

---


Electronic Theses and Dissertations, 2020-

---

2020

## Modeling Flow and Nitrate Transport in Karst Groundwater Basins

Yuan Gao  
*University of Central Florida*

 Part of the [Civil Engineering Commons](#), and the [Water Resource Management Commons](#)  
Find similar works at: <https://stars.library.ucf.edu/etd2020>  
University of Central Florida Libraries <http://library.ucf.edu>

This Doctoral Dissertation (Open Access) is brought to you for free and open access by STARS. It has been accepted for inclusion in Electronic Theses and Dissertations, 2020- by an authorized administrator of STARS. For more information, please contact [STARS@ucf.edu](mailto:STARS@ucf.edu).

---

### STARS Citation

Gao, Yuan, "Modeling Flow and Nitrate Transport in Karst Groundwater Basins" (2020). *Electronic Theses and Dissertations, 2020-*. 215.  
<https://stars.library.ucf.edu/etd2020/215>

MODELING FLOW AND NITRATE TRANSPORT IN KARST GROUNDWATER BASINS

by

YUAN GAO

B.S. Xidian University, 2008

M.S. Colorado State University, 2017

A dissertation submitted in partial fulfillment of the requirements  
for the degree of Doctor of Philosophy  
in the Department of Civil, Environmental, and Construction Engineering  
in the College of Engineering and Computer Science  
at the University of Central Florida  
Orlando, Florida

Summer Term

2020

Major Professor: Dingbao Wang

©2020 YUAN GAO

## **ABSTRACT**

Understanding the groundwater flow in karst aquifers and the effect of best management practices (BMPs) on nitrate decrease in spring discharge is critical for effective management and protection of karst water resources. However, the control on the conduit network's impacts on spring discharge and nitrate concentration is not fully understood, and the cumulative effects of BMP on reducing nitrate in karst groundwater systems have not been evaluated at the basin scale. In this dissertation, a coupled Conduit Flow Process (CFPv2) and Conduit Mass Three-Dimensional (CMT3D) model was applied to evaluate the biosorption-activated media (BAM)-based BMP on nitrate removal in Silver Springs in Florida. It is found that the effect of BMP by implementing BAM blanket filters in twenty-six stormwater retention basins is limited; whereas, for implementing BAM blanket filters in 50% of the urban area, the nitrate-N concentration in spring discharge would be decreased by 10.7% in a normal hydrologic year. The controls on the contribution of conduit flow to spring discharge are evaluated. For aquifer with turbulent flow in a single conduit, the effects of three dimensionless numbers (Reynolds number, relative surface roughness, and hydraulic conductivity ratio) and recharge on conduit flow contribution are quantified. Moreover, the effects of conduit geometry and density on conduit flow contribution are evaluated for conduit networks. Finally, the prediction of long-term average discharge in ungauged basins is assessed for improving recharge estimation.

## **ACKNOWLEDGMENTS**

I cannot express enough thanks to my advisor, Dr. Wang, for his dedication and inspiration. It is his guidance, timely advice, and meticulous scrutiny helped me to accomplish dissertation. His kind and patient support throughout my doctoral study is gratefully appreciated.

I would also like to thank all of my committee members, Dr. Kelly Kibler, Dr. Ni-Bin Chang, and Dr. Melanie Beazley, for their comments and suggestions which considerably enlightened my research and help improve the quality of my dissertation.

I am deeply grateful to my former and current research and project group members: Mohammad Shokri, Dr. Dan Wen, Lili Yao, Andrea Valencia, Diana Ordonez, and Eranildo Lustosa. They always show me their professional attitude and critical thinking along my doctoral study, which inspired me greatly on successfully conducting research and project.

Special thanks are given to my family for their immense love and support in my entire life. I cannot complete my Ph.D. degree without their support.

In the end, I am very grateful for the financial support provided by the University of Central Florida and the Florida Department of Transportation.

## TABLE OF CONTENTS

ABSTRACT .....	iii
ACKNOWLEDGMENTS .....	iv
TABLE OF CONTENTS .....	v
LIST OF FIGURES .....	viii
LIST OF TABLES .....	xii
CHAPTER 1 INTRODUCTION .....	1
1.1 Background .....	1
1.2 Study objectives .....	4
CHAPTER 2 EVALUATING THE PERFORMANCE OF BAM-BASED BLANKET FILTER ON NITRATE DECREASE IN A KARST SPRING .....	7
2.1 Introduction .....	7
2.2 Study area and methodology .....	11
2.2.1 Study area: Silver Springs, FL .....	11
2.2.2 Model description .....	17
2.2.3 Model calibration and validation .....	29
2.2.4 BAM-based blanket filter scenarios .....	30
2.3 Results .....	32
2.3.1 Groundwater flow .....	32

2.3.2 Nitrate transport .....	35
2.3.3 Effects of BMP .....	38
2.4 Discussions .....	41
2.4.1 Effects of conduits on flow and nitrate transport.....	41
2.4.2 Sensitivity analysis.....	42
2.5 Summary .....	44
 CHAPTER 3 EVALUATING PHYSICAL CONTROLS ON GROUNDWATER FLOW IN KARST CONDUIT NETWORK.....	
3.1 Introduction.....	47
3.2 Methodology .....	50
3.2.1 Mechanisms governing the flow in a single-conduit karst aquifer .....	50
3.2.2 Mechanisms governing the flow in conduit network.....	52
3.2.3 Evaluation methods.....	53
3.3 Evaluation results.....	58
3.3.1 Controls on the contribution of single conduit to spring discharge .....	58
3.3.2 Controls on the contribution of conduit networks with different conduit density to spring discharge .....	67
3.3.3 Controls on the contribution of conduit networks with same conduit density to spring discharge .....	69

3.4 Case study and discussion.....	70
3.4.1 Descriptions of the study area.....	70
3.4.2 Configuration and calibration of the regional scale models .....	72
3.4.3 Comparison of $Q_c/Q$ between the evaluation results and regional scale models	74
3.5 Summary .....	76
 CHAPTER 4 DIAGNOSIS TOWARD PREDICTING MEAN ANNUAL RUNOFF IN	
UNGAUGED BASINS.....	
4.1 Introduction.....	79
4.2 Methodology .....	83
4.2.1 Mean annual runoff model.....	83
4.2.2 Parameter estimation.....	85
4.2.3 Study watersheds .....	89
4.3 Results and discussion .....	91
4.3.1 Estimated average soil water storage capacity.....	91
4.3.2 Estimated shape parameter .....	94
4.3.3 Diagnosing mean annual runoff prediction.....	97
4.4 Summary .....	100
 CHAPTER 5 CONCLUSION.....	
REFERENCES .....	106



## LIST OF FIGURES

Figure 1: (a) Nitrate treatment through BAM blanket filter constructed in a stormwater retention basin. (b) The design concepts and general dimensions of blanket filters. (c) A constructed blanket filter in City of Ocala, Florida (Wen et al., 2019). .....	12
Figure 2: The observation wells, sinkholes, conduits and rivers in the springshed of Silver Springs in Florida.....	13
Figure 3: The land use and land cover (LULC) (a) and the percentage of area for each LULC type (b) in the Silver Springs springshed in 2000, 2009, and 2014.....	15
Figure 4: (a) Population density from 2000 to 2016 for City of Ocala in Florida. (b) Observed nitrate-N concentration in the discharge of Silver Springs. (c) Observed nitrate-N concentration in the discharge of Silver Springs (the green-dash arrows indicate the trend of observed nitrate-N concentration from 2000 to 2016). (d) A linear relationship between the observed nitrate-N concentration in spring discharge and population density in City of Ocala from 2000 to 2016.....	17
Figure 5: The flow chart for modelling the nitrate-N concentration in groundwater and spring discharge. ....	19
Figure 6: The horizontal (a) and vertical (b) discretization of the groundwater model.....	19
Figure 7: Injection and sampling sites for the tracer dyes. ....	26
Figure 8: Tracer samplers at well-2 (A), well-3 (B), and Silver Springs (C). ....	26

Figure 9: Calibration relationship between absorbance and concentration of eosin solution. .... 27

Figure 10: (A) Rhodamine WT concentration detected in Silver Springs with fitted curve based on the two-region non-equilibrium model; (B) Fluorescein dye concentration detected in well-2. .... 28

Figure 11: The twenty-six stormwater retention basins (SRB) owned by Florida Department of Transportation (FDOT) and the boundary of the City of Ocala. .... 32

Figure 12: (a) The observed versus simulated hydraulic heads for the steady state and transient models; and (b) The observed and simulated discharge of Silver Springs. .... 35

Figure 13: Estimated nitrate concentration in groundwater recharge for agricultural land, residential & transportation, and forest land. .... 36

Figure 14: Projected effects of blanket filter on decrease of nitrate concentration in the discharge of Silver Springs when BAM implemented in twenty-six stormwater retention basins owned by Florida Department of Transportation (FDOT) and 50% of the drainage area in City of Ocala. .... 38

Figure 15: The control of recharge on the percentage of flow volume (a) and nitrate mass (b) in conduits. .... 42

Figure 16: (a) Sensitivity of spring discharge to diameter, conductance, and roughness height of conduits. (b) Sensitivity of nitrate-N concentration in spring discharge to effective porosity (n). .... 43

Figure 17: Model configuration for karst aquifers with single conduit (a), three-conduit network (c), two seven-conduit networks (e) and (g). The numbers of nodes and tubes for one-conduit (b), three-conduit network (d), and seven-conduit networks (f) and (h). ..... 56

Figure 18: Relation between  $K_c/K$  and  $Q_c/Q$  (a) and  $Re$  and  $Q_c/Q$  (b) for a single conduit 60

Figure 19: For a defined  $\epsilon/D$  and different  $K_c/K$ , changes in contours of hydraulic head in aquifers with (a) single conduit; (b) three-conduit network; (c) and (d) seven-conduit network under laminar flow conditions. .... 64

Figure 20: When flow in the conduit is turbulent, (a) controls of  $\epsilon/D$  on  $Q_c/Q$  when  $K_c/K = 0.033$ ; (b) for same Reynolds number, controls of  $\epsilon/D$  on  $Q_c/Q$  with different  $K_c/K$  and recharge..... 66

Figure 21: For same recharge values, different conduit densities and geometries, (a) controls of  $K_c/K$  on  $Q_c/Q$  and (b) controls of  $Re$  on  $Q_c/Q$  under laminar flow conditions..... 68

Figure 22: For same recharge value and  $K_c/K$  and different conduit density and geometry, controls of  $\epsilon/D$  on  $Q_c/Q$  under turbulent flow conditions. .... 69

Figure 23: Conduit structure settings in the steady-state groundwater flow model for Silver Springs springshed. .... 71

Figure 24: The observed and simulated hydraulic heads for the steady-state groundwater flow model for Silver springshed. .... 74

Figure 25: Controls of  $\epsilon/D$  on  $Q_c/Q$  for regional scale karst models developed in present and

previous studies..... 76

Figure 26: The degree of saturation  $S/S_b$  under long-term average climate versus climate aridity index  $\Phi$ . ..... 87

Figure 27: The spatial distribution of land use and land cover for Fox River watershed in Wisconsin (a) and Spoon River watershed in Illinois (d), the hydrologic soil groups for Fox River watershed (b) and Spoon River watershed (e), and the curve numbers for Fox River watershed (c) and Spoon River watershed (f)..... 93

Figure 28: The estimated average soil water storage capacity ( $S_b$ ) as a function of  $S_{CN}$  and climate aridity index (a) and shape parameter from soil data (b)..... 94

Figure 29: The estimated shape parameter for the spatial distribution of soil water storage capacity based on soil data and the calibrated shape parameter based on mean annual water balance in the Fox River watershed (a) and the Spoon River watershed (b). ..... 95

Figure 30: (a) Observed versus simulated mean annual runoff using shape parameter based on soil data; (b) Soil data-based versus calibrated shape parameter; and (c) Observed versus simulated mean annual runoff using shape parameter based on calibration. .... 96

Figure 31: The effects of soil, land surface topography, and bedrock topography on the shape parameter of the spatial distribution of soil water storage capacity..... 100

## LIST OF TABLES

Table 1: The injection well and the amount of injected dye for each tracer type. ....	25
Table 2: Background concentrations of RWT at the sampling point in Silver Springs. ....	28
Table 3: The calibrated values of diameter, conductance, roughness height, tortuosity for each conduit. ....	33
Table 4: The calibrated values of diameter, conductance, roughness height, tortuosity for each conduit in the regional model for Silver Springs springshed.....	73
Table 5: The USGS gage stations, climate aridity index, the estimated potential maximum retention of curve number method ( $S_{CN}$ ), and the average soil water storage capacity ( $S_b$ ) for the study watersheds.....	90

# CHAPTER 1 INTRODUCTION

## 1.1 Background

Karst aquifers, which are widely distributed around the world and provide the water resources for about one quarter of the global population, display considerable complexity due to the large contrast in physical parameters within the coupled conduit-matrix system (Ford and Williams, 2007; Giese et al, 2018). The highly permeable karst conduits, draining the fractures and matrix, are the most important hydraulic features adding a fast flow component to the groundwater discharge (Quinlan and Ewers, 1985; Marechal et al., 2008), and numerical modeling of karst aquifers also has demonstrated that conduits may comprise a large proportion of spring discharge, with increasing effective transmissivity or hydraulic conductivity as the spring outlet is approached, suggesting the convergence of groundwater flow in a network of high-permeability conduits (Liedl et al., 2003; De Rooij et al., 2013). Therefore, much importance has been placed on the investigation of conduit flow in karst aquifers (Worthington, 2009, 2015) and numerous studies on the influence of variable of conduit properties on groundwater flow in karst conduits have been published. The studies thus far have focused on the effects of conduit properties on flow and transport in karst systems either conceptually or numerically, or just applicable to specific regions; however, to our knowledge, literatures provide few researches about the controls which are independent of the magnitude of the physical parameters on the conduit flow under laminar

and turbulent conditions in karst aquifers.

Understanding the aquifer and conduit properties on conduit flow is critical for effective management and protection of karst water resources. Due to high flow velocity usually occurred in karst conduit network, karst aquifers are highly vulnerable to contaminants. For example, the concentration of nitrate has been steadily increasing over the last 30 years in many Florida's karst springs (Katz et al., 2009; Heffernan et al., 2010) which serve as important locations where groundwater outlets interact with surface water and are a common feature of Florida's landscape (Katz, 2004). Over fertilization of agricultural and residential areas has led to nitrate pollution in Florida's largest spring group: Silver Springs. Over the past few decades, the nitrate-N concentration in Silver Springs have significantly exceeded the 0.35 mg/L standard as a result of human activities (Katz et al., 2009). Best management practices (BMPs) for stormwater treatment have been developed to reduce both nitrate contaminants in urban surface runoff and in groundwater that are discharged to the Silver Springs. For example, recently, Wen et al. (2019) reported that a BAM-based blanket filter implemented in an SRB can reduce the nitrate by 62%. Field experiments and process-based numerical models have been used for evaluating the cumulative effects of BMPs implemented at various spatial scales (Almasri and Kaluarachchi, 2007; Sahu and Gu, 2009; Shultz et al., 2018), serving as tools for decision making on mitigation measures. However, to our knowledge, due to the lack of systematic understanding of the aquifer and conduit properties on conduit flow, contaminant transport in karst systems by the effects of

BMPs have not been deeply studied and evaluated.

Numerical models are usually employed to study the effects of BMPs on subsurface contaminant transport. Improved estimation of surface runoff provides opportunities for improving the calculation of input contaminant concentration thus enhancing the model fidelity. The factors controlling mean annual runoff have been studied in the literature. Mean climate has been identified as the first order control on mean annual runoff and evaporation and it has been quantified by climate aridity index, which is defined as the ratio between the mean annual potential evapotranspiration and precipitation (Turc, 1954; Pike, 1964). Other controlling factors include the temporal variability of climate (Troch et al., 2013), vegetation (Zhang et al., 2001), soil (Yokoo et al., 2008), and topography (Woods, 2003). Mean annual runoff or evaporation has been modeled as a function of climate aridity index and the equation is usually called as Budyko equation (Budyko, 1958). The effects of other factors are represented by including a parameter to Budyko equations (Fu, 1981; Yang et al., 2008; Wang and Tang, 2014). Among these factors, climate including its mean and temporal variability, and soil water storage capacity including its mean and spatial variability are dominant catchment characteristics controlling mean annual runoff, especially for saturation excess runoff generation-dominated catchments (Milly, 1994). Soil water storage capacity exerts a powerful control on mean annual runoff. Research has been conducted to reveal the role of soil water storage capacity through the linkage of vegetation and model parameter (Yang et al., 2008). It has also been suggested that the spatial variability of soil



water storage capacity could suppress the actual evaporation and therefore promote the runoff generation indirectly (Yao et al., 2020). Climate variability and soil water storage capacity need to be explicitly incorporated into the model for predicting mean annual runoff. The effect of climate variability could be taken into account by driving the model with daily precipitation and potential evaporation which are usually available. The spatial distribution of soil water storage capacity could be modelled by a distribution function, and it is usually modelled by the generalized Pareto distribution (Moore, 1985; Zhao, 1992). However, the estimated parameters in the distribution function from previous methods bring much uncertainty in runoff estimation, and the two parameters of the generalized Pareto distribution are usually estimated by model calibration using observed streamflow data (Wood et al., 1992; Alipour and Kibler, 2018, 2019).

## 1.2 Study objectives

Based on the background and study limitations describe above, there are three main objectives seek to obtain in this dissertation. The first objective of this dissertation is to evaluate effects of a BMP on nitrate decrease in karst springs: Silver Springs which is located near the City of Ocala, in Florida by using an integrated groundwater model. A version of MODFLOW Conduit Flow Process (CFPv2) and the Conduit Mass Transport Three-Dimensional model (CMT3D) (Spiessl et al., 2007; Reimann et al., 2013a, b, c) were integrated to address the variability of nitrate-N concentration in blanket filter effluent. The integrated model simulates

flow and contaminant transport in both porous medium and conduits (Xu et al., 2015; Sullivan et al., 2019). The integrated model is used to evaluate the effects of the BMP which are implemented in twenty-six SRBs in transportation corridors. An aggressive BAM implementation scenario that considers multiple BMPs having a combined drainage area equivalent to 50% of the urban area near the Silver Springs (i.e., City of Ocala) is also considered. This scenario is included to provide guidance on nutrient control policies and future investment plans of nutrient decrease technologies. There are two questions seek to answer: 1) What is the potential for the BMP in stormwater basins to mitigate groundwater nitrate as compared to the baseline condition in a karst aquifer? 2) What is the long-term effectiveness of the BMP in reducing nitrate-N concentrations in spring discharge?

The second objective of this dissertation is to quantify the roles of following factors on conduit flow: conduit relative surface roughness, flow regime for conduit flow, hydraulic conductivity of porous matrix, aquifer recharge rate, and conduit density and morphology. To achieve the objective, synthetic groundwater models with conduits will be developed using the code of MODFLOW-CFP (Shoemaker et al., 2008). General relations are developed for several dimensionless numbers, which are used to characterize the coupled conduit-matrix system. The obtained general relations are applied to the Silver Springs in Florida to estimate the percentage of conduit flow over the total spring discharge.

The final objective of this dissertation is toward developing nonparametric mean annual

water balance model for predicting mean annual runoff in ungauged basins. The mean annual water balance model is forced by daily precipitation and potential evaporation; therefore, the climate variability at different timescales is represented explicitly in the climate input. The runoff generation is quantified by a distribution function for describing the spatial distribution of soil water storage capacity (Wang, 2018). The mean and the shape parameter of the distribution function need to be estimated from the available data in ungauged basins. Therefore, the model serves as a diagnosis tool for evaluating the data requirement for estimating soil water storage capacity.

## **CHAPTER 2 EVALUATING THE PERFORMANCE OF BAM-BASED BLANKET FILTER ON NITRATE DECREASE IN A KARST SPRING**

### 2.1 Introduction

Groundwater serves as the primary source of drinking water for many municipalities and rural areas in Florida (Bradner, 1994; Dufresne and Drake, 1999). Springs serve as important locations where groundwater outlets interact with surface water and are a common feature of Florida's landscape (Katz, 2004). Over fertilization of agricultural and residential areas has led to nitrate pollution in Florida's groundwater and surface water systems (Ritter et al., 2007; Castro et al., 2018). Elevated nitrate concentrations in drinking water can cause serious health problems, specifically to infants (e.g., methemoglobinemia). The National Drinking Water Regulations have the maximum contaminant level for nitrate in drinking water set to 10 mg/L, measured as nitrate-nitrogen (NO<sub>3</sub>-N). Excess concentrations of dissolved nitrate in surface water will lead to eutrophication and may increase the gross primary production of water bodies (Coinly, 1945; Sfriso and Marcomoni, 1994; Gardner and Vogel, 2005). Water quality standards including Numeric Nutrient Criteria help to protect and restore the quality of water bodies such as streams, lakes, and springs. In response to the *Florida Springs and Aquifer Protection Act* passed in 2014, the *Springshed Initiative* began to monitor and reduce nutrient contamination in all springsheds in Florida. In this context, the Florida Department of Environmental Protection (FDEP) has set the

nitrate limit to 0.35 mg/L to maintain spring health (FDEP, 2014).

Over the past few decades, the nitrate-N concentration in Florida's springs have significantly exceeded the 0.35 mg/L standard as a result of human activities (Katz et al., 2009) such as, over fertilization of agricultural lands and lawns, leakage from septic tanks, polluted stormwater runoff from transportation corridors, and contamination from wastewater effluent (Reed et al., 2018). An analysis of 328 private drinking water wells in Florida revealed that 66% of the wells were heavily contaminated by nitrate-N (FDEP, 2012). The Upper Floridan Aquifer (UFA), the most productive groundwater system in the U.S., is highly vulnerable to contaminants due to the karstification of its landscape, characterized by the change of porosity in interconnected caves, conduits, and underground drainage channels (Ritter et al., 2007; Ghasemizadeh et al., 2012).

Nitrogen exists as multiple species in natural water systems (e.g., organic nitrogen, nitrite, and nitrate), but nitrate is the most prevalent groundwater contaminant in freshwater aquifers (Smith et al., 2001). Organic nitrogen is usually present in the form of sediment and suspended solids and is usually not observed in groundwater (Rivett et al., 2008). Nitrite is relatively unstable and the conversion to nitrate, through nitrification, occurs quickly (Rivett et al., 2008). Excess nitrate generated from non-point sources (e.g., fertilizer run-off from agricultural lands) and point sources (e.g., septic tanks in urban areas) may exceed the denitrification capacity in topsoil and allow nitrate to leach into groundwater systems (Shamrukh et al., 2001). This is

common since nitrate is highly mobile with a low sorption capacity (Robertson et al., 2000). Nitrate can be converted to nitrogen gas through denitrification; however, this process requires anaerobic conditions (Korom, 1992; Smith et al., 2004). Therefore, denitrification in the vadose zone is limited, and nitrate is the main nitrogen specie in groundwater (Exner et al., 2014).

Best management practices (BMPs) for stormwater treatment have been developed to reduce both nitrate contaminants in urban surface runoff and in groundwater recharge. Bratieres et al. (2008) reported that biofilters remove 70% of nitrate in urban runoff. Studies have shown that the water quality of BMP effluent can be improved by up to 50% when using bio-infiltration media in stormwater retention basins (SRBs) (Ermilio, 2005). The potential of a biosorption-activated media (BAM) on removing nitrogen has been highlighted in several studies (Chang et al., 2010, 2011, 2018; Hossain et al., 2010; Xuan et al., 2010) and has already been implemented in constructed wetlands (Chang et al., 2013; Xuan et al., 2009), SRBs (O'Reilly et al., 2012a,b,c), roadside swales (Hood et al., 2013), linear ditches (Chang et al., 2019; Wen et al., 2019), and rapid infiltration basins (Wen et al., 2020). Recently, Wen et al. (2019) reported that a BAM-based blanket filter implemented in an SRB can reduce the nitrate by 62%. The construction of a BAM blanket filter is shown in Figure 1, further details are presented in Section 2.2. Field experiments and process-based numerical models have been used for evaluating the cumulative effects of BMPs implemented at various spatial scales (Almasri and Kaluarachchi, 2007; Sahu and Gu, 2009; Shultz et al., 2018), serving as tools for decision making on mitigation measures. However, to our

knowledge, current studies have not evaluated the performance of BAM nitrate removal in karst systems.

The objective of this study is to evaluate the effect of BAM blanket filters on the decrease in nitrate in karst groundwater systems. The Silver Springs springshed located near the City of Ocala, in Florida was evaluated using a coupled groundwater model. A version of MODFLOW Conduit Flow Process (CFPv2) and the Conduit Mass Transport Three-Dimensional model (CMT3D) (Spiessl et al., 2007; Reimann et al., 2013a, b, c) were coupled to address the variability of nitrate-N concentration in blanket filter effluent. The integrated model simulates flow and contaminant transport in both porous medium and conduits (Xu et al., 2015; Sullivan et al., 2019). In this study, the integrated model is used to evaluate the effects of BAM blanket filters which are implemented in twenty-six SRBs in transportation corridors. This study also considers an aggressive BAM implementation scenario that considers multiple BMPs having a combined drainage area equivalent to 50% of the urban area near the Silver Springs (i.e., City of Ocala). This scenario is included to provide guidance on nutrient control policies and future investment plans of nutrient decrease technologies. This study seeks to answer the following questions: 1) What is the potential for BAM blanket filter in stormwater basins to mitigate groundwater nitrate as compared to the baseline condition in a karst aquifer? 2) What is the long-term effectiveness of BAM blanket filter in reducing nitrate-N concentrations in spring discharge?

## 2.2 Study area and methodology

This section is organized as follows: 1) introduction of the study area; 2) model description; 3) model calibration and validation, and 4) BAM blanket filter scenarios.

### 2.2.1 Study area: Silver Springs, FL

#### 2.2.1.1 Springshed characteristics

The Silver Springs springshed, with an area of about 2,323 km<sup>2</sup>, is delineated using the potentiometric surface of the UFA (Figure 2). Silver Springs, which is the head water of the Silver River, is the largest spring group in Florida, with an average discharge of 8.1 m<sup>3</sup>/s during the period of 2010 to 2016. The climate is humid subtropical with rainy summers and dry winters (Phelps, 2004). The average annual temperature is 21.8 °C and the average annual precipitation is 1,290 mm.



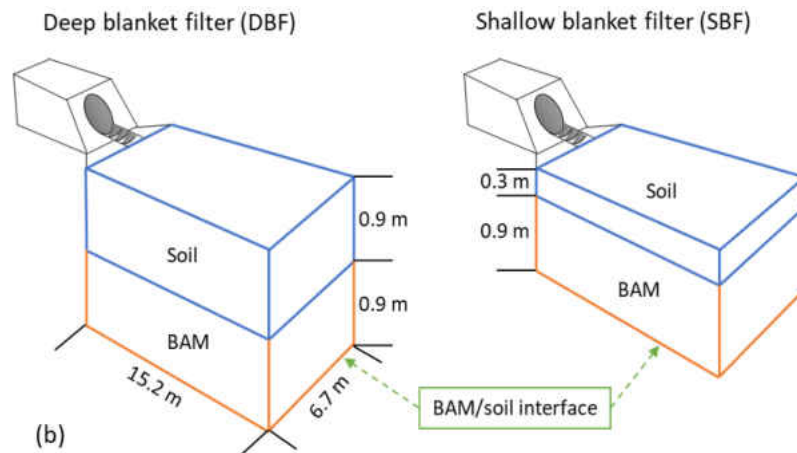
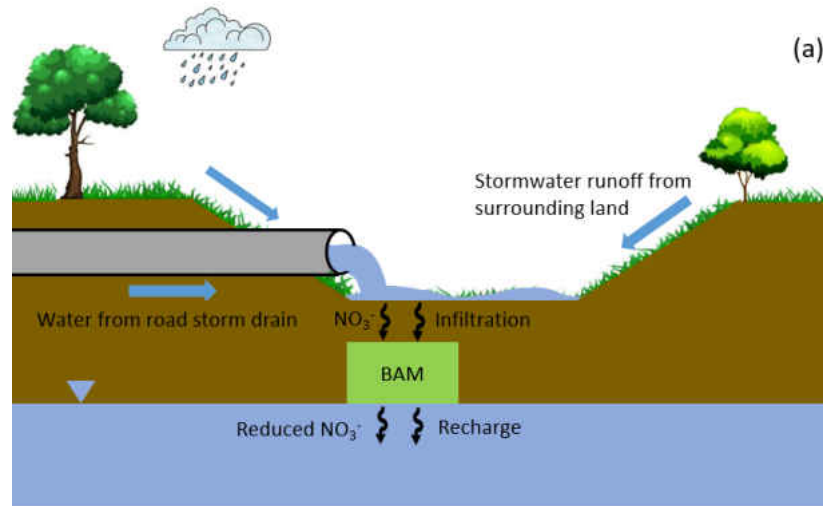


Figure 1: (a) Nitrate treatment through BAM blanket filter constructed in a stormwater retention basin. (b) The design concepts and general dimensions of blanket filters. (c) A constructed blanket filter in City of Ocala, Florida (Wen et al., 2019).

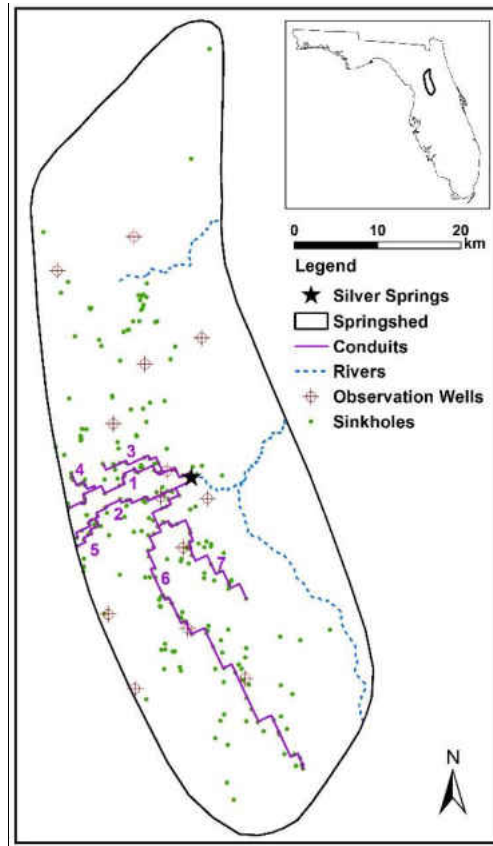


Figure 2: The observation wells, sinkholes, conduits and rivers in the springshed of Silver Springs in Florida.

The aquifer system of the springshed is comprised of the UFA, a middle semi-confining unit, and the lower Floridan aquifer. The UFA is mainly composed of Ocala Limestone and the thickness of the UFA is about 90 m (Sepulveda, 2002; Canion et al., 2019). A majority (86%) of spring discharge is from the upper 30 m of the UFA (Faulkner, 1973). The UFA is confined in most parts of the springshed except some areas where the Ocala limestone crops out (Phelps, 2004). The UFA in the western part of the springshed is near the land surface where the recharge rates are relatively higher, especially in the central-western portion of the springshed where there are numerous closed sinkhole depressions (Phelps, 2004). Most of the rainfall either drains directly

into sinkholes or seepages into the unconfined limestone of the UFA since surface drainage is not abundant (Phelps, 2004). Groundwater flow in the UFA may occur both in the rock matrix and fractures due to the dual-porosity characteristics of the aquifer (Phelps, 2004). Fractures are distributed mainly around the spring outlet, where the hydraulic conductivity and groundwater flow velocity are relatively higher compared with the rock matrix (Faulkner, 1973). These karstified features facilitate the recharge activity and correspondingly nitrate transport to the aquifer.

#### 2.2.1.2 LULC, population density, and trends in nitrate-N concentration

The land use and land cover (LULC) in the springshed is comprised of agriculture, residential, forest, barren land (i.e., sparse vegetation and fallow ground), transportation, rangeland, wetlands and streams, and lakes (Figure 3; data obtained from <https://data-floridaswater.opendata.arcgis.com/>). The predominant LULC prior to 1995 included agricultural land and forest. Since the nitrogen source in forested land is atmospheric deposition and the associated nitrogen load is small, fertilizer seepage from agriculture land is the main source of nitrate in groundwater. With population growth, the urban area including residential and transportation areas has gradually replaced agricultural and forest lands since 1995. Most of the residents within the springshed use onsite sewage disposal systems, such as septic tanks (FDEP, 2012), and the transportation land has an impervious surface, producing runoff with accumulated

nutrient loads from residential lawns. The leakage from septic tanks, fertilizer applications to lawns, and stormwater runoff from roads contribute significant nitrate loads to groundwater.

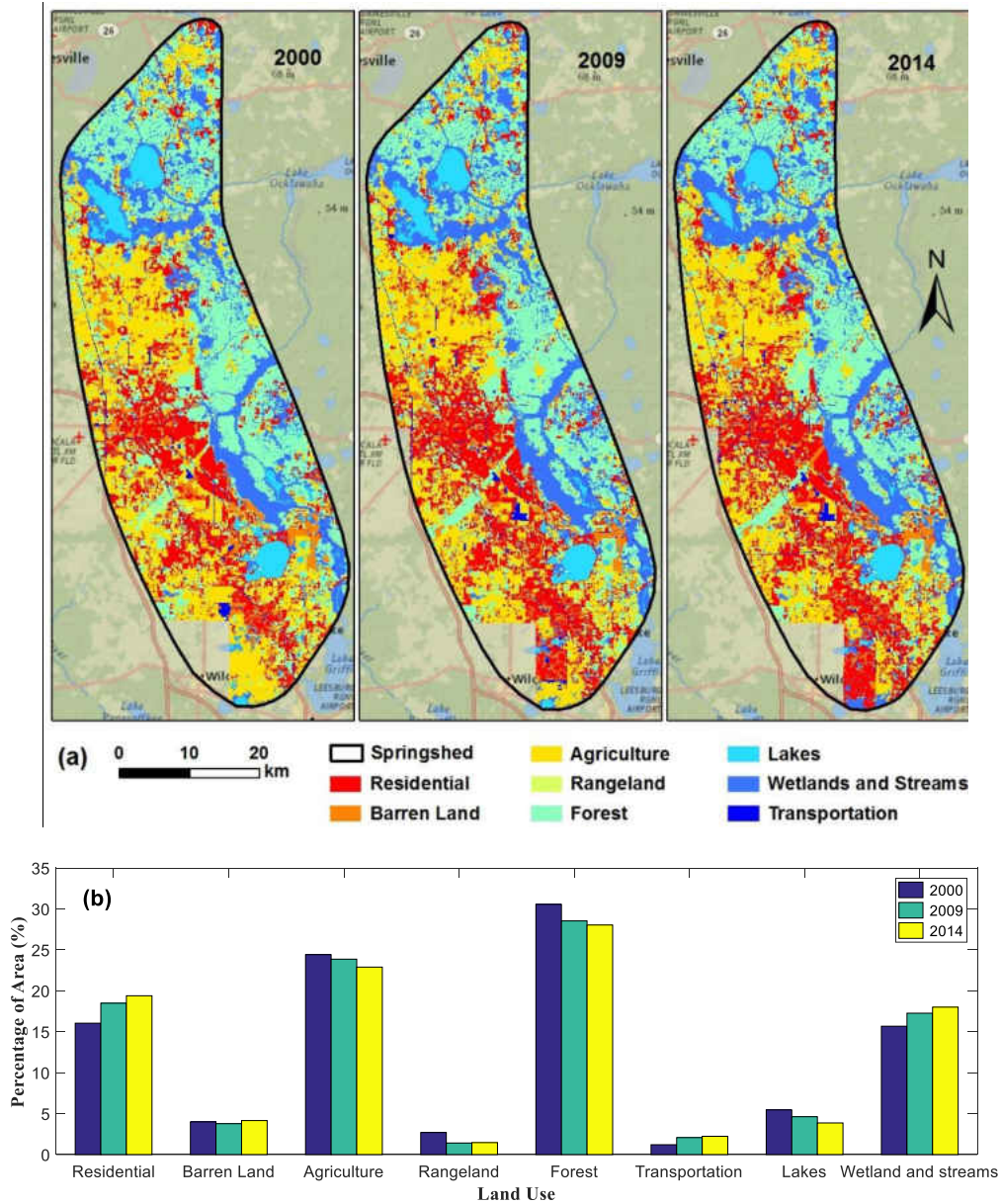


Figure 3: The land use and land cover (LULC) (a) and the percentage of area for each LULC type (b) in the Silver Springs springshed in 2000, 2009, and 2014.

The population in the springshed is mainly concentrated in the City of Ocala, which is

located at the west side of the Silver Springs. Data obtained from the U.S. Census Bureau indicate that population density has increased by 22% from 2000 to 2014 (Figure 4a). Figure 4b and 4c show the observed nitrate-N concentrations in the Silver Springs, which were obtained from the literature (FDEP, 2006; FDEP, 2012) and St. Johns River Water Management District (<https://www.sjrwmd.com/data/>). From the 1900s to the 1960s, a period with less anthropogenic influences on the environment, the nitrate-N concentration was 0.3-0.4 mg/L on average (Figure 4c). This nitrate-N concentration can be considered as the natural level and is the restoration target for the spring. Since the 1960s, the nitrate-N concentration has dramatically increased due to agricultural development and urbanization. Population density and nitrate-N concentration in the spring discharge have increased from 2000 to 2014, and there is a linear correlation ( $R^2 = 0.62$ ) between them as shown in Figure 4d, indicating that increase of nitrate-N concentration is correlated with the growth of population density.

Actions have been undertaken for protecting the spring in the past 10 years, and particularly, spring restoration projects have been conducted in 2015 for reducing the nitrogen load from human activities. The total nitrogen has been reduced by 12.5% (i.e., 42,565 kg-N) for urban fertilizer, 2.8% (i.e., 96,668 kg-N) for agricultural fertilizer, and 1.5% (i.e., 11,022 kg-N) for onsite sewage treatment and disposal systems (FDEP, 2015). The observed mean annual nitrate-N concentration has been reduced from 1.26 mg/L in 2015 to 1.14 mg/L in 2016 following the restoration projects (green arrows in Figure 4b).

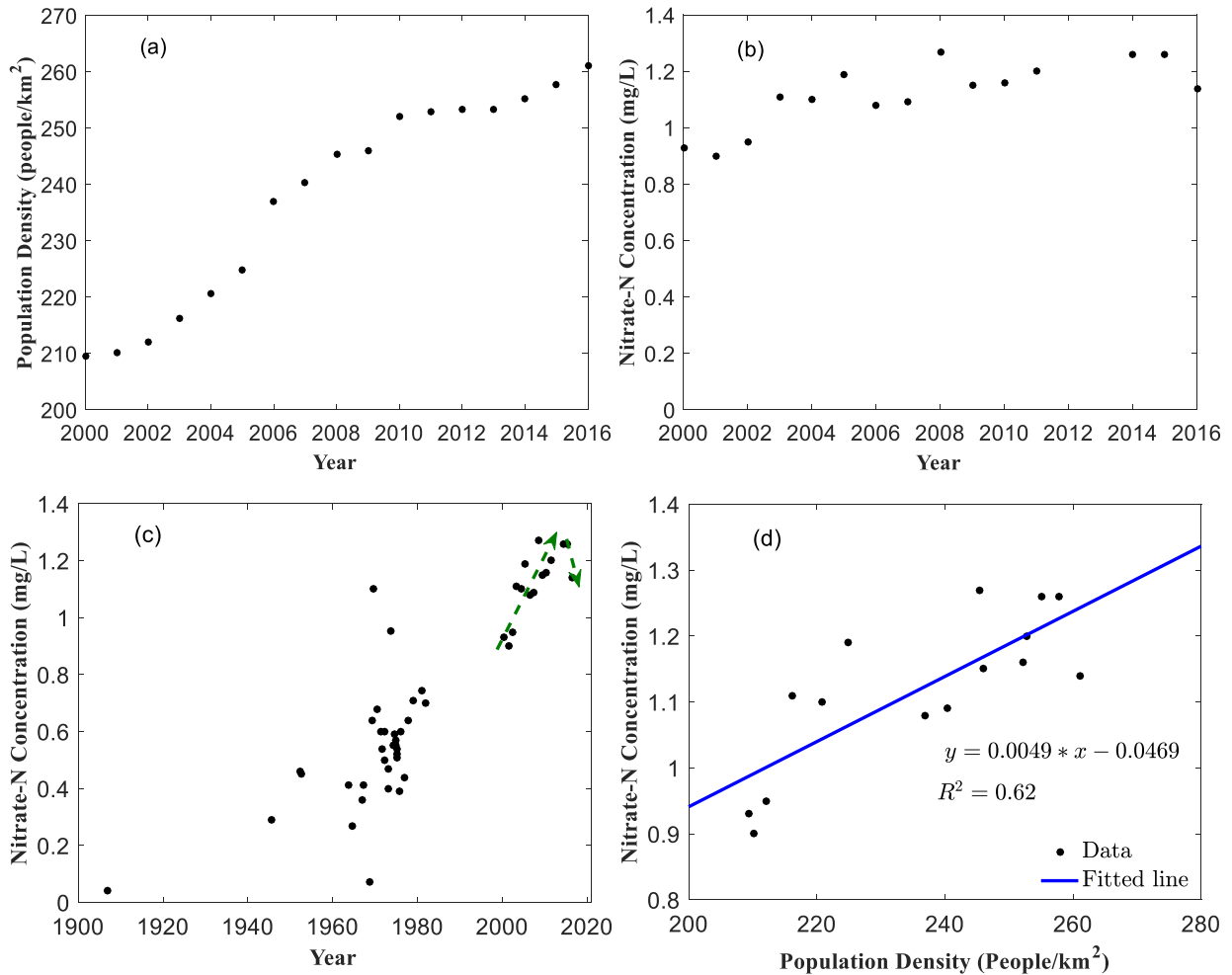


Figure 4: (a) Population density from 2000 to 2016 for City of Ocala in Florida. (b) Observed nitrate-N concentration in the discharge of Silver Springs. (c) Observed nitrate-N concentration in the discharge of Silver Springs (the green-dash arrows indicate the trend of observed nitrate-N concentration from 2000 to 2016). (d) A linear relationship between the observed nitrate-N concentration in spring discharge and population density in City of Ocala from 2000 to 2016.

## 2.2.2 Model description

### 2.2.2.1 The EPM model

Figure 5 shows the flow chart of model development. The first step is to develop and calibrate a groundwater flow model without conduits using MODFLOW. Three-dimensional

groundwater flow EPM model was created using MODFLOW and the model domain is discretized into 496 rows and 236 columns with the cell size of 190.5 m by 190.5 m (Figure 6a). The model includes 4 layers with variable thickness representing the surficial aquifer (Layer 1), the middle semi-confining unit (Layer 2), the UFA (Layer 3), and the lower Floridan aquifer (Layer 4) (Figure 6b). The springshed boundary is set as a no-flux boundary condition, and the head-dependent flux boundary is used for internal boundaries such as rivers, lakes, and streams. The top and bottom elevations of each layer, average hydraulic conductivity, boundary conditions for river, lake, streams, recharge, and evapotranspiration within the springshed were obtained from the large scale North Florida Southeast Georgia (NFSEG) model which was developed by St. Johns River Water Management District (SJRWMD) (Durdan et al., 2013). In the EPM model, high hydraulic conductivity cells were allowed for representing karst features in the UFA.

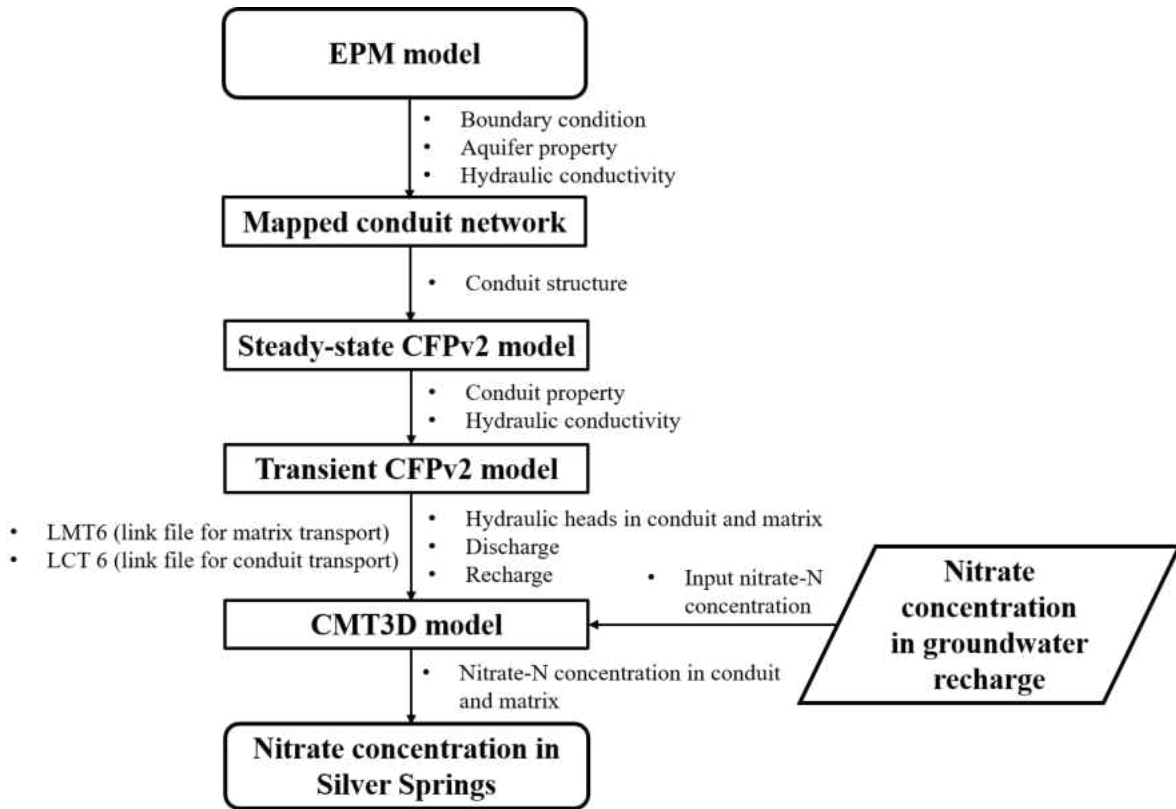


Figure 5: The flow chart for modelling the nitrate-N concentration in groundwater and spring discharge.

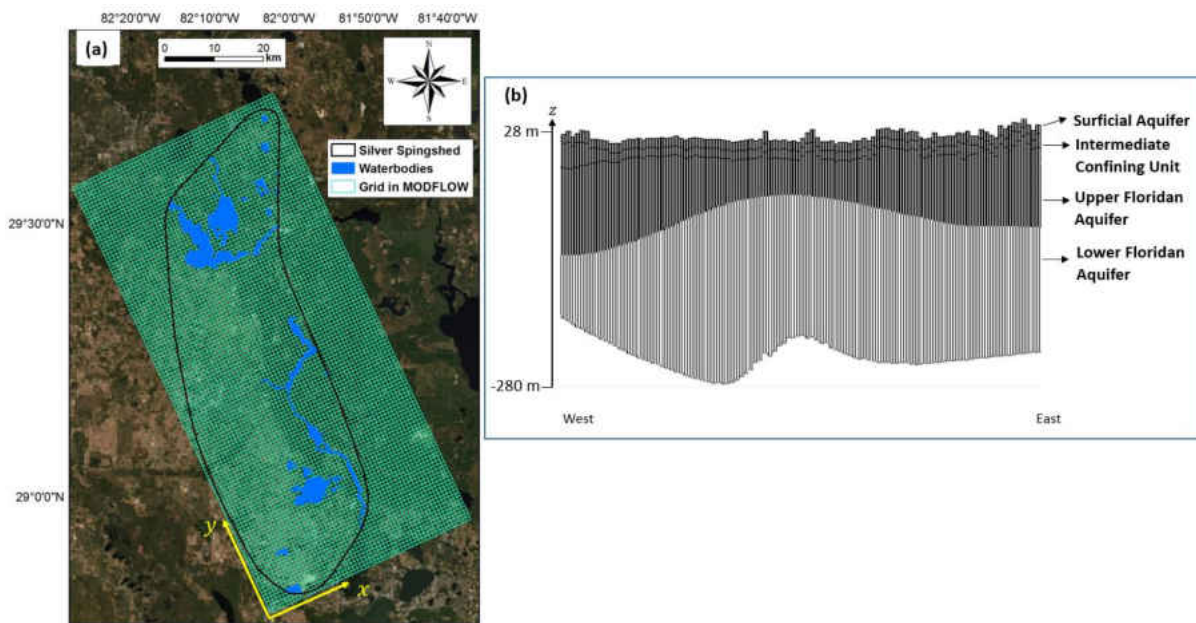


Figure 6: The horizontal (a) and vertical (b) discretization of the groundwater model.



### 2.2.2.2 CFPv2 for flow modeling

CFPv2 simulates flows in both rock matrix and conduits. Darcy's law is applicable in the rock matrix where the flow is laminar, and the governing equation is:

$$\frac{\partial}{\partial x} \left( K_x \frac{\partial h}{\partial x} \right) + \frac{\partial}{\partial y} \left( K_y \frac{\partial h}{\partial y} \right) + \frac{\partial}{\partial z} \left( K_z \frac{\partial h}{\partial z} \right) = S_s \frac{\partial h}{\partial t} - W \quad (2.1)$$

where  $K_x$ ,  $K_y$ , and  $K_z$  ( $\text{LT}^{-1}$ ) are the hydraulic conductivity along the  $x$ -,  $y$ - and  $z$  directions, respectively;  $h$  (L) is the hydraulic head;  $W$  is the source and/or sink term ( $\text{T}^{-1}$ );  $S_s$  ( $\text{L}^{-1}$ ) is the specific storage of the porous material; and  $t$  (T) is time. Equation (2.1) is solved by MODFLOW (Harbaugh, 2005). The flow in conduits is turbulent, and the Darcy-Weisbach equation is used for calculating the hydraulic head (Shoemaker et al., 2007):

$$h_L = f \frac{\Delta l V^2}{d 2g} \quad (2.2)$$

where  $h_L$  is the head loss along the conduit length  $\Delta l$  (L);  $f$  is the friction factor (-);  $d$  is the conduit diameter (L);  $V$  is the average velocity ( $\text{LT}^{-1}$ ); and  $g$  is the gravitational acceleration constant ( $\text{LT}^{-2}$ ). Conduit network consists of discrete cylindrical tubes and nodes in the model. The nodes located in each MODFLOW cell compute the exchange between tubes and rock matrix. The flow exchange between the rock matrix and a conduit node is computed by the following equation:

$$Q_{ex} = \alpha_{i,j,k} (h_n - h_{i,j,k}) \quad (2.3)$$

where  $Q_{ex}$  is the volumetric exchange flow rate ( $\text{L}^3\text{T}^{-1}$ );  $\alpha_{i,j,k}$  is the pipe conductance at cell  $i, j, k$  ( $\text{L}^2\text{T}^{-1}$ );  $h_n$  is the head at the conduit node  $n$ ; and  $h_{i,j,k}$  is the head at the cell  $i, j, k$ .

### 2.2.2.3 The CMT3D modeling

CMT3D simulates the contaminant transport in both the rock matrix and conduits (Reimann et al., 2013a), and is an extension of MT3DMS (Zheng and Wang, 1999) which is a three-dimensional groundwater solute transport model. The nitrate transport in the rock matrix is modelled by:

$$\frac{\partial(\theta C_{NO_3})}{\partial t} = \frac{\partial}{\partial x_i} \left( \theta D_{ij} \frac{\partial C_{NO_3}}{\partial x_j} \right) - \frac{\partial}{\partial x_i} (\theta v_i C_{NO_3}) + q_s C_{sNO_3} + R \quad (2.4)$$

where  $\theta$  (-) is the porosity of the porous medium;  $C_{NO_3}$  (ML<sup>-3</sup>) is the nitrate-N concentration;  $t$  (T) is time;  $x_i$  (L) is the distance along the direction  $i$ ;  $D_{ij}$  (L<sup>2</sup>T<sup>-1</sup>) is the hydrodynamic dispersion coefficient;  $v_i$  (LT<sup>-1</sup>) is the linear pore water velocity;  $q_s$  (T<sup>-1</sup>) is the volumetric flow rate per unit volume of aquifer representing sources and sinks;  $C_{sNO_3}$  (ML<sup>-3</sup>) is the nitrate-N concentration of the source and sink flux; and  $R$  (ML<sup>-3</sup>T<sup>-1</sup>) is the chemical reaction term which is not considered in the simulation in this research. The porosity values for the surficial aquifer, intermediate semi-confining unit, and UFA are set to 0.25, 0.05, and 0.30, respectively (Phelps, 2004). The sorption of nitrate is assumed to be negligible due to its high mobility (Exner et al., 2014; Wei et al., 2018). In this study,  $C_{sNO_3}$  represents the nitrate-N concentration in groundwater recharge. The method for quantifying the spatial and temporal variability of  $C_{sNO_3}$  is described in the following section. The nitrate transport in conduits is modeled by advective transport module (Clark, 2009):

$$\frac{\partial C_j}{\partial t} = -v_j \frac{\partial C}{\partial x} + D \frac{\partial^2 C}{\partial x^2} \quad (2.5)$$

where  $C_j$  ( $\text{ML}^{-3}$ ) is the nitrate-N concentration in a conduit tube;  $v_j$  is the velocity ( $\text{LT}^{-1}$ ); and  $D$  ( $\text{L}^2\text{T}^{-1}$ ) is the dispersion coefficient. The dispersion and chemical reaction in conduits are not considered in this study due to the limited residence time.

#### 2.2.2.4 Conversion of EPM to CFPv2

The CFPv2 model was developed based on the EPM model and the model boundary conditions described above were retained in the CFPv2 model. The steady-state CFPv2 model was created by incorporating the pipes into the UFA (the third layer of the model) where karstic features are mostly distributed (Faulkner, 1973; Phelps, 2004). Since groundwater enters the system both through surface infiltration and direct injection of runoff into karstic conduits via sinkholes, locations of sinkholes provide an indication of conduit arrangement (Faulkner, 1973; Ghasemizadeh et al., 2012). As such, the locations of conduits were assigned according to the distribution of sinkholes (Figure 2). Specifically, the cells where high density of sinkholes around were replaced with CFPv2 pipes. The hydraulic conductivity values in these cells were in succession of lowering to the average hydraulic conductivity values of the surrounding matrix. This methodology was successfully used to set up conduits locations to model groundwater flow and nitrate transport in Woodville Karst Plain using CFPv2 and UMT3D models (Xu et al., 2015). A tracer study conducted by FDEP (2011) reported that there are no mature conduits in the upper portion of the springshed, therefore, conduits were assigned mostly in the central-west portion of

the domain although several sinkholes are also distributed in the upper portion (Figure 2). The steady-state model uses a single, one-day time step and long-term average recharge values. The transient model was created by updating the recharge data to cover the periods 2000-2016. Annual stress periods with a one-day time step were used.

#### 2.2.2.5 Nitrate-N concentration in groundwater recharge

Opportunities for improving model fidelity can be found in improved estimation of nitrate-N concentration in groundwater recharge, for which the observation data is usually not available. It has been reported that LULC (Appleyard, 1995; Robertson et al., 2000; Trojan et al., 2003; McMahon et al, 2008) and population density (Gardner and Vogel, 2005) affects the recharge nitrate-N concentrations. Nitrate-N concentration in groundwater recharge was estimated for each type of LULC, and the area change for each LULC type has been calculated as described in Section 2.1.2. The nitrate-N concentration in groundwater recharge was set to 4 mg/L for agricultural land and 0.12 mg/L for forested land (Phelps, 2004). For residential and transportation lands, the population density was used as the factor for estimating the spatial and temporal change of nitrate-N concentration in groundwater recharge. As population increases, the nitrate-N concentration from septic tanks and lawn fertilizer may also increase within a given residential area. Further, more impervious areas (i.e., transportation corridors) may be developed as a result of population growth, and more stormwater runoff from these areas are generated.

Figure 4d shows the linear relationship between population density in City of Ocala and observed nitrate-N concentration in spring discharge. In this study, the nitrate-N concentrations in groundwater recharge ( $C_{input}$ , [M/L<sup>3</sup>]) for urban and transportation lands were assumed to be linearly proportional to population density ( $P_d$  [pop./L<sup>2</sup>]):

$$C_{input} = kP_d - B \quad (2.6)$$

The slope  $k$  [M/L<sup>3</sup>] and the background concentration  $B$  [M/L<sup>3</sup>] were estimated during calibration of the transport model. Since the transport model is a cold start model (concentration of contaminant is simulated from zero at the beginning of the modeling period), the initial conditions were initialized by running the model from 1995 to 2000 with recharge nitrate-N concentration estimated using population densities from this respective period. During calibration, the simulated annual nitrate-N concentration was compared with its observed counterpart. The focus of this study is to analyze the potential for BMP in SRBs to mitigate nitrate at a given nitrate-N concentration in groundwater recharge as compared to the condition without BMP implementation. Simulation of nitrate-N concentration in groundwater recharge through time is outside the scope of this study. Further, after the implementation of spring restoration projects from 2015 described in Section 2.1.3, nitrogen loads at the land surface should be controlled. Therefore, it was assumed that nitrate-N concentrations in groundwater recharge for the years from 2017 were the same as that in 2016 till the implementation of BMP in 2021, assuming no changes in LULC and population density.

#### 2.2.2.6 Estimating dispersivity from a tracer test

A tracer test was conducted for estimating the dispersivity. Three types of tracer dyes with different emission wavelengths were injected into the three wells (Table 1 and Figure 7). These dyes are easily soluble and stable in water, have low toxicity, and are detectable at low concentrations.

The tracer test included tracer mixing, injection, flushing, and sampling. Permission to use the fire hydrants at each site was approved by the Customer Service Office of City of Ocala and the Utility Office of Marion County. On May 22, 2019, tracer dyes were mixed with water (1:1) from the fire hydrants. The mixed dyes were injected into the wells through a funnel, and 100 gal of hydrant water were injected into the wells for flushing. On May 23, 2019, 200 gal of water was injected into the wells for further flushing. After flushing the wells, tracer dyes were sampled at well-2, well-3, and Silver Springs (Figure 7) using the Sigma 900 Max Portable Sampler (Figure 8). During each sampling period, 24 samples were collected.

Table 1: The injection well and the amount of injected dye for each tracer type.

Tracer type	Injection Well	Amount of Injected Dye (pound)
Fluorescein dye	well-1	25
Eosin dye	well-2	30
Rhodamine WT	well-3	25



Figure 7: Injection and sampling sites for the tracer dyes.

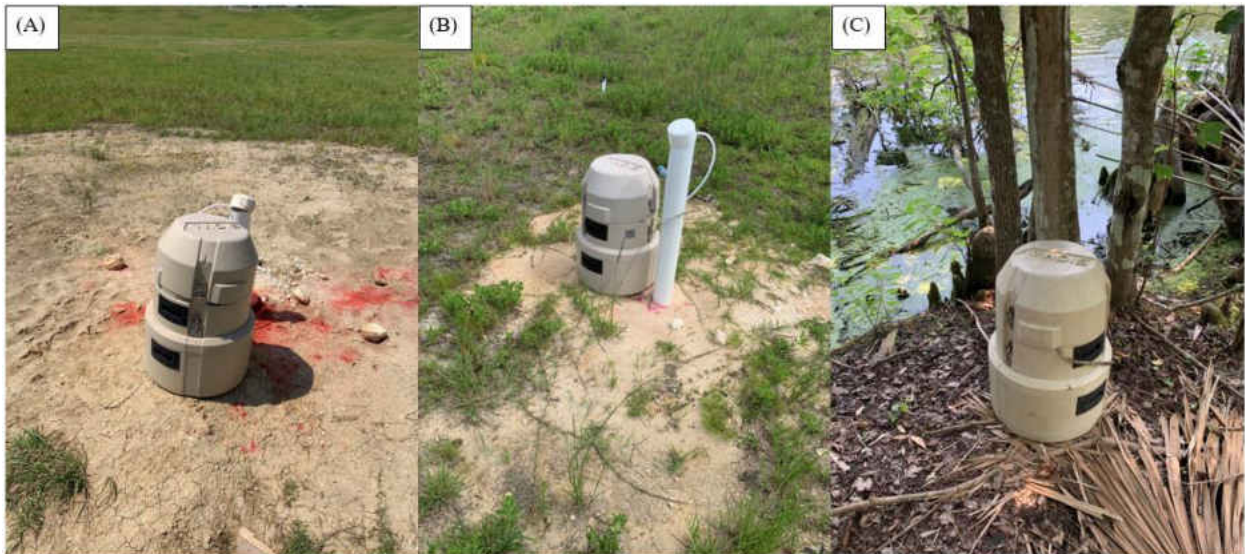


Figure 8: Tracer samplers at well-2 (A), well-3 (B), and Silver Springs (C).

The concentrations of fluorescein and RWT were measured by the AquaFluor handheld fluorometer using two different channels. The concentration of eosin was estimated by measuring the absorbance of eosin solutions using a RF 5000 spectrofluorophotometer. The wavelength of the spectrofluorophotometer was set to 519 nm with the maximum absorbance for eosin. The relationship between eosin concentration and absorbance at 519 nm was calibrated using eosin solutions with known concentrations in the lab (Figure 9). This linear relation will be used for estimating the eosin concentrations of tracer test samples based on the measured absorbance. Since a tracer test using RWT was conducted at Basin 9b in July 2017, the background concentration of RWT was measured as shown in Table 2. The low concentration of RWT indicates the effect of previous tracer test is negligible. The background concentration for the tracer test in this project is set to 0.023 ppb.

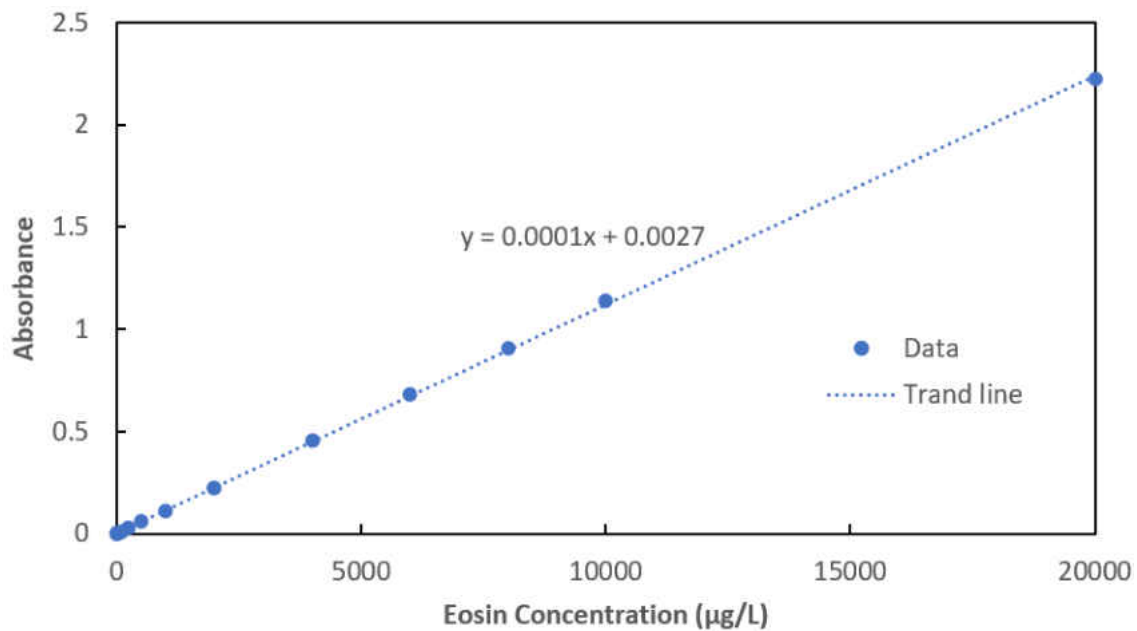


Figure 9: Calibration relationship between absorbance and concentration of eosin solution.



Table 2: Background concentrations of RWT at the sampling point in Silver Springs.

Date	Concentration (ppb)
Feb 15, 2019	0.018
Mar 29, 2019	0.059
Apr 30, 2019	0.023

RWT was detected in Silver Springs almost immediately, suggesting a subsurface travel time of less than 1 hour (Figure 10A). This indicates the existence of subsurface karst features. The breakthrough curve from 200 to 2400 hours (8 days to 3.5 months) after dye injection captured most of the RWT tracer mass. The small peaks following the main breakthrough curve suggest the complexity of flow paths in the karst aquifer. Fluorescein dye (injected upstream in well-1) was detected in well-2 after 144 hours (6 days). Fluorescein concentrations increased steadily and stabilized after 2000 hours (2.5 months) (Figure 10B). Fluorescein and eosin were never detected in Silver Springs or well-3, suggesting lack of an efficient karst network from well-2 to areas downstream.

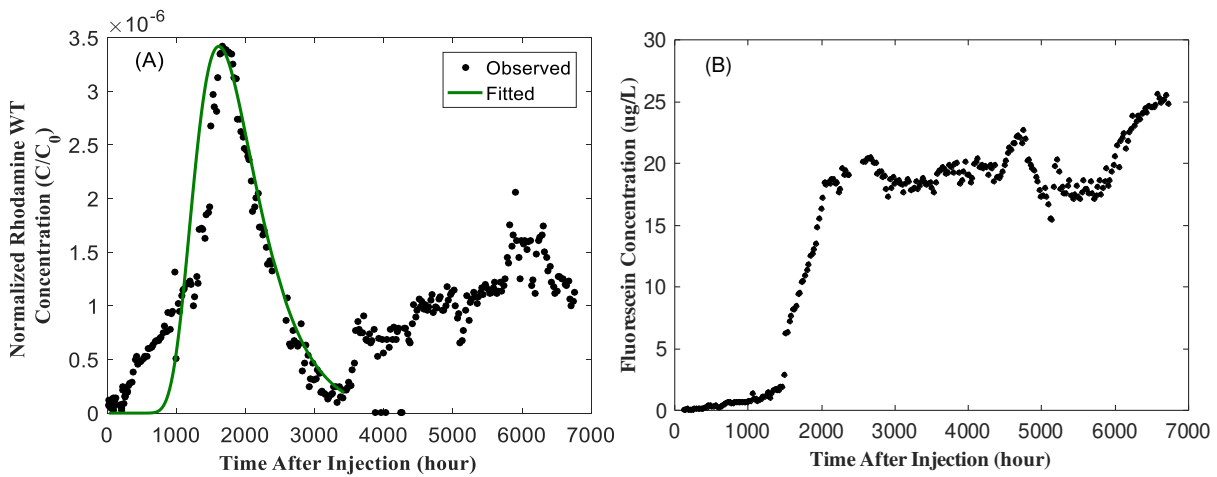


Figure 10: (A) Rhodamine WT concentration detected in Silver Springs with fitted curve based on the two-region non-equilibrium model; (B) Fluorescein dye concentration detected in well-2.

The two-region non-equilibrium model (Toride et al., 1999) is capable of reproducing the peak and skewness of the observed breakthrough curve (Figure 10A). The recovered tracer mass and mean tracer velocity were quantified as 10% and 0.0003 m/s using the QTRACER2 program (U.S. EPA, 2002). The relative low recovery is mainly caused by tracer loss in the rock matrix as well as delays in stagnant zones in the fractures and conduits, and the magnitude of mean velocity indicates limestone of geologic media (Freeze and Cherry, 1979). Longitudinal dispersivity yielded from the fitted breakthrough curve is 1.8 m, and the ratio of longitudinal to transverse dispersivity is set as 0.1. Both values are on the same magnitudes as previously reported ones in the UFA (Xiao et al., 2016; Reed et al., 2017).

### 2.2.3 Model calibration and validation

As shown in Figure 5, the calibration of the flow and nitrate transport model is achieved by conducting the following calibrations sequentially. Model calibration begin with hydraulic calibration of the steady-state model, recharge calibration of the transient model, then progressed to calibration of nitrate transport model. The hydraulic conductivity from the NFSEG model was further calibrated in the steady-state model based on the observed mean water levels in the monitoring wells (Figure 2) and the observed mean discharge of the Silver Springs during January 1<sup>st</sup>, 2000 -- December 31<sup>st</sup>, 2016. The conduit diameter ( $d$ ), tortuosity, and conductance ( $\alpha_{i,j,k}$ ) were calibrated in the steady-state CFPv2 model. The inter-annual variability of groundwater

recharge is estimated through the calibration of the transient CFPv2 model by taking the observed water levels in 13 monitoring wells (Figure 2) and the observed discharge of the Silver Springs as calibration targets. The variable annual recharge was calibrated by applying an adjustment factor to the recharge used in the steady-state model. The sources of groundwater recharge in the springshed include net precipitation (rainfall minus evapotranspiration), surface flow into sinkholes, irrigation on agricultural lands, and discharge from onsite sewage disposal system. Finally, the nitrate transport model (CMT3D) is calibrated and validated by matching the observed annual average nitrate-N concentration in spring discharge (Figure 4b). The two parameters in equation (2.6) are estimated during the calibration period (2000-2008), and the nitrate transport model is validated during 2009-2016.

#### 2.2.4 BAM-based blanket filter scenarios

BAM-based blanket filter, as a BMP, could be used to further reduce the nitrate-N concentration. BAM is a type of green sorption medium and made from a mixture of natural and recycled materials containing sand, clay, and tire crumb. The clay content in BAM helps to keep moisture within the medium for a longer time, which is essential for the survival of microbial community for denitrification (O'Reilly et al., 2014; Salamah, 2014). BAM requires relatively less area compared to other BMPs (Sirianuntapiboon et al., 2006). BAM was set up within a depth of 1.2 m in an SRB near the Silver Springs so that the blank filter is above the local

groundwater table (Figure 1). Such shallow blanket filter has been tested in the field, and the average nitrate decrease over seven rainfall events is 57% (Wen et al., 2019).

The calibrated and validated groundwater and nitrate transport model was utilized to assess the effectiveness of the BAM-based blanket filter on nitrate decrease by comparison with a baseline condition in which no blanket filter is implemented. A portion of nitrate in stormwater is removed by natural soil profile before stormwater recharges the groundwater. The spatial heterogeneity of soil removal efficiency for nitrate was considered in this study, and the results for an average removal efficiency of 74% are reported. Two BMP scenarios are considered in this study, both of which are assumed to be implemented in 2021. The first BMP scenario is to implement filter media in the twenty-six SRBs owned by the Florida Department of Transportation (FDOT); and the second scenario is to implement filter media in multiple SRBs located in Ocala, for a combined drainage area of half of the city area (Figure 11). The total drainage area of the twenty-six SRBs is 14.9 km<sup>2</sup>, which accounts for 0.64% of the springshed area. The drainage area for the second scenario is 111.9 km<sup>2</sup> and accounts for 9.6% of the springshed area. Assuming a 10-year longevity of BAM, the effects of BMP on nitrate decrease are assessed for the period of 2021--2030, during which the input nitrate-N concentrations are assumed to be constant. The recharge for this period is adopted from the period of 2001-2010.

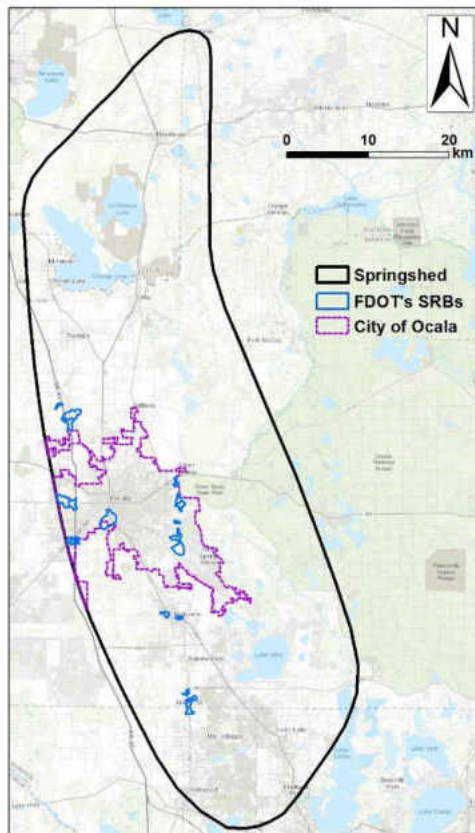


Figure 11: The twenty-six stormwater retention basins (SRB) owned by Florida Department of Transportation (FDOT) and the boundary of the City of Ocala.

## 2.3 Results

### 2.3.1 Groundwater flow

#### 2.3.1.1 Steady-state CFPv2 model

The calibrated conduit parameters from the steady-state CFPv2 flow model are shown in Table 3, and the index for each conduit is shown in Figure 2. The conduit diameter and conductance are estimated for each conduit. The calibrated values for conduit diameter range

from 1.5 m to 6.0 m. The diameters for conduits 1, 2, 6 and 7, which are the main conduits (Figure 2), are estimated as 6.0 m. The conduit 5 has a diameter of 1.5 m, which merges to conduit 2 (Figure 2). The vent diameter for Silver Spring has been reported to be 11 m (Sepúlveda, 2009; Ghosh et al., 2016); and the conduit diameter in the UFA has been reported as ranging from 3 m to 6 m (Xu et al., 2015). Higher conductance values are calibrated for some conduits (e.g., conduit 1, 2, 6, and 7 shown in Table 1). Hovorka et al. (1995) reported that the conductance for karst aquifer ranges from  $3 \times 10^{-6}$  to  $1.8 \text{ m}^2/\text{day}$ . The roughness height was assumed to be uniform over the 7 conduits, and the estimated value is 0.05 m. The range of tortuosity carbonate aquifers has been reported from 1 to 3.9 (Worthington, 2015; Assari and Mohammadi, 2017), and the tortuosity for each conduit in this study was estimated as 1.5.

The observed versus simulated average water levels during 2000-2016 in the monitoring wells (Figure 2) are shown in Figure 8a. The average root mean square error (RMSE) and relative error between simulated and observed water levels are 0.47 m and 2%, respectively. The relative error for the simulated mean spring discharge is 5%.

Table 3: The calibrated values of diameter, conductance, roughness height, tortuosity for each conduit.

Parameters	Conduit Index						
	1	2	3	4	5	6	7
Diameter (m)	6.0	6.0	3.0	3.0	1.5	6.0	6.0
Conductance ( $\text{m}^2/\text{day}$ )	0.45	0.45	0.30	0.30	0.20	0.45	0.45
Roughness height (m)	0.05						
Tortuosity	1.5						

### 2.3.1.2 Transient CFPv2 model

The range of the adjustment factor is 1-1.5 for dry years and 3-4.5 for wet years. Figure 12a shows the scatter plot of observed versus simulated water levels in the monitoring wells. The RMSE of simulated heads is 0.66 m (0.62 m) for the calibration (validation) period; and the relative errors are 4% for both the calibration and validation periods. Figure 12b shows the time series of simulated and observed annual spring discharge. The Nash-Sutcliffe efficiency (NSE) for simulated discharge is 0.93 (0.94) for the calibration (validation) period; and the relative error is 2% (3%) for the calibration (validation) period. These statistics indicate the good performance of the transient groundwater flow model.

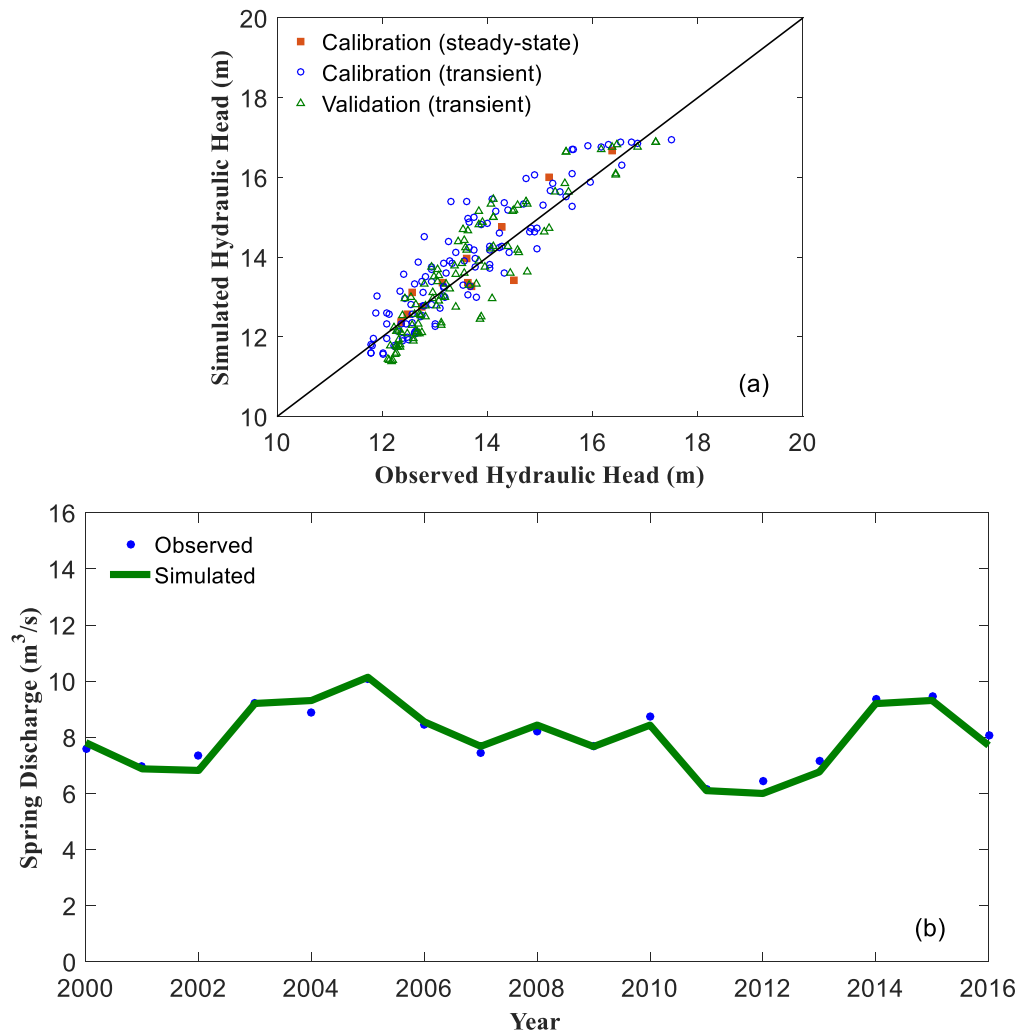


Figure 12: (a) The observed versus simulated hydraulic heads for the steady state and transient models; and (b) The observed and simulated discharge of Silver Springs.

### 2.3.2 Nitrate transport

The calibrated nitrate-N concentration in groundwater recharge for three types of LULC from 2000 to 2014 is shown in Figure 13. The nitrate-N concentrations in recharge for agricultural and forested lands are constants as described in Section 2.4. The slope ( $k$ ) and intercept ( $B$ ) in equation (2.6) are calibrated as  $7000 \text{ (mg/L)} \cdot (\text{km}^2/\text{people})$  and  $0.03 \text{ mg/L}$ ,



respectively. The natural background concentration of nitrate in 200 wells was smaller than 0.10 mg/L in the study by Panno et al. (2006). In Figure 4c, nitrate-N concentration was 0.04 mg/L in 1904 with population around 3,380 (USCB, 1995). Therefore, it is reasonable to consider the calibrated intercept as the background concentration of nitrate.

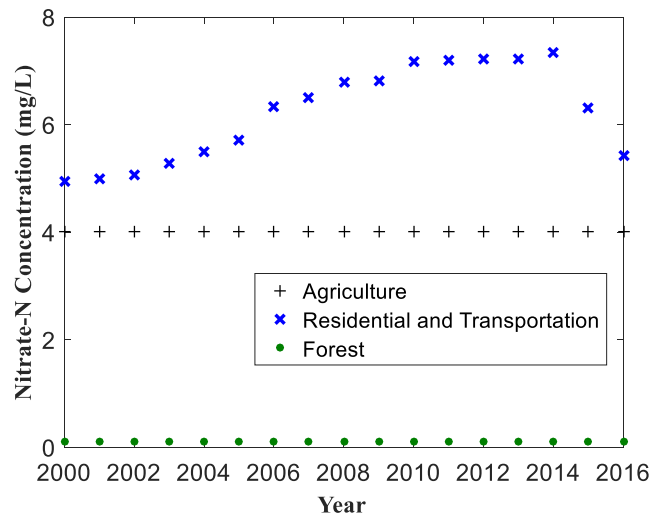


Figure 13: Estimated nitrate concentration in groundwater recharge for agricultural land, residential & transportation, and forest land.

Dispersivity in the transport model was estimated by a tracer test conducted in the field from May 2019 to November 2019 in the City of Ocala. The two-region non-equilibrium transport model in the program CXTFIT (Toride et al., 1999) was applied to analyze the tracer test dataset. The longitudinal dispersivity yielded from the data is 1.8 m, and the ratio of longitudinal to transverse dispersivity is set to 0.1. Both values are on the same magnitudes as previously reported ones in the UFA (Xiao et al., 2016; Reed et al., 2017).

Figure 14 shows the simulated and observed mean annual nitrate-N concentration in spring discharge during the calibration (2000-2008) and validation periods (2009-2016). The RMSE for

the calibration (validation) period is 0.06 mg/L (0.09 mg/L), and the relative error for the calibration (validation) period is 4% (5%). The difference between observed and simulated nitrate-N concentration (i.e., 2010) could be due to other factors than LULC and population density, such as the variation of fertilizer application rates (Harper, 2014). As shown in Figure 10, the nitrate-N concentration positively correlates with recharge and spring discharge. For example, the observed nitrate-N concentration reached to a high value at a peaked spring discharge (i.e., 2005) and decreased gradually as the discharge reduced (i.e., 2005-2007). Groundwater recharge during storm events strongly depends on hydrologic conditions and land use (Hem, 1985; Huebsch et al., 2014). Nitrate in the soil is accumulated to a high level prior to storm events in agricultural and urban lawn areas. Higher recharge in wet years mobilizes and transports more nitrate into the aquifer. Therefore, the nitrate in this system is transport-limited (instead of nitrate supply-limited), and the recharge rate has an enrichment effect on nitrate-N concentration. The relation between hydrologic conditions and concentration is similar as that reported in Duncan et al. (2017) and it shows the higher concentrations coupled with higher discharge values contributed to higher nitrate fluxes in the higher hydrologic conditions based on the observations of nitrate time series over multiple seasons.

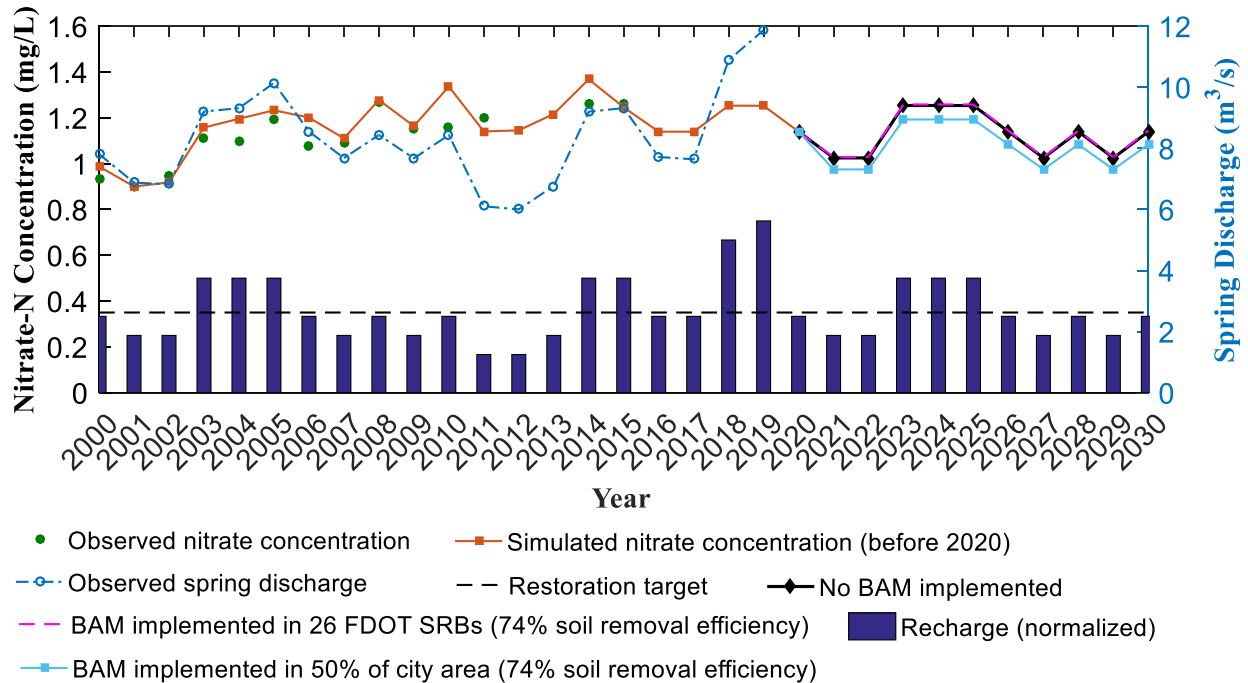


Figure 14: Projected effects of blanket filter on decrease of nitrate concentration in the discharge of Silver Springs when BAM implemented in twenty-six stormwater retention basins owned by Florida Department of Transportation (FDOT) and 50% of the drainage area in City of Ocala.

The implementation of spring restoration projects in 2015 and 2016 were included in the simulation by importing the nitrate decrease into CMT3D model and the annual nitrate showed a decline after 2015 besides the effect of variation of annual recharge. The nitrate-N concentration increased from 2016 to 2018 due to the increasing recharge, and then reduced to 1.14 mg/L in 2020, which is about 4 times of the restoration target (Figure 14).

### 2.3.3 Effects of BMP

The effects of two BMP scenarios on nitrate decrease in the spring discharge are shown in Figure 14. Considering the effect of restoration project (Section 2.1.2), the input nitrate-N

concentration in 2016 is used for the period of 2017-2020. The fluctuation of nitrate-N concentration during 2017-2020 and the projection period (2021-2030) is due to the inter-annual variation of recharge. For example, the nitrate-N concentration in a wet year (e.g., 2030) is higher than that in a dry year (e.g., 2029). In scenario 1, BAM-based blanket filters have almost no effect on decrease of the nitrate-N concentration in the spring discharge in a normal year (e.g., 2026) compared to that in 2020 (without BAM implemented). This is due to the limited drainage area which only accounts for 0.64% of the springshed area and small amount of stormwater treated by BAM-based blanket filters in the 26 FDOT SRBs. The BMP investigated in this study involves the removal and replacement of part of the soil profile with BAM media. Whether BAM BMP lead to net water quality improvements or degradation depends on whether BAM removes more or less nitrate from stormwater than the unaltered soil profile. Therefore, the slight effect of this scenario is also probably caused by the very small performance difference between the nitrate removal of BAM (57%) and unaltered soil (74%). In scenario 2, the nitrate-N concentration will be reduced to 1.08 mg/L in 2026 (i.e., a 10.7% decrease relative to the baseline condition). Moreover, the nitrate-N concentration will be 1.19 mg/L in the wet year of 2023 and 0.97 mg/L in the dry year of 2029. The nitrate-N concentration in spring discharge will have quick responses to the BAM-based blanket filters. For example, from a dry year (2022) to a wet year (2023), nitrate-N concentration will increase without a delay. Similarly, due to the insufficient recharge, a quick and continuous decline on nitrate-N concentration will occur over

the period from 2025 to 2027. These quick responses are resulted from the flow and nitrate transport in conduits (Huebsch et al., 2014). As shown in Figure 11, most of the BAM-implementation areas are located at the central springshed where subsurface medium has been maturely karstified (Faulkner, 1973). A large proportion of attenuated nitrate filtered in the top soil and BAM layers of the blanket filters may mobilize into conduits from the surrounding rock matrix or from blanket filters directly. However, treated nitrate in the rock matrix can hardly change nitrate-N concentrations within groundwater storage, given the large volume (Peterson et al., 2002). Hence, the proportion of treated nitrate in conduits may dominate the fluctuations of the nitrate-N concentration in the aquifer. Lack of denitrification capacity leads to few nitrate decrease occurring in conduits, and the nitrate-N concentration in the aquifer does not continue to decline before it reaches the springs. The quantitative analysis of nitrate in conduits is discussed in the following section.

The modeling study indicates that BAM BMP benefit is likely to scale with penetration (i.e. greater water quality benefits can be expected with greater BMP implementation). However, this study suggests that even the maximum expected benefits may be nominal. The greatest possible net improvement (scenario 2) was achieved assuming BAM-based blanket filters were installed in multiple FDOT SRBs, which will be a great investment for water resources management. Other restoration measures are necessary to meet the restoration target (0.35 mg/L). For example, considering that nitrate from agricultural lands accounts for a large proportion of pollution in

groundwater, other BMPs on or near agricultural lands could be implemented for further nitrate removal.

## 2.4 Discussions

### 2.4.1 Effects of conduits on flow and nitrate transport

The conduit network in the springshed plays an important role on the groundwater's flow path and by association, the nitrate transport. Using the conduit network shown in Figure 2 for model calibration, it was estimated that 48% of spring discharge and 47% of nitrate mass is transported through the conduits for the validation period. It is expected that a higher percentage of groundwater discharge and nitrate would be transported through the conduit network in wet years. For instance, when considering just 2019, a wet year, the percentage of spring discharge (and nitrate) through conduits is 51% (and 61%). As shown in Figure 15, the percentage of flow and nitrate contributed from conduits increase with recharge. A positive trend line fit to the data with an  $R^2$  value of 0.61 for flow and 0.79 for nitrate indicates the increasing contribution of conduit flow and transport for wet years and high flow springsheds. In the wet years with higher recharge, the hydraulic head in the matrix is higher, which induces more flow into the conduits from the matrix.

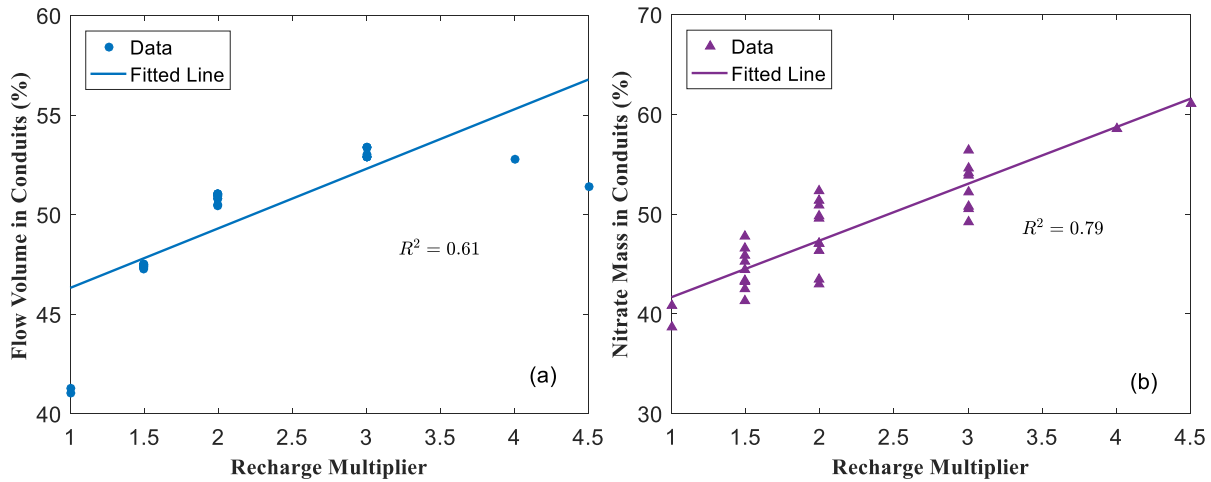


Figure 15: The control of recharge on the percentage of flow volume (a) and nitrate mass (b) in conduits.

#### 2.4.2 Sensitivity analysis

The sensitivity of spring discharge to model parameters was evaluated for assessing the discharge uncertainty in the model characterization. Sensitivity simulations were conducted by increasing and decreasing the calibrated conduit parameters by 25%, 50%, and 75%. Figure 16a shows the sensitivity of spring discharge averaged over the 2000-2016 period to changes in selected parameters: conduit diameter, conductance, and roughness height. The spring discharge is most sensitive to conduit diameter, shown in Figure 16a. Specifically, if the conduit diameter were increased by 25%, spring discharge would be increased by 25%. If conduit conductance were to increase by 25%, spring discharge would only be increased by 7%. The spring discharge is least sensitive to the conduit roughness height, showing just a 2% decrease in spring discharge when roughness height was increased by 25%. The conduit diameter is the most important

parameter among the three due to its strong relationship with the average velocity. Theoretically, higher conduit diameter and conductance mean higher drainage capacity of matrix and conduit network. Therefore, the parameter sets of the conduit network play important roles on the variation of spring discharge.

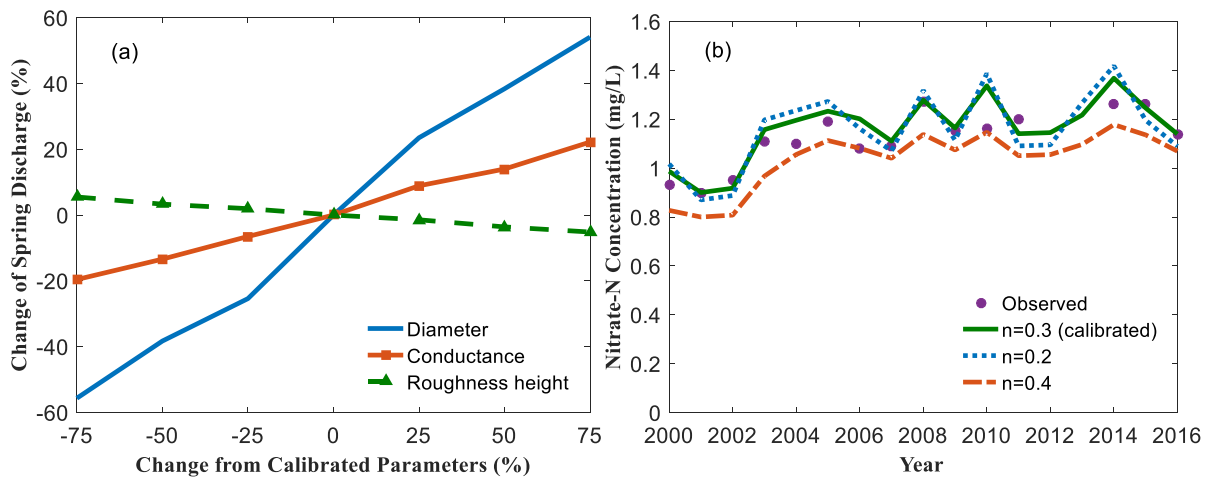


Figure 16: (a) Sensitivity of spring discharge to diameter, conductance, and roughness height of conduits. (b) Sensitivity of nitrate-N concentration in spring discharge to effective porosity (n).

The impact of aquifer properties on nitrate presence in spring discharge was assessed by performing a sensitivity analysis on the effective porosity. Figure 16b shows simulated nitrate-N concentrations in spring discharge with effective porosities of the UFA ranging from 0.2 to 0.4, as compared to the calibrated value (0.3). Higher effective porosities of the UFA results in lower nitrate concentrations present in spring discharge. Aquifers with lower effective porosities, tends to show nitrate transport being more sensitive to the recharge variation (Ho and Webb., 1998).



## 2.5 Summary

In this study, a coupled CFPv2 and CMT3D model was applied to discover the effect of a BAM-based stormwater BMP on nitrate removal in the discharge of Silver Springs. Given the nitrate removal efficiency of BAM-based blanket filter and soil tested by field experiments, the net effect of BMP on nitrate removal in karst area was evaluated using the coupled model. Modeling results show that the nitrate-N concentration present in karst springsheds is higher in wetter years with higher recharge. Therefore, the inter-annual variation of nitrate concentration is controlled by the hydrologic condition. For the scenario of implementation of 26 SRBs having a combined drainage area of 14.9 km<sup>2</sup> with a 74% of soil removal efficiency, the decrease of nitrate in spring discharge will be less than 1%. When considering the more aggressive scenario, implementation of multiple BMPs with a combined drainage area of 111.9 km<sup>2</sup>, the nitrate-N concentration in spring discharge will be reduced by 10.7% for a normal recharge year and can decline to up to 0.97 mg/L for a dry year.

The BMP investigated involves the removal and replacement of part of the soil profile with BAM media. Therefore, whether BAM-based BMP leads to net water quality improvements or degradation depends on whether BAM removes more or less nutrients from stormwater than the unaltered soil profile. In some places, replacing the soil profile with BAM will lead to greater transformation and removal of nutrients; in other cases the natural remediation of the unaltered soil profile will exceed that of BAM. The spatial heterogeneity of soil nutrient remediation

properties introduces considerable uncertainty to the potential cumulative water quality improvements offered by BAM-based BMP. Therefore, managers' most pressing concern is: how to differentiate between soils that will benefit from BAM replacement and those which will not? This requires addressing a critical knowledge gap regarding the relative nutrient remediation potential of BAM versus soils of variable properties. This knowledge gap should be resolved before large-scale investments are made to implementing BAM-based BMP. When this is accomplished, a modelling study in this research may assess the potential cumulative effects of BAM-based BMP with greater precision. The uncertainty in soil heterogeneity can be resolved, but only after achieving greater understanding of nutrient transformations within soils of variable properties and then understanding how those variable soils are distributed spatially. These two pieces of information are also critically needed to assist managers in making cost-effective decisions regarding BMP implementation.

Conduit networks play an important role in groundwater flow and nitrate transport; in the Silver Springs springshed, an average percentage of mass transport from conduits is 48% for water and 47% for nitrate. Moreover, the linear relationship between recharge and flow (nitrate) contribution of conduits indicate that higher percentages of flow and nitrate are transported through conduits to the spring outlets in wetter years.

This study is the first regional scale application of the numerical model to evaluate the effect of BMP nitrate removal in karst springsheds, providing a useful tool for water resources

managers. The input nitrate-N concentration is simply assumed as a function of land use and land cover change and population density. Future analysis could focus on 1) including more factors to quantify the input nitrate concentration, and 2) determining the location and treatment scale of blanket filter based on this regional-scale modeling of BMP implementation. A comprehensive restoration plan is recommended to achieve the restoration goal for Silver Springs that considers both decrease of nitrate sources (e.g., fertilizer run-off and septic tank leakage) and implementation of different BMP technologies.

## **CHAPTER 3 EVALUATING PHYSICAL CONTROLS ON GROUNDWATER FLOW IN KARST CONDUIT NETWORK**

### 3.1 Introduction

Karst aquifers, which are widely distributed around the world and provide the water resources for about one quarter of the global population, display considerable complexity due to the large contrast in physical parameters within the coupled conduit-matrix system (Ford and Williams, 2007; Giese et al, 2018). The strongly heterogeneous distributions of porosity, hydraulic parameters of conduit, fissures, and the porous matrix control groundwater flow paths thus having groundwater fluxes varied by several orders of magnitude from local to catchment scale (Halihan et al., 2000; Kiraly, 2002). For example, slow laminar may occur through the matrix and second porosity such as fractures (Shuster and White, 1971), while fast turbulent flow may occur through conduits (Worthington, 1999). The highly permeable karst conduits, draining the fractures and matrix, are the most important hydraulic features adding a fast flow component to the groundwater discharge (Quinlan and Ewers, 1985; Marechal et al., 2008), and numerical modeling of karst aquifers also has demonstrated that conduits may comprise a large proportion of spring discharge, with increasing effective transmissivity or hydraulic conductivity as the spring outlet is approached, suggesting the convergence of groundwater flow in a network of high-permeability conduits (Liedl et al., 2003; De Rooij et al., 2013).

Therefore, much importance has been placed on the investigation of conduit flow in karst aquifers (Worthington, 2009, 2015) and numerous studies on the influence of variable of conduit properties on groundwater flow in karst conduits have been published. For example, Peterson and Wicks (2006) quoted that slight changes of roughness significantly affect the simulated spring discharge as well as solute transport. Gallegos et al. (2013) argues an insensitivity of relative roughness height with respect to hydraulic head, spring discharge, and residence time for a well-developed karst aquifer. Chang et al. (2015) analyzes the effects of diameter of conduit and recharge events in laminar and turbulent conditions on spring hydrograph, and concludes that the turbulent conduit influences the early recession curve and the influence decreases with the spring discharge or rainfall intensity. Under turbulent and laminar flow, influence of hydraulic properties of conduit system on drawdown in conduit is also studied by Giese et al. (2018) which solves the question to which extent different conduit flow regimes will affect the drawdown in conduit and matrix depending on the hydraulic properties of the conduit system. Additionally, regards to conduit geometry and distributions, Ronayne (2013) and Yang et al. (2019) evaluates their influences on solute transport and spring discharge in karst aquifers using numerical and analytical approaches, respectively. The studies thus far have focused on the effects of conduit properties on flow and transport in karst systems either conceptually or numerically, or just applicable to specific regions; however, to our knowledge, literatures provide few researches about the controls which are independent of the magnitude of the physical parameters on the conduit

flow under laminar and turbulent conditions in karst aquifers. Understanding the physical controls on conduit flow is critical for effective management and protection of karst water resources. For example, the concentration of nitrate has been steadily increasing over the last 30 years in many Florida's karst springs (Katz et al., 2009; Heffernan et al., 2010). In order to protect and manage spring water from pollutants, it is essential to understand the responses of spring discharge to physical controls of conduit and natural stresses (e.g., recharge).

The objectives of this study are therefore to evaluate the physical controls on the contributions of conduit(s) to spring discharge ( $Q_c/Q$ ,  $Q_c$  and  $Q$  are flow in the conduit(s) and the spring discharge [ $L^3$ ]). The specific research questions addressed in this study include (1) How do the physical controls on the contribution of single conduit and conduit network to spring discharge under laminar and turbulent conditions, respectively? (2) Can the evaluations on the physical controls help estimate the groundwater discharge in regional scale karst aquifers? In this study, in addition to recharge, conduit density and geometry, firstly we employed three dimensionless physical factors to evaluate their controls on the contributions of single conduit and conduit network to spring discharge under laminar and turbulent conditions. To this end, four simple models with different conduit networks are developed using MODFLOW-CFP model to simulate the groundwater flow in karst conduits. The second focus is to validate whether the evaluations of physical controls on conduit flow can be applicable to the estimation of groundwater discharge for regional karst aquifers. In this context, a regional scale model for Silver Springs

springshed in Florida, USA is developed in this study. The modeling results, as well as the results from a regional karst model in a previous study are compared with the evaluation results of physical controls on conduit flow.

The study is organized as follows: section 3.2 briefly describes the mechanisms governing the flow in conduit(s) and rock matrix, model configuration, and parameter settings used in the evaluation. In section 3.3, the evaluation results of controls on the contributions of single conduit and conduit network to spring discharge are presented. A region scale model developed for Silver Springs springshed and the discussion between the results from regional scale models and evaluations are described in section 3.4. Finally, conclusions are shown in section 3.5.

## 3.2 Methodology

### 3.2.1 Mechanisms governing the flow in a single-conduit karst aquifer

Flow regime in a continuum medium or a pipe (conduit) has been deeply studied, respectively (Bear, 1972; Jeppson, 1976). It's reasonable to consider a karst aquifer is a hybrid system which is composed of a continuum medium (matrix) embedded by a conduit or a pipe. Groundwater flow in a matrix is laminar whereas both laminar and turbulent flow can be occurred in the conduit. For karst systems with a permeable matrix, evaluation of controls on the contribution of conduit to spring discharge must consider both conduit and matrix flow. In the matrix, groundwater flow is governed by a partial-differential equation based on Darcy's law and

mass conservation (Harbaugh, 2005):

$$\frac{\partial}{\partial x} \left( K_x \frac{\partial h}{\partial x} \right) + \frac{\partial}{\partial y} \left( K_y \frac{\partial h}{\partial y} \right) + \frac{\partial}{\partial z} \left( K_z \frac{\partial h}{\partial z} \right) = S_s \frac{\partial h}{\partial t} - W \quad (3.1)$$

where  $K_x$ ,  $K_y$ , and  $K_z$  ( $\text{LT}^{-1}$ ) are the hydraulic conductivity along the  $x$ -,  $y$ - and  $z$  directions, respectively;  $h$  (L) is the hydraulic head;  $W$  is the source and/or sink term ( $\text{T}^{-1}$ );  $S_s$  ( $\text{L}^{-1}$ ) is the specific storage of the porous material; and  $t$  (T) is time.

Similar to be applied in the urban pipe flow area, the Hagen-Poiseuille equation is also used to govern the laminar flow ( $R_e < 2300$ ) in the conduit in the hybrid system (Liedl et al., 2003):

$$Q_c = -\frac{\pi g d^4}{128 \nu} I \quad (3.2)$$

where  $Q_c$  is the flow in the conduit [ $\text{L}^3\text{T}^{-1}$ ],  $d$  is the conduit diameter [L],  $\nu$  is the kinematic viscosity of groundwater [ $\text{L}^2\text{T}^{-1}$ ],  $g$  is the gravitational acceleration constant [ $\text{LT}^{-2}$ ], and  $I$  is the hydraulic gradient in the conduit.

On the other hand, when flow in the conduit is turbulent ( $R_e > 4000$ ; Liedl et al., 2003), two distinct flow regimes may occur in the hybrid system including laminar flow in the matrix. Turbulent flow in the conduit in the hybrid system is described based on the Darcy-Weisbach equation and the Colebrook-White equation which is also widely used in the urban pipe flow area:

$$Q_c = -2A \log \left( \frac{\varepsilon}{3.71d} + \frac{2.51\nu}{d\sqrt{2gdI}} \right) \sqrt{2gdI} \quad (3.3)$$

where  $\varepsilon$  is the mean roughness height of the conduit wall micro-morphology [L].

Further, in the hybrid system, groundwater flow can be exchanged between the matrix



and conduit through their boundary depending on the head differences in the two mediums (Bauer and Liedl, 2003). The exchange flux ( $Q_{ex}$ ) it is governed by a linear steady state exchange term (Shoemaker at al., 2007):

$$Q_{ex} = \alpha_{ex}(h_c - h) \quad (3.4)$$

where  $h_c$  is the hydraulic head in the conduit [L];  $\alpha_{ex}$  is the exchange coefficient [ $L^2T^{-1}$ ] and it is a lump parameter which depends on the conduit wall hydraulic conductivity, conduit size and geometry, and local flow system geometry (Shoemaker at al., 2007; Chang et al., 2015). When flow in the matrix and conduit are both laminar, the flow regime in the conduit can be deemed to merge into the matrix thus leading the hybrid system to a continuum medium. Consequently, the parameter  $\alpha_{ex}$  is lumped into the hydraulic conductivity of this continuum and equation (3.1) is therefore similar to the equation  $Q = KIA$  in which  $K$  can be treated as  $\alpha_{ex}$ . On the contrast, when flow in the conduit is transferred from laminar to turbulent, the flow regimes in the conduit and matrix are quite distinct from each other. The system is consequently evolved from a continuum medium to a hybrid system.

### 3.2.2 Mechanisms governing the flow in conduit network

The mechanisms governing the flow in conduit network are similar to the case for single conduit described above. To study the physical controls, especially conduit density and geometry on the contribution of networks to spring discharge, karst aquifers with different conduit networks

are employed, which are explained in the following sections.

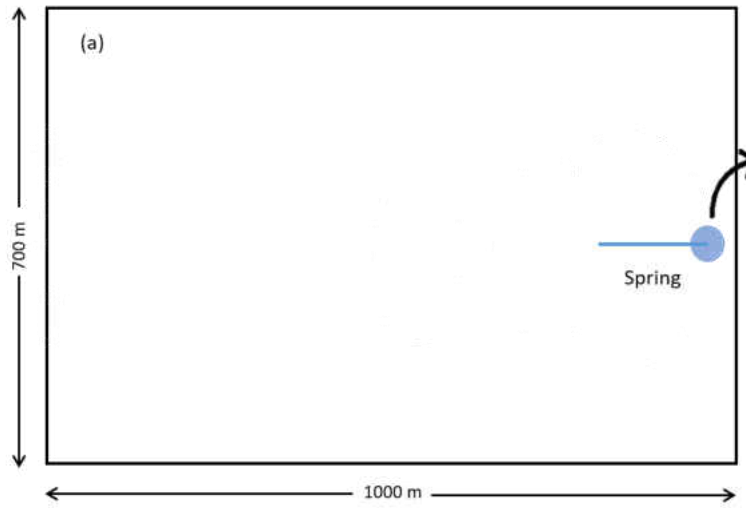
### 3.2.3 Evaluation methods

#### 3.2.3.1 Simulation tool

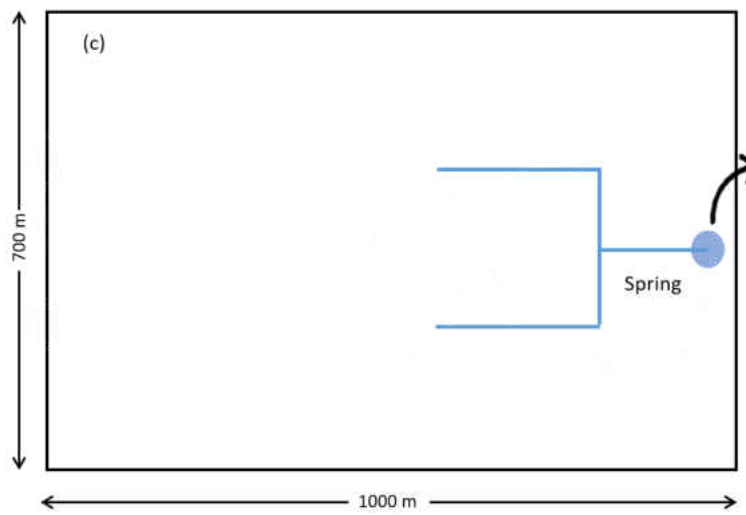
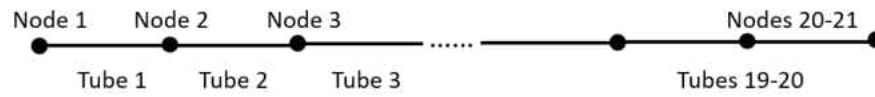
The MODFLOW-CFP is employed to simulate laminar and turbulent conduit flow in this study. This model could simulate groundwater flow in a hybrid system by coupling Darcy groundwater flow equation in continuum porous medium with discrete network of cylindrical pipes (Shoemaker et al., 2007).

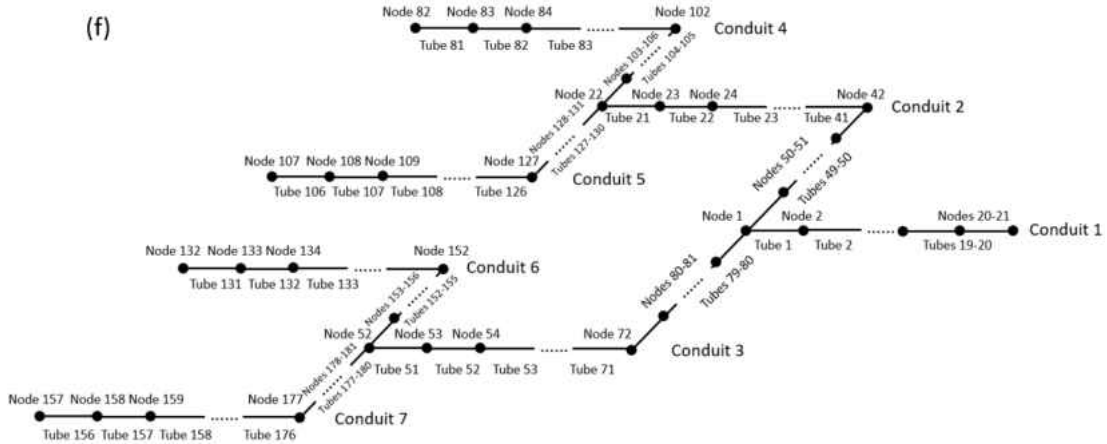
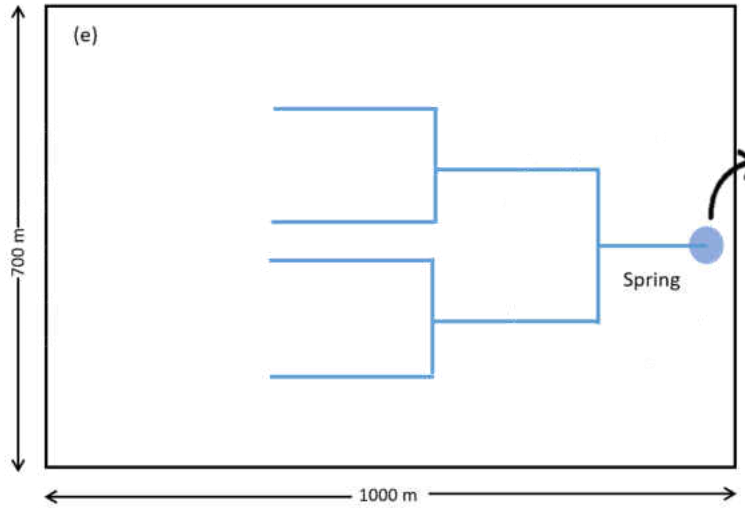
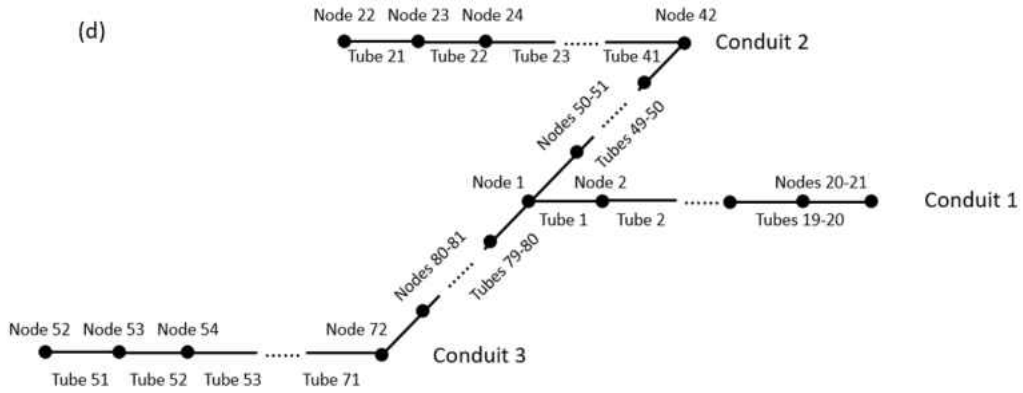
#### 3.2.3.2 Model configurations

The structures of conduit network in karst aquifers are usually complex and challenging to characterize. In this study, one single-conduit aquifer (Figure 17a, 17b) and three aquifers with different conduit networks which have three conduits (Figure 17c, 17d), and seven conduits with different geometries (Figure 17e-17h) are considered. Both single conduit and conduit networks are surrounded by low permeability matrix, and controls on the contribution of single conduit and conduit networks to spring discharge in laminar and turbulent conditions are respectively evaluated.



(b)





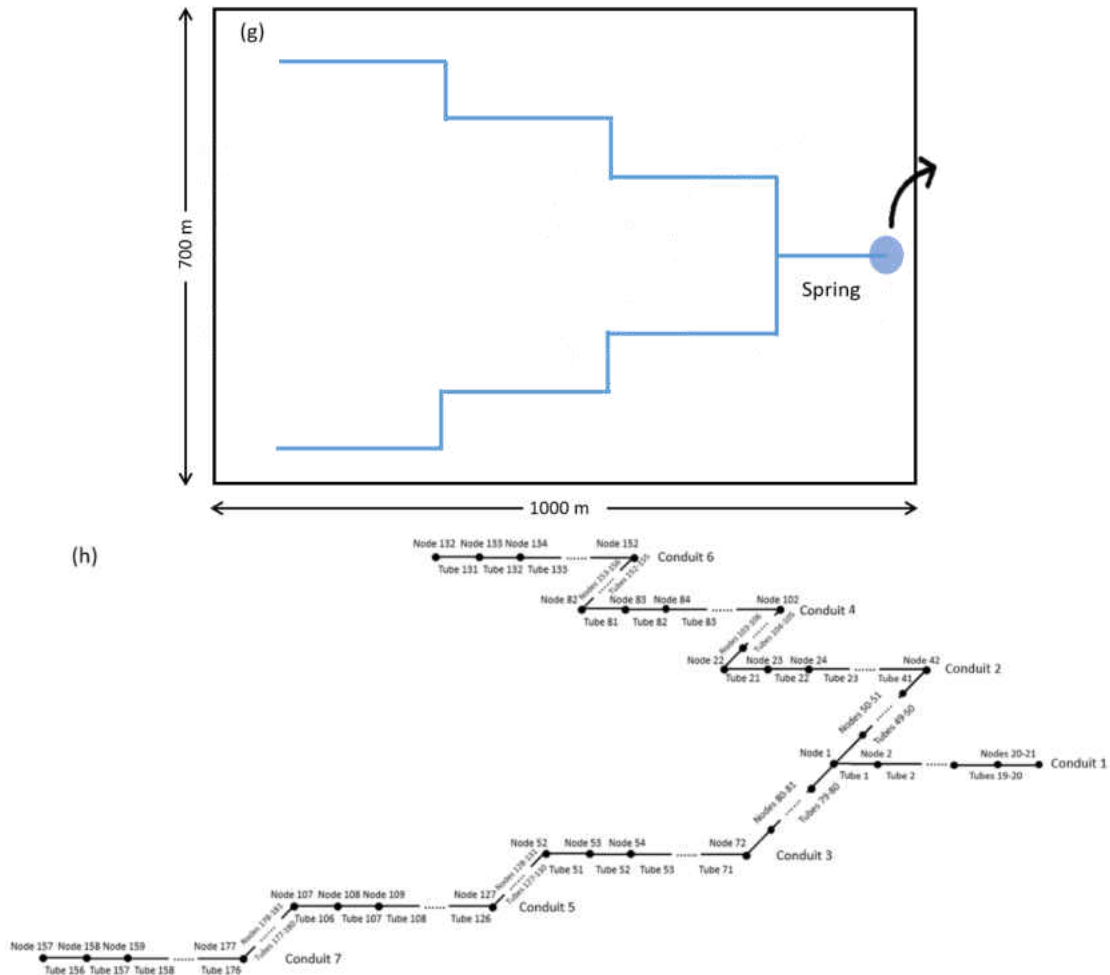


Figure 17: Model configuration for karst aquifers with single conduit (a), three-conduit network (c), two seven-conduit networks (e) and (g). The numbers of nodes and tubes for one-conduit (b), three-conduit network (d), and seven-conduit networks (f) and (h).

The matrix for each aquifer is 1000 m long and 700 m width, and the width of both columns and rows is set to 10 m for each cell (Figure 17). Each model consists of one layer and the thickness of the aquifer is 200 m with the elevation of aquifer bottom set as 0 m. Neumann type (no flow) boundaries are set around the matrix. For the aquifer with single conduit, the conduit is located in the middle of the matrix (36<sup>th</sup> row) with 200 m long and is also discretized in 10 m long tubes (Figure 17b). The aquifers with conduit networks were developed based on the

single-conduit aquifer, and the conduit geometries are shown in Figure 17c, 17e, and 17g. In particular, although the aquifers shown in Figure 17e and 17g own different conduit geometries, conduit densities between them are identical. There are, take the single-conduit aquifer as an instance, 21 conduits nodes and 20 tubes with their numbers increasing successively from left to right (Figure 17b). The end of conduit is set to a constant head boundary to represent a spring. To investigate the control on the contribution of single conduit and conduit network to spring discharge from the diffuse recharge, the precipitation was set to only recharge the matrix in the model and none of conduit nodes receive the recharge. The setting described herein represents simple karst aquifers without allogenic or point recharge on the conduit(s) and the matrix receives the precipitation and then is dewatered by the conduit(s) to the right spring. The simulations for the model are all steady state.

### 3.2.3.3 Parameter settings

The matrix for each aquifer is assumed to be a homogeneous media with 0.03 m/d for hydraulic conductivity. The fixed head of the spring at right-hand side of the conduit(s) is set to 31 m (Figure 17a, 17c, 17e, 17g). The conduit node height is set to 20 m. The groundwater temperature in the conduit is set to 20 °C. Besides recharge ( $R$ ), conduit density ( $Cd$ , *conduit length/area of aquifer*,  $[L^{-1}]$ ), conduit geometry, three dimensionless factors are used for the evaluations to keep them be independent of the magnitude of the physical parameters

(e.g.,  $\varepsilon$ ,  $D$ ,  $K_c$ , etc.) (Bourdet, 2001):  $\varepsilon/D$ ,  $K_c/K$  ( $K_c = \alpha_{ex}/\text{cell size}$ ), and  $R_e$  (Reynolds number, the ratio of inertial forces versus viscous forces). Specifically,  $\varepsilon/D$ , relative roughness, represents the controlling effects of conduit roughness.  $K_c/K$  represents the conduit-matrix hydraulic conductivity contrast. Ranges of conduit properties values are employed in the evaluation. For example, exchange coefficient ( $\alpha_{ex}$ ) are ranged from  $1 \times 10^{-6}$  m<sup>2</sup>/day - 1 m<sup>2</sup>/day (Hovorka et al., 1995), conduit diameter ( $D$ ) 0.1 m – 5 m (Sullivan et al., 2019), and roughness height ( $\varepsilon$ )  $1 \times 10^{-9}$  m – 0.99 m. Each of the controlling factor will be investigated regarding the influence on the contribution of sing conduit and conduit network to spring discharge ( $Q_c/Q$ ) under laminar and turbulent conditions.

### 3.3 Evaluation results

#### 3.3.1 Controls on the contribution of single conduit to spring discharge

For the condition that conduit flow is laminar, the evaluation results for controls of  $K_c/K$  on  $Q_c/Q$  is shown in Figure 18a. First, the seven curves representing different values of  $\varepsilon/D$  are virtually congruent. Therefore, the impact of changes in  $\varepsilon/D$  on  $Q_c/Q$  is insignificant. Second,  $Q_c/Q$  increases with increasing  $K_c/K$  for each  $\varepsilon/D$ . When hydraulic conductivity of conduit wall increases but still remains a very low value compared to that of matrix (e.g., lower than  $3.3 \times 10^{-4}$ ), groundwater flow is dominated by the matrix so that a small proportion of groundwater (e.g., lower than 5%) could flow into the conduit from surrounding matrix. It can

be also observed in Figure 19a, in which most of the groundwater flows directly into the spring from the matrix and there are insignificant changes in contours of hydraulic head when  $K_c/K$  is smaller than  $3.3 \times 10^{-4}$ . Correspondingly, conduit flow is insensitive to the low  $K_c/K$ . On the other hand,  $Q_c/Q$  increases dramatically from 5% to 80% as  $K_c/K$  increases from  $3.3 \times 10^{-4}$  to 0.033. The results are reasonable because as  $K_c/K$  increases, more groundwater could flow into the conduit instead of moving along its original direction in the matrix. This finding is also supported by Figure 19a, in which the contour lines of hydraulic head are gradually converged to the conduit when  $K_c/K$  is larger than  $3.3 \times 10^{-4}$ , indicative of increasing proportion of groundwater could flow into the conduit other than into the spring directly from the matrix. When hydraulic conductivity of conduit wall is much higher and even overwhelms that of the surrounding matrix (e.g.,  $K_c/K$  beyond 0.033),  $K_c/K$  reaches the maximum where the conduit could deliver 95% of groundwater to the spring. Meanwhile, increase of  $Q_c/Q$  turns into a slower rate again as shown in Figure 18a. This is because as more groundwater flows to the outlet carried by the conduit, spring discharge is nearing saturated resulting from the recharge is specified and the mass conservation. Thus, although more groundwater could flow into the conduit as  $K_c/K$  increases, the difference in  $Q_c/Q$  will not be remarkable. It also indicates that conduit flow is insensitive to the situation where  $K_c/K$  is very high, which is similar as the situation where  $K_c/K$  is less than  $3.3 \times 10^{-4}$ . Results shown in Figure 19a also assist in these points, where contours of hydraulic head around the conduit are almost parallel to it and there are



no obvious changes in terms of contours when  $K_c/K$  is larger than 0.033. These results imply that instead of the controls of  $K_c/K$  on  $Q_c/Q$  is monotonous ascending or decreasing, there are two threshold values of  $Q_c/Q$  existed at the extremes of  $K_c/K$ .

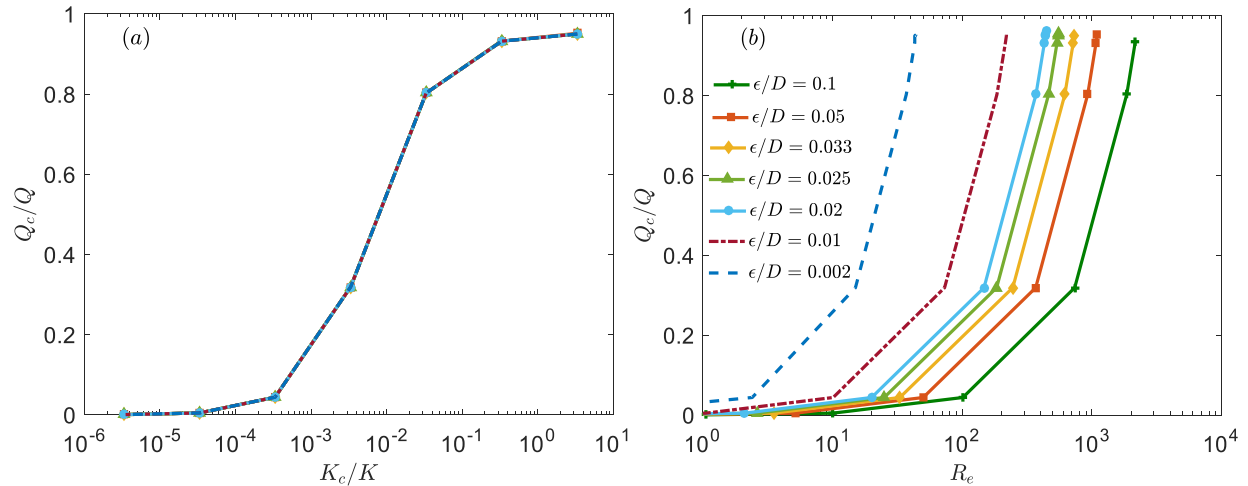
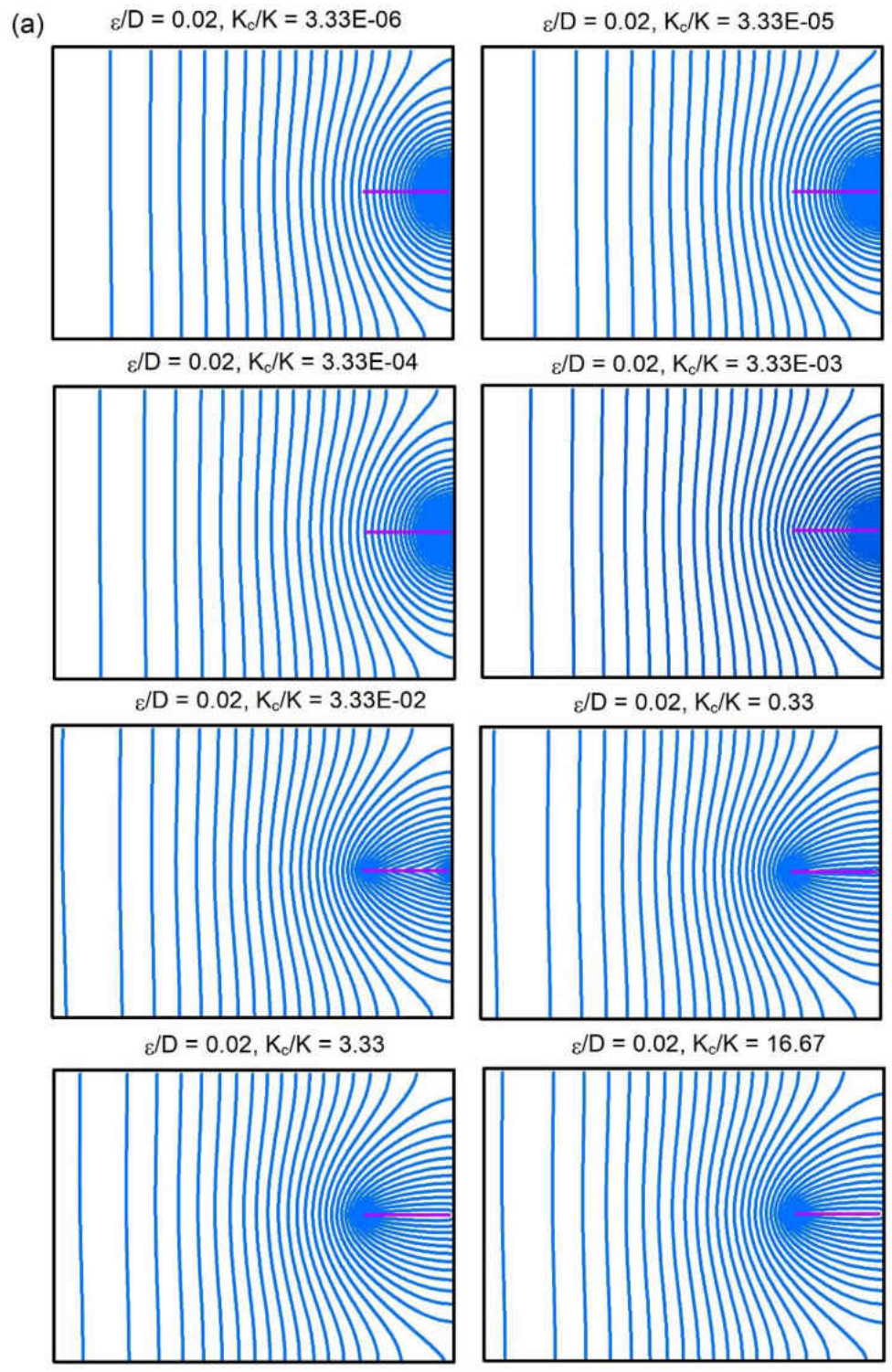
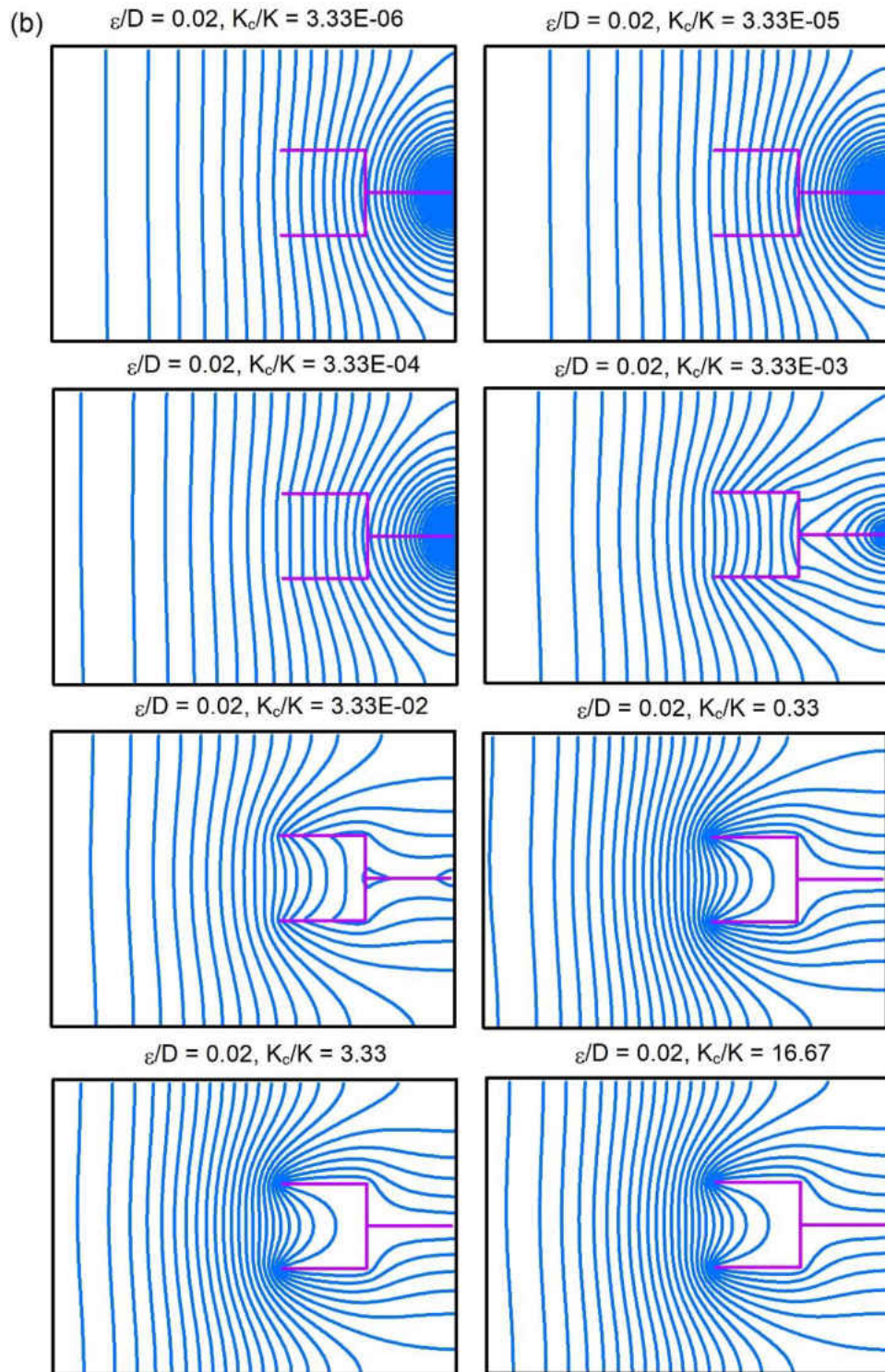
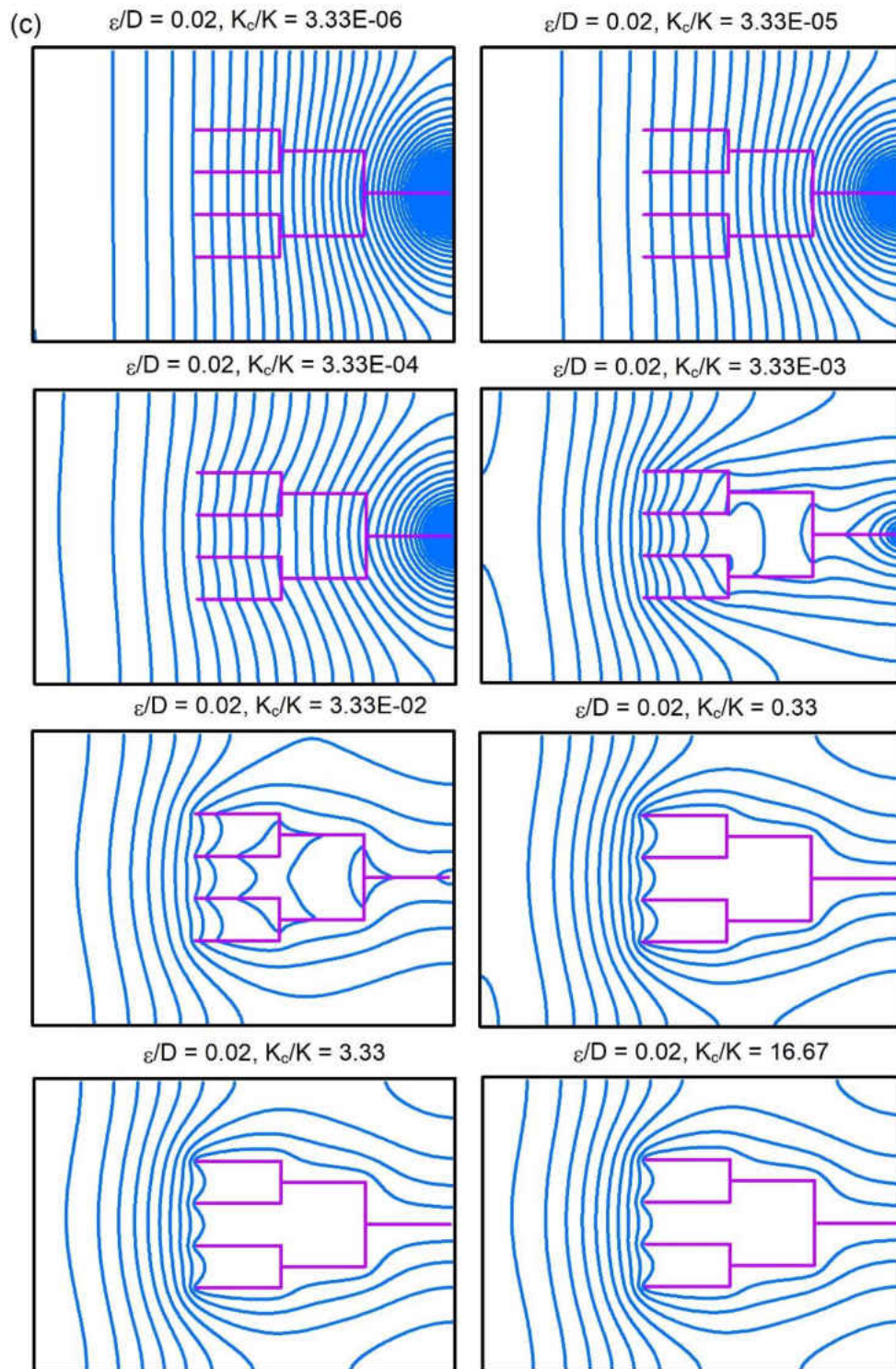


Figure 18: Relation between  $K_c/K$  and  $Q_c/Q$  (a) and  $R_e$  and  $Q_c/Q$  (b) for a single conduit karst aquifer under laminar flow condition.

Figure 18b shows the variation of  $Q_c/Q$  with  $R_e$  for different  $\epsilon/D$  when conduit flow is laminar. When  $\epsilon/D$  keeps the same, due to the increasing  $K_c/K$ ,  $Q_c/Q$  increases with  $R_e$  (e.g., when  $\epsilon/D = 0.1$ ). Figure 18b also analyzes the controls of  $\epsilon/D$  on  $Q_c/Q$ . An increase in  $\epsilon/D$  does not affect  $Q_c/Q$  but increases  $R_e$ , due to the increase in cross sectional area ( $v = Q_c/A$ ). Based on the results shown in Figure 18, it can be concluded that  $Q_c/Q$  is both controlled by  $K_c/K$  and  $R_e$  when conduit flow is laminar.







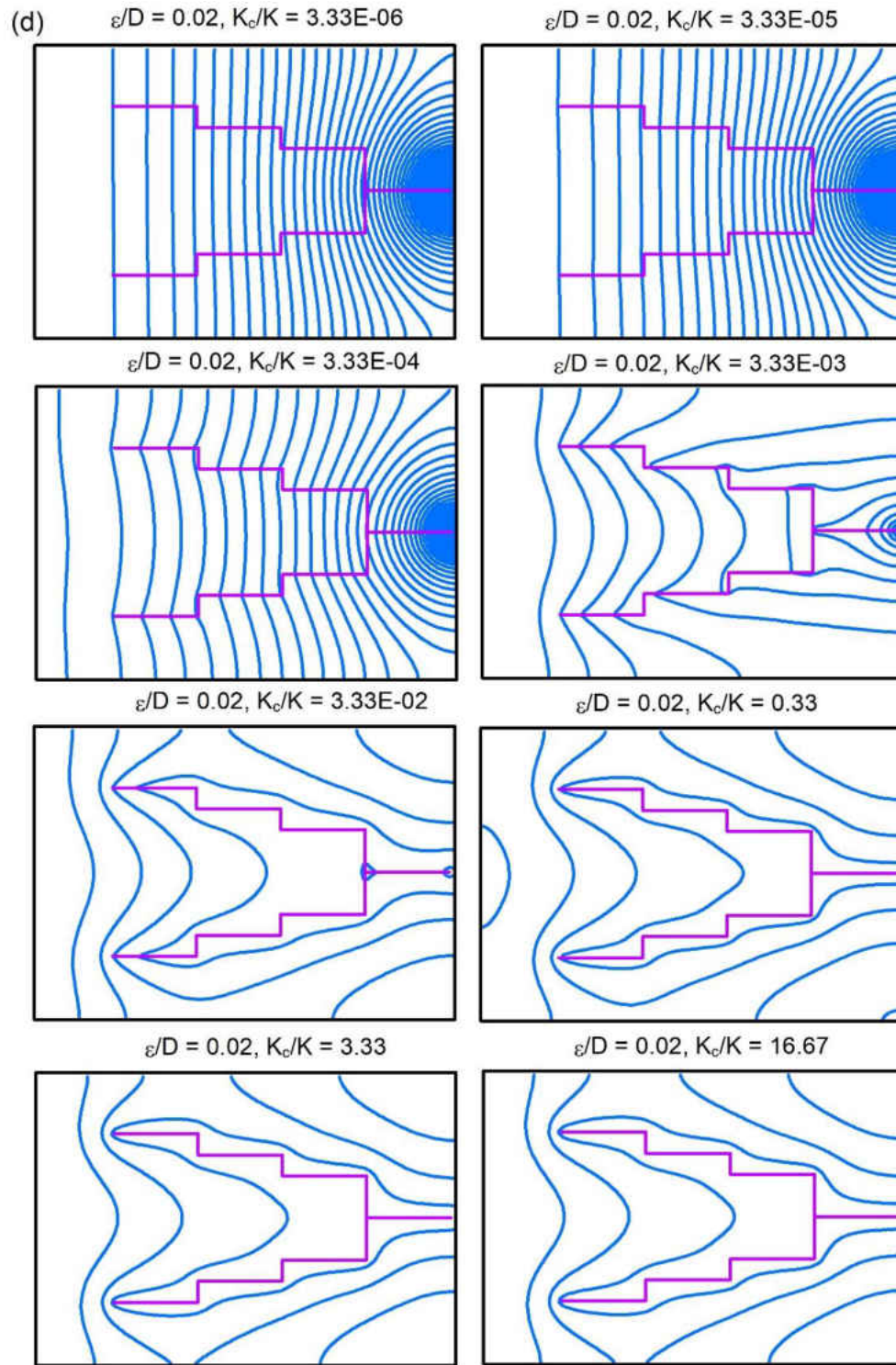


Figure 19: For a defined  $\varepsilon/D$  and different  $K_c/K$ , changes in contours of hydraulic head in aquifers with (a) single conduit; (b) three-conduit network; (c) and (d) seven-conduit network under laminar flow conditions.

The evaluations for the controls of  $\varepsilon/D$  on  $Q_c/Q$  when flow in single conduit is turbulent is presented in Figure 20a, in which  $Q_c/Q$  both varies with  $\varepsilon/D$  and  $R_e$  can be observed. As shown in Figure 20a, when  $K_c/K$  keeps the same, the variations of  $Q_c/Q$  with  $\varepsilon/D$  for different conduit sizes present unidentical curves. For example, when  $D = 0.1\text{ m}$ ,  $Q_c/Q$  does not change with  $\varepsilon/D$  until  $\varepsilon/D$  is larger than 0.001 and it sharply decreases from 0.61 to 0.56, showing a distinct downward concave curve from others. Compared to the smooth conduit or large-diameter conduit, for the conduit with small diameter, an increase in the mean roughness height influences the conduit flow properties, e.g., increase the turbulent core zone (Giese et al., 2018). The interferences caused by the wall roughness decrease the conductivity and thus the flux along the conduit. Therefore, the effect of flow restriction is further increased, causing a reduced  $Q_c/Q$ . This result is also documented in Peterson and Wicks (2006) which stated that slight changes in Manning's roughness coefficient can highly alter the simulated output for turbulent flow in small-diameter conduits. As conduit diameter increases,  $Q_c/Q$  decreases over a narrow range, and the concave curve gradually almost changes into a line (e.g.,  $D = 0.3\text{ m}$ ). Moreover, it is worthwhile to notice that  $R_e$  decreases with the reduction of the controls of  $\varepsilon/D$  on  $Q_c/Q$ . As a consequence, it seems reasonable to conclude that the curve will turn into a line when  $R_e$  is small enough, and this result will be consistent with the situation already explained when conduit flow is laminar, which shows  $Q_c/Q$  does not change with  $\varepsilon/D$  (Figure 18a).

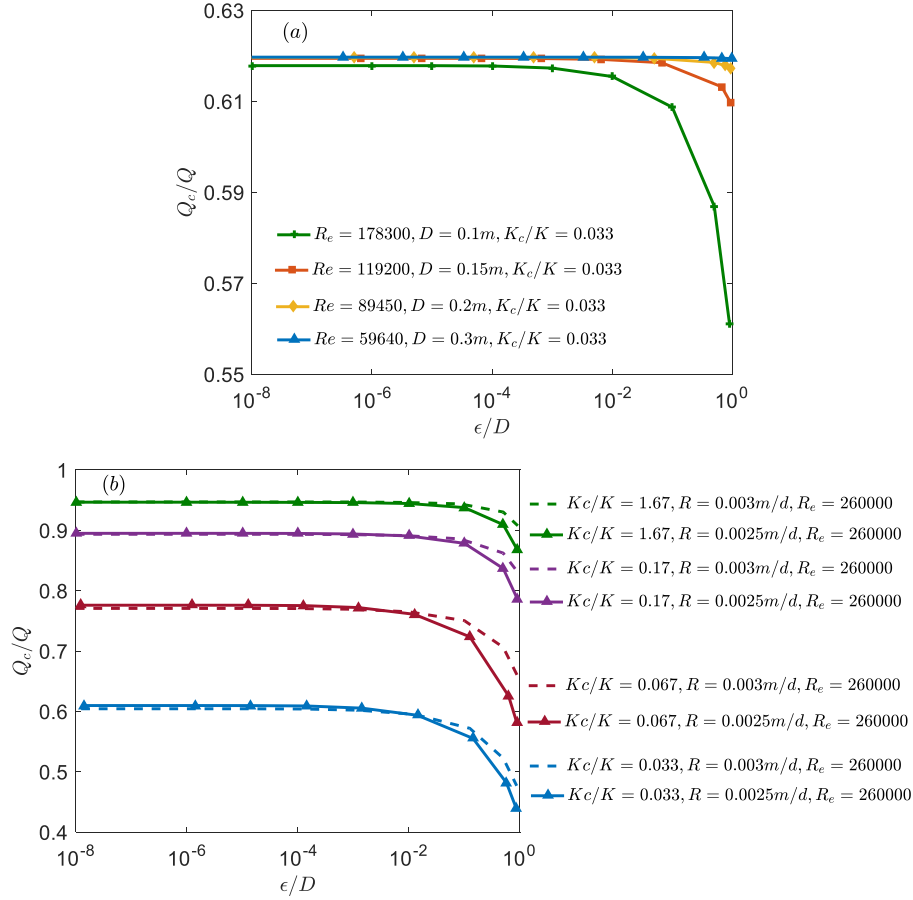


Figure 20: When flow in the conduit is turbulent, (a) controls of  $\epsilon/D$  on  $Q_c/Q$  when  $K_c/K = 0.033$ ; (b) for same Reynolds number, controls of  $\epsilon/D$  on  $Q_c/Q$  with different  $K_c/K$  and recharge.

For the condition that conduit flow is turbulent, the evaluations for the controls of  $\epsilon/D$  on  $Q_c/Q$  with different  $K_c/K$  and  $R$  are shown in Figure 20b. For different values of  $K_c/K$ , the patterns of the curves are similar as that shown in Figure 20a. As a consequence of a rising in  $K_c/K$ , more groundwater could flow into the conduit. Therefore, with the same  $\epsilon/D$  and  $Re_e$ , increase in  $K_c/K$  lifts  $Q_c/Q$ . Meanwhile, besides the three dimensionless parameters ( $\epsilon/D$ ,  $Re_e$ , and  $K_c/K$ ),  $R$  could also influence  $Q_c/Q$ . When  $\epsilon/D$ ,  $Re_e$  and  $K_c/K$  are defined the same, changes in  $R$  have a negligible influence on  $Q_c/Q$  until  $\epsilon/D$  is larger than 0.01. It

indicates higher  $R$  may boost  $Q_c/Q$  and the results are also shown in Chang et al. (2015) which reported that the influence of turbulent conduit flow decreases with rainfall intensity. The present study further highlights that  $Q_c/Q$  may not be increased with  $R$  until  $\varepsilon/D$  beyond a certain threshold.

### 3.3.2 Controls on the contribution of conduit networks with different conduit density to spring discharge

When flow in conduit network is laminar, the evaluation for the controls of  $K_c/K$  on  $Q_c/Q$  is shown in Figure 21a. Comparable to single-conduit aquifer, for the aquifers with different conduit networks,  $Q_c/Q$  changes with  $K_c/K$  but not  $\varepsilon/D$ . With higher conduit density ( $Cd$ ), there is a greater chance for groundwater interaction between conduit network and matrix. This geometric influence is analogous to sinuosity-driven hyporheic exchange in stream-aquifer systems (Cardenas, 2009; Gomez et al., 2012). The enhanced mixing means that more groundwater is traveling through the conduit (Ronayne, 2013). Consequently, with the same  $K_c/K$ , higher  $Cd$  may enhance more  $Q_c/Q$ . Further,  $Q_c/Q$  increases slowly when  $K_c/K$  is less than  $3.3 \times 10^{-4}$  or higher than 0.33 while the value is dramatically increased in between, indicating for karst aquifers with conduit network,  $Q_c/Q$  is also insensitive to the low or high  $K_c/K$ , which can be observed in Figure 19b-19d. Similar to the single-conduit aquifer, a rise in  $\varepsilon/D$  could cause a decrease in  $R_e$  of conduit flow in aquifers with conduit network when flow is laminar (Figure 18b). While, when  $\varepsilon/D$  is defined the same, differing in  $Cd$  would permit



the flow in conduit network to have the same  $R_e$ , which is shown in Figure 21b. It indicates  $Cd$  does not affect the relation between  $Q_c/Q$  and  $R_e$  for laminar flow regime. Generally, the analysis for the condition when flow is laminar implies that, for karst aquifers with conduit network,  $K_c/K$ ,  $\epsilon/D$ ,  $R_e$ , and  $Cd$  may all pose controls on  $Q_c/Q$ .

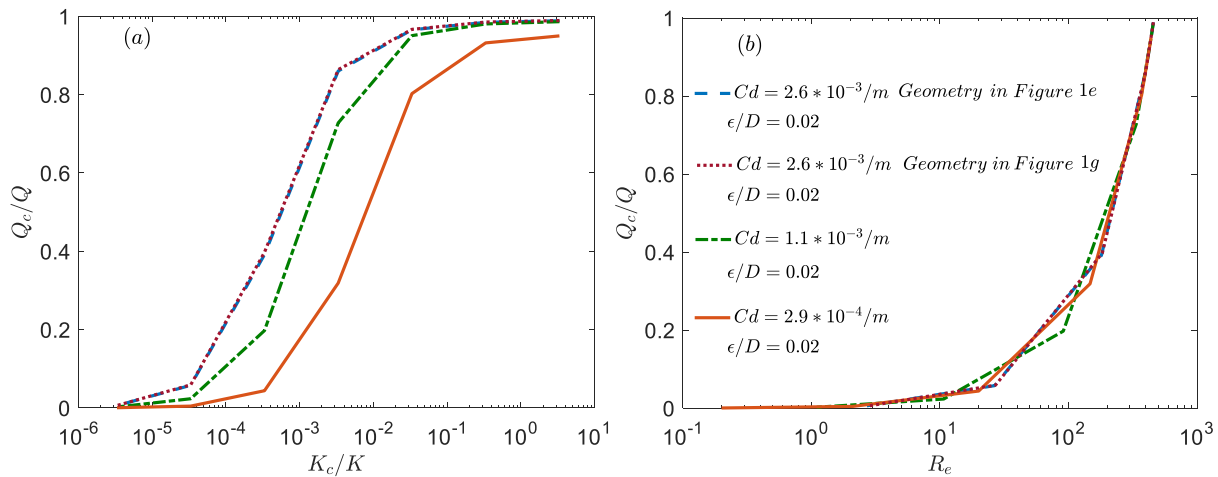


Figure 21: For same recharge values, different conduit densities and geometries, (a) controls of  $K_c/K$  on  $Q_c/Q$  and (b) controls of  $R_e$  on  $Q_c/Q$  under laminar flow conditions.

Figure 22 presents the evaluation for the controls of  $\epsilon/D$  on  $Q_c/Q$  under turbulent flow conditions. A rise in  $\epsilon/D$  causes a decrease in  $Q_c/Q$  for each defined  $Cd$ , which is similar to the condition analyzed for single-conduit aquifer (Figure 18a). Meanwhile, when  $K_c/K$  and  $R$  keep the same, the aquifer with higher  $Cd$  may allow larger proportion of groundwater to flow into conduit network, resulting in more groundwater could be delivered by conduit network to the spring. Further, when  $\epsilon/D$  is higher than 0.01, noticeable decreasing trends can be observed in Figure 22. The decreasing trend of  $Q_c/Q$  with  $\epsilon/D$  could be more significant in the aquifer with higher  $Cd$ . This suggests that, even though the aquifers may have different  $Cd$ , changes in

$Q_c/Q$  with  $\varepsilon/D$  all show similar patterns and when large  $\varepsilon/D$  existed in conduits, the aquifer with higher  $Cd$  could be more inclined to be impacted.

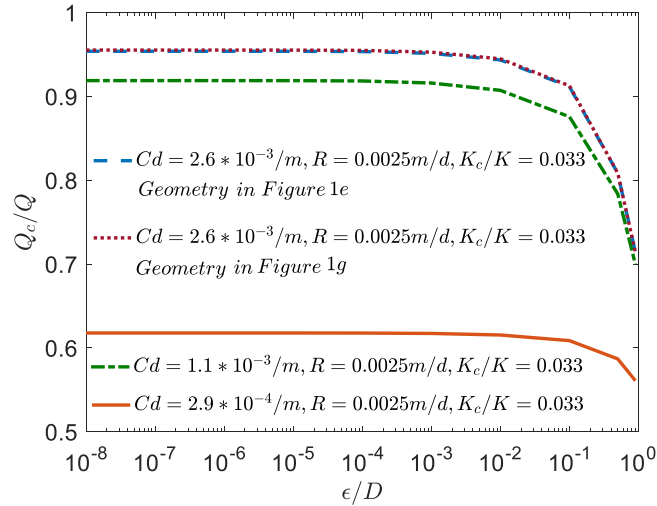


Figure 22: For same recharge value and  $K_c/K$  and different conduit density and geometry, controls of  $\varepsilon/D$  on  $Q_c/Q$  under turbulent flow conditions.

### 3.3.3 Controls on the contribution of conduit networks with same conduit density to spring discharge

When conduit flow is laminar, the evaluation for the controls of  $K_c/K$  on  $Q_c/Q$  for same  $Cd$  but different geometry (Figure 19e and 19g) is shown in Figure 21a. The changes in  $Q_c/Q$  with  $K_c/K$  for both of these two aquifers are the same, albeit the geometries are different. Meanwhile, for a defined  $\varepsilon/D$ , no difference in  $R_e$  of flow regimes in the conduits for the two aquifers is observed (Figure 21b). Moreover, when conduit flow is turbulent, for the same  $K_c/K$ ,  $R$  and  $Cd$ , variations of  $Q_c/Q$  with  $\varepsilon/D$  present the same patterns between the two aquifers with different geometries of conduit network (Figure 22). Consequently, the results indicate that,

comparable to laminar conduit flow, if  $Cd$  keeps the same, differing in conduit geometry does not affect  $Q_c/Q$ .

### 3.4 Case study and discussion

The results evaluated above thus far highlight the controls on the contribution of single conduit and conduit networks to spring discharge under laminar and turbulent conditions, respectively. In this section, behaviors of conduit flow from two regional scale models for simulating groundwater flow in karst aquifers located in Florida, Silver Springs springshed and Woodville Karst Plain (WKP), are used as case studies to validate the evaluated controls on  $Q_c/Q$ . The controls on  $Q_c/Q$  are evaluated based on the aquifer and conduit properties from the two regional scale models. The values of  $Q_c/Q$  from the regional scale models are compared with that from the evaluations, to examine whether the controlling analysis are able to provide clues on the estimation of conduit flow in regional karst aquifers instead of building more complex regional scale models.

#### 3.4.1 Descriptions of the study area

The Silver Springs springshed, with an area of about 2,323 km<sup>2</sup>, is delineated using the potentiometric surface of the UFA (Figure 23). Silver Springs, which is the head water of the Silver River, is the largest spring group in Florida, with an average discharge of 8.1 m<sup>3</sup>/s during

the period of 2010 to 2016. The aquifer system of the springshed is comprised of the UFA, a middle semi-confining unit, and the lower Floridan aquifer. A majority (86%) of spring discharge is from the upper 30 m of the UFA (Faulkner, 1973). Groundwater flow in the UFA may occur both in the rock matrix and fractures due to the dual-porosity characteristics of the aquifer (Phelps, 2004). Fractures are distributed mainly around the spring outlet, where the hydraulic conductivity and groundwater flow velocity are relatively higher compared with the rock matrix (Faulkner, 1973). These karstified features facilitate the recharge activity and correspondingly nitrate transport to the aquifer. The characteristics of the WKP is provided in detail in Xu et al. (2015).

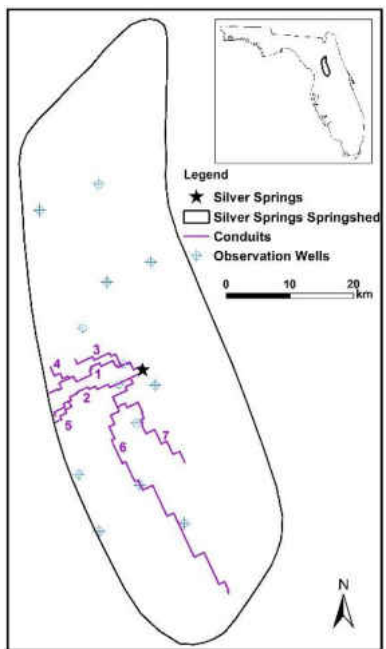


Figure 23: Conduit structure settings in the steady-state groundwater flow model for Silver Springs springshed.

### 3.4.2 Configuration and calibration of the regional scale models

The steady-state groundwater flow model for the Silver springshed is developed by MODFLOW-CFP. The model domain is discretized into a uniform grid of finite difference cells consisting 496 rows of 190.5 m-length cells and 236 columns of 190.5 m-length cells. The model has 4 layers of variable thickness, with layer 1 representing the surficial aquifer, layer 2 middle semi-confining unit, layer 3 upper Floridan aquifer (UFA), and layer 4 lower Floridan aquifer. No-flux boundary corresponds to the springshed boundary; head-dependent flux boundary is used to simulate rivers, lakes and streams in the domain. Data for the aquifer properties (top and bottom elevations, hydraulic conductivities) and boundary conditions (river, lake, and streams) were obtained from North Florida Southeast Georgia (NFSEG) Model which was developed by St. Johns River Water Management District (SJRWMD) in 2013 (Durdan et al., 2013). There are seven conduits set up in the UFA and the arrangement of conduit network is shown in Figure 23.

The calibration targets include mean observed hydraulic heads in 13 monitoring wells (data obtained from St. Johns River Water Management District) (Figure 23) and mean observed discharge of the Silver Springs during the period from 2000 to 2016 (data obtained from USGS website). Conduit diameter ( $D$ ), wall conductance ( $\alpha_{ex}$ ) and roughness height ( $\epsilon$ ) are estimated for each conduit in Figure 19, which are shown in Table 2 (Sepúlveda, 2009; Xu et al., 2015; Ghosh et al., 2016). Higher conductance values are calibrated for some conduits (e.g., conduit 1, 2, 6, and 7 shown in Table 4) (Hovorka et al., 1995). The roughness height was assumed to be

uniform over the 7 conduits, and the estimated value is 0.05 m. The scatter plot of observed versus simulated steady-state head values is shown in Figure 24, which shows a good agreement without apparent over- or under-estimation bias. The average root mean square error (RMSE) and relative error between simulated and observed heads are 0.14 ft and 2%. The relative error for the simulated mean spring discharge is 5%. Based on the alignment of calibrated conduit parameters with published values and acceptable calibration statistics for head values and the spring, the steady-state model calibration is acceptable. The steady-state groundwater flow model for the WKP is also developed by MODFLOW-CFP. More details on the model configuration and calibration are described in Xu et al., 2015.

Table 4: The calibrated values of diameter, conductance, roughness height, tortuosity for each conduit in the regional model for Silver Springs springshed.

Parameters	Conduit Index							Mean
	1	2	3	4	5	6	7	
Diameter (m)	6.0	6.0	3.0	3.0	1.5	6.0	6.0	4.5
Conductance (m <sup>2</sup> /day)	0.45	0.45	0.30	0.30	0.20	0.45	0.45	0.37
Roughness height (m)				0.05				0.05
Tortuosity				1.5				1.5
Conduit density (/m)				$5.7 \times 10^{-5}$				$5.7 \times 10^{-5}$

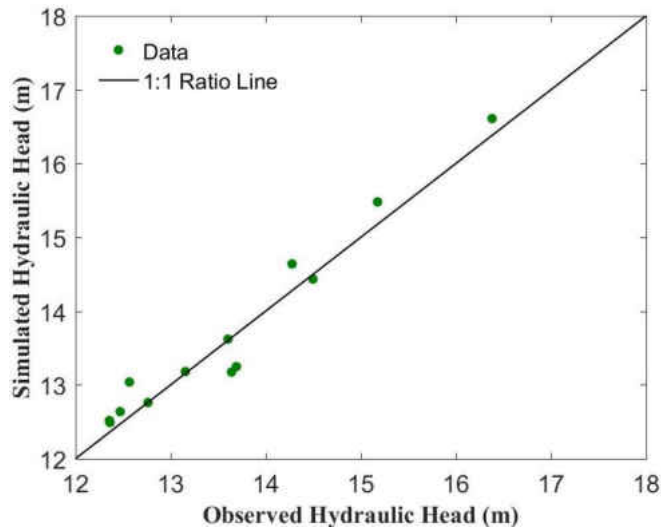


Figure 24: The observed and simulated hydraulic heads for the steady-state groundwater flow model for Silver springshed.

### 3.4.3 Comparison of $Q_c/Q$ between the evaluation results and regional scale models

$Q_c/Q$  corresponded to the specific  $\varepsilon/D$  for the two regional models are shown in Figure 25. Groundwater flow in conduit networks in the Silver springshed and WKP are both turbulent (minimum  $Re > 4000$ ). As shown in Figure 9, when  $\varepsilon/D = 0.011$ , 46% of groundwater flows through the conduit network to the spring in the springshed and 88% of groundwater is delivered by conduit network in the WKP when  $\varepsilon/D = 0.0033$ . Given the same values of  $R$ ,  $K_c/K$ , and  $Cd$  from the regional models, the controls of  $\varepsilon/D$  on  $Q_c/Q$  are evaluated, which are shown in Figure 25. Both curves are slimier as that shown in Figure 18. For conduit flow in Silver springshed, 48% of groundwater flows through the conduit network when  $\varepsilon/D$  is less than 0.55, and 96% of groundwater flows through conduit network in WKP when  $\varepsilon/D$  is less than 0.1. Between the results from regional models and evaluations, corresponding to the same  $\varepsilon/D$ , the

differences in  $Q_c/Q$  are small, particularly for the Silver springshed. The differences are mainly caused by the types of boundary conditions assigned in the regional models, which can pose impact on groundwater flow. For example, head-dependent boundaries are employed to simulate rivers in the regional model for Silver springshed and the interaction between the aquifer and river may influence the inflow and outflow of groundwater. However, even though the differences existed, the values from the evaluation results have well agreements with that from the regional models, which convinces us the evaluation for the controls on  $Q_c/Q$  established in this study is efficacious. Normally, developments of regional scale models are complex not only because the hydraulic properties of karst conduits are partly or totally unknown and acquiring the measured values of conduit properties is not possible, but also calibration of the model is time consuming. Hence, the process to attain the conduit flow or spring discharge is a cumbersome journey. Given appropriate physical properties, evaluating the controls on  $Q_c/Q$ , however, could efficiently provide clues on conduit flow in specific flow regimes, thus they may be served as solid tools to predict groundwater discharge in karst aquifers instead of building a more complex regional scale model.



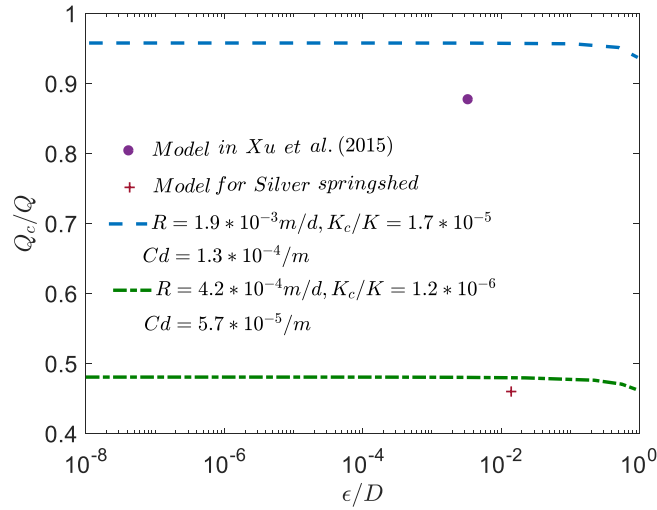


Figure 25: Controls of  $\varepsilon/D$  on  $Q_c/Q$  for regional scale karst models developed in present and previous studies.

### 3.5 Summary

In this study, physical controls on the contribution of single conduit and conduit network to spring discharge ( $Q_c/Q$ ) are evaluated under laminar and turbulent conditions. Three dimensionless parameters representing the conduit-matrix hydraulic conductivity contrast ( $K_c/K$ ), relative roughness ( $\varepsilon/D$ ), Reynolds number ( $R_e$ ), as well as recharge ( $R$ ), conduit density ( $Cd$ ) and different conduit geometries are employed to be as controlling factors in the evaluation.

When conduit flow is laminar, other than relative roughness, conduit-matrix hydraulic conductivity contrast and Reynolds number as well as conduit density could pose significant controls on the contribution of single conduit or conduit network to spring discharge. The contribution of single conduit or conduit network to spring discharge could increase with conduit-matrix hydraulic conductivity contrast and its variation is insensitive to the low and high conduit-

matrix hydraulic conductivity contrast while it could be dramatically changed in between, indicative of the controls of conduit-matrix hydraulic conductivity contrast on the contribution of single conduit or conduit network to spring discharge is not monotonous ascending or decreasing, however, there are two threshold values of the contribution of single conduit or conduit network to spring discharge existed at the extremes of the conduit-matrix hydraulic conductivity contrast.

When flow in the conduit(s) is turbulent, in addition to conduit-matrix hydraulic conductivity contrast, conduit density, and Reynolds number, the contribution of single conduit or conduit network to spring discharge could also be controlled by relative roughness and recharge. For the aquifers with same conduit-matrix hydraulic conductivity contrast and conduit density, a rise in relative roughness could pose negative impact on the contribution of single conduit or conduit network to spring discharge. Particularly when the relative roughness is larger than 0.01, noticeable decreasing trends can be observed. Meanwhile, when conduit-matrix hydraulic conductivity contrast and recharge keep the same, the aquifer with higher conduit density may allow larger proportion of groundwater to flow into conduits, resulting in more groundwater could be delivered by conduits to the spring. Further, when conduit density is defined the same, changes in conduit geometry do not impact conduit flow whether it is in laminar or turbulent conditions.

The evaluation for the controls on the contribution of single conduit and conduit network to spring discharge also show good predictions on the contributions of conduit networks to spring

discharge of the two regional scale models developed in present and previous studies, indicating given appropriate aquifer and conduit properties, the evaluation for the controls on the contribution of single conduit and conduit networks to spring discharge could provide clues to estimate groundwater discharge in karst aquifers instead of building a more complex regional scale model. The results presented in this study are based on steady-state flow simulations. Future research should consider the influence of these parameters on conduit flow during transience, which is particularly important for shallow eogenetic karst systems that are directly recharged during precipitation events.

# CHAPTER 4 DIAGNOSIS TOWARD PREDICTING MEAN ANNUAL RUNOFF IN UNGAUGED BASINS

## 4.1 Introduction

Hydrologists have a long-standing interest in mean annual water balance modeling and prediction. The factors controlling mean annual runoff have been studied in the literature. Mean climate has been identified as the first order control on mean annual runoff and evaporation and it has been quantified by climate aridity index, which is defined as the ratio between the mean annual potential evapotranspiration and precipitation (Turc, 1954; Pike, 1964). Other controlling factors include the temporal variability of climate (Troch et al., 2013), vegetation (Zhang et al., 2001), soil (Yokoo et al., 2008), and topography (Woods, 2003). Mean annual runoff or evaporation has been modeled as a function of climate aridity index and the equation is usually called as Budyko equation (Budyko, 1958). The effects of other factors are represented by including a parameter to Budyko equations (Fu, 1981; Yang et al., 2008; Wang and Tang, 2014). Among these factors, climate including its mean and temporal variability, and soil water storage capacity including its mean and spatial variability are dominant catchment characteristics controlling mean annual runoff, especially for saturation excess runoff generation-dominated catchments (Milly, 1994).

Intra- and inter-annual climate variability introduces non-steady state conditions to finer

timescale water balances and the non-steady state effect could propagate to the mean annual runoff. The effects of seasonal variations of precipitation and potential evaporation on long-term runoff have been studied in several studies. Milly (1994) showed that seasonality tends to increase mean annual runoff through a stochastic soil moisture model. The seasonality effects have been demonstrated through a top-down model by Hickel and Zhang (2006) and a classification study by Berghuijs et al. (2016). Mean annual water balance also receives impacts from climate variability at the inter-annual and daily timescales. Li (2014) showed that the inter-annual variability of precipitation and potential evaporation could increase the mean annual runoff up to 10% based on a stochastic soil moisture model. Shao et al. (2012) found that daily precipitation with a larger variation potentially increases mean annual runoff especially in the catchments where infiltration excess runoff is prevalent. Yao et al. (2020) quantified the relative contribution of daily, monthly and inter-annual climate variabilities to mean annual runoff and showed that the contribution decreases, by average, from monthly to inter-annual scale, and then daily scale.

Soil water storage capacity exerts a powerful control on mean annual runoff. A smaller soil water storage capacity creates favorable conditions for runoff generation because the precipitation in excess of the available storage capacity would be lost as runoff directly, while catchments with a larger soil water storage capacity could hold more precipitation for evaporation (Sankarasubramanian and Vogel, 2002; Porporato et al., 2004). Soil water storage capacity is closely related to vegetation since the root structure of vegetation could affect soil water holding

capacity significantly. Research has been conducted to reveal the role of soil water storage capacity through the linkage of vegetation and model parameter (Yang et al., 2008). Gerrits (2009) developed equations for transpiration and interception by considering the root zone and interception storage capacity as two of the most important catchment characteristics affecting evapotranspiration. In addition to the magnitude of the average soil water storage capacity, the spatial variability of storage capacity within a catchment also influences precipitation partitioning at the event scale, and further influences the cumulative runoff at the mean annual scale (Moore, 1985). It has also been suggested that the spatial variability of soil water storage capacity could suppress the actual evaporation and therefore promote the runoff generation indirectly (Yao et al., 2020).

Therefore, climate variability and soil water storage capacity need to be explicitly incorporated into the model for predicting mean annual runoff. The effect of climate variability could be taken into account by driving the model with daily precipitation and potential evaporation which are usually available. The spatial distribution of soil water storage capacity could be modelled by a distribution function, and it is usually modelled by the generalized Pareto distribution (Moore, 1985; Zhao, 1992). The distribution function includes two parameters, i.e., the shape parameter and the maximum storage capacity over the watershed. In ungauged basins, soil water storage capacity and its spatial variability need to be estimated directly from available data. Gao et al. (2014) adopted the mass curve technique, which has been used for designing the

storage capacity of reservoir, to estimate the average water storage capacity of the root zone using precipitation and potential evaporation data. The shape parameter of the distribution function has been estimated from soil data (Huang et al., 2003). However, the estimated parameters from these methods bring much uncertainty in runoff estimation, and the two parameters of the generalized Pareto distribution are usually estimated by model calibration using observed streamflow data (Wood et al., 1992; Alipour and Kibler, 2018, 2019).

The objective of this study is toward developing nonparametric mean annual water balance model for predicting mean annual runoff in ungauged basins. The mean annual water balance model is forced by daily precipitation and potential evaporation; therefore, the climate variability at different timescales is represented explicitly in the climate input. The runoff generation is quantified by a distribution function for describing the spatial distribution of soil water storage capacity (Wang, 2018). The mean and the shape parameter of the distribution function need to be estimated from the available data in ungauged basins. Therefore, the model serves as a diagnosis tool for evaluating the data requirement for estimating soil water storage capacity. The mean of the distribution is estimated from curve number and climate since the distribution function leads to the SCS curve number method. The estimation of the shape parameter is diagnosed in terms of the data requirement including soil, land surface topography, and bedrock topography. Section 4.2 introduces the new mean annual water balance model and the study watersheds. Results and discussion are presented in Section 4.3, followed by Section 4.4 for conclusions.

## 4.2 Methodology

### 4.2.1 Mean annual runoff model

As discussed in the introduction, the mean annual runoff model takes daily precipitation and potential evaporation as inputs, and calculates daily soil wetting (infiltration) and evaporation by tracking the soil water storage. Mean annual runoff is estimated by aggregating the daily values. The daily soil wetting is calculated using the concept of saturation excess runoff generation by modeling the spatial variability of soil moisture and storage capacity. To facilitate the parameter estimation of storage capacity distribution in ungauged basins, the following distribution function is used for modeling the spatial distribution of storage capacity (Wang, 2018):

$$F(C) = 1 - \frac{1}{a} + \frac{C+(1-a)S_b}{a\sqrt{(C+S_b)^2-2aS_bC}} \quad (4.1)$$

where  $F(C)$  is the cumulative distribution function (CDF), representing the fraction of the watershed area for which the storage capacity is equal to or less than  $C$ ;  $a$  is the shape parameter of the distribution and varies between 0 and 2; and  $S_b$  is the average soil water storage capacity over the watershed (i.e., the mean of the distribution). As shown in Wang (2018), this distribution function leads to the SCS curve number (SCS-CN) method when the initial storage is set to zero. Therefore, there is a linkage between  $S_b$  and the “potential maximum retention after runoff begins” in the SCS-CN method, denoted as  $S_{CN}$ .

Daily soil wetting and runoff generation is computed as a function of daily precipitation ( $P$ ), initial storage ( $S_0$ ),  $a$ , and  $S_b$ . As shown in Wang (2018), the average soil wetting ( $W$ ) is computed by:



$$W = \frac{P+S_b\sqrt{(m+1)^2-2am}-\sqrt{[P+(m+1)S_b]^2-2amS_b^2-2aS_bP}}{a} \quad (4.2)$$

where  $m = \frac{S_0(2S_b-aS_0)}{2S_b(S_b-S_0)}$ . Setting  $S_0 = 0$  and dividing  $P$  on both sides of equation (4.2), a Budyko-type equation, representing  $\frac{W}{P}$  as a function of  $\frac{S_b}{P}$ , is obtained (Wang and Tang, 2014), which has been used to model long-term soil wetting (Tang and Wang, 2017). Therefore, equation (4.2) can be interpreted as a non-steady state Budyko equation which accounts for the effect of water storage. Daily evaporation is computed as (Yao et al., 2020):

$$E = \frac{W+S_0}{S_b} \frac{E_p+S_b-\sqrt{(E_p+S_b)^2-2aS_bE_p}}{a} \quad (4.3)$$

The first component on the right-hand side of equation (4.3),  $\frac{W+S_0}{S_b}$ , is the percentage of storage, and the second component is the evaporation for the condition when the entire watershed is saturated, i.e., the spatial distribution of soil water storage is same as that of storage capacity (Yao et al., 2020). Dividing  $W + S_0$  on both-hand sides, equation (4.3) represents  $\frac{E}{W+S_0}$  as a function of  $\frac{E_p}{S_b}$ , and the function is same as the Budyko-type equation derived by Wang and Tang (2014). Mean annual evaporation ( $\bar{E}$ ) is computed by aggregating the daily evaporation, and mean annual runoff ( $\bar{Q}$ ) is computed as the difference of mean annual precipitation and evaporation.

This mean annual water balance model applies two non-steady Budyko-type equations at the daily scale, one for daily soil wetting and the other for daily evaporation. Runoff routing is not necessary since the model is for long-term water balance. As a result, the mean annual water balance model includes two parameters, i.e., the shape parameter ( $a$ ) and the average soil water storage capacity ( $S_b$ ). For studies where a one-parameter Budyko equation is applied to long-

term scale directly, the effects of climate variability (seasonality, inter-annual variability, and daily storminess) on mean annual water balance are attributed to the single parameter of Budyko equation (e.g., Fu, 1981; Zhang et al., 2001). This creates the challenge to estimate the single parameter in ungauged basins; whereas, the mean annual water balance model used in this study takes daily precipitation and potential evaporation as inputs, and the effects of climate variability are taken into account explicitly. To achieve the goal of predicting mean annual runoff in ungauged basins,  $a$  and  $S_b$  need to be estimated in ungauged basins.

#### 4.2.2 Parameter estimation

##### 4.2.2.1 Average soil water storage capacity

Under a given soil moisture condition, soil water storage capacity is the sum of actual water storage and the remaining (or effective) storage capacity. The effective storage capacity corresponding to the normal antecedent moisture condition defined in the SCS-CN method,  $S_{CN}$  (mm), is computed as a function of CN (SCS, 1972):

$$S_{CN} = 25.4(1000/CN - 10) \quad (4.4)$$

where CN is computed based on land use and land cover (LULC) and hydrologic soil group (HSG) for each catchment. The LULC data can be obtained from the National Land Cover Database (Homer et al., 2015), and the HSG data can be extracted from the Gridded Soil Survey Geographic (gSSURGO) database with a spatial resolution of 10 m (USDA, 2014). In HSG, soils are assigned to one of the four groups (A, B, C, and D) and three dual classes (A/D, B/D, and C/D)

according to the rate of infiltration when the soils are not protected by vegetation and receive precipitation from long-duration storms. For the cells characterized by dual classes, the CN value is calculated as the average of the two CN values corresponding to the two soil groups.

The average soil water storage capacity ( $S_b$ ) is the sum of the actual storage under the normal condition ( $\bar{S}$ ) and its corresponding effective storage capacity:

$$S_b = \bar{S} + S_{CN} \quad (4.5)$$

Since the “normal antecedent moisture” can be interpreted as the steady-state soil moisture condition,  $\bar{S}$  is the long-term average storage over the watershed. The values of  $\bar{S}$  for 59 MOPEX (MOdel Parameter Estimation Experiment) watersheds are estimated based on the long-term water balance model in Yao et al. (2020); and these watersheds do not include any watersheds studied in this study. The long-term water balance model used in their study has a same model structure but the two parameter, i.e., the mean value of the soil water storage capacity and its shape parameter in the distribution function, were obtained by model calibration. The ratio between  $\bar{S}$  and  $S_b$  is defined as the long-term storage ratio  $\left(\frac{\bar{S}}{S_b}\right)$ . It is found that the values of  $\frac{\bar{S}}{S_b}$  for all the watersheds were larger than 0.5. As shown in Figure 26,  $\frac{\bar{S}}{S_b}$  has a linear relationship with the climate aridity index:

$$\frac{\bar{S}}{S_b} = -0.46\Phi + 1.2 \quad (4.6)$$

where  $\Phi$  is the climate aridity index. Substituting equations (4.5) and (4.6) into equation (4.4), one can estimate the average soil water storage capacity as a function of curve number and

climate aridity index:

$$S_b = \frac{S_{CN}}{0.46\Phi - 0.2} \quad (4.7)$$

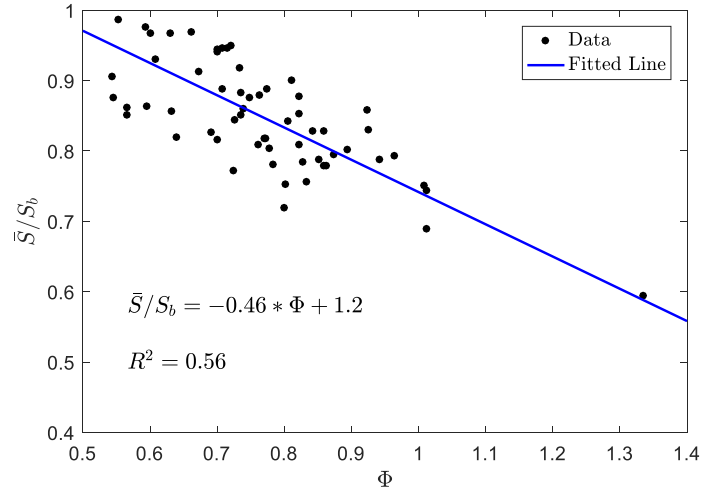


Figure 26: The degree of saturation  $\left(\frac{\bar{S}}{S_b}\right)$  under long-term average climate versus climate aridity index ( $\Phi$ ).

#### 4.2.2.2 Shape parameter

The spatial variability of storage capacity is determined by the spatial distribution of point-scale pore space across the watershed. The volume of soil pores at point scale can be determined by soil thickness and porosity in different soil layers. The porosity ( $\theta_s$ ) for each layer is calculated from the soil bulk density:

$$\theta_s(j) = 1 - \frac{\rho_b(j)}{\rho} \quad (4.8)$$

where  $j$  denotes the  $j^{th}$  soil layer;  $\rho_b(j)$  is the bulk density of the  $j^{th}$  soil layer;  $\rho$  is the particle density (2.65 g/cm<sup>3</sup>). After obtaining the porosity, the point-scale storage capacity can be

calculated as the following equation (Huang et al., 2003):

$$C = \sum_1^n z_j \cdot \theta_s(j) \quad (4.9)$$

where  $C$  is the point-scale soil storage capacity;  $n$  is the number of soil layers;  $z_j$  and  $\theta_s(j)$  are the thickness and porosity of the  $j^{th}$  soil layer, respectively. In the gSSURGO database, the soil thickness and bulk density for each layer are available for shallow soil from the land surface to ~ 2 m soil depth.

The total soil thickness at each point is the elevation difference from the land surface to the fresh bedrock. However, the bedrock topography is difficult to obtain especially at the catchment scale. Alternatively, it is assumed that the spatial distribution of the actual soil water storage capacity is same as the spatial distribution of water storage capacity computed from the gSSURGO database. In order to compare the shape parameter evaluated from the soil data with its counterparts evaluated from other methods, the point-scale storage capacity is normalized with the average storage capacity over the watershed, and Equation (4.1) is rewritten as:

$$F(x) = 1 - \frac{1}{a} + \frac{x+(1-a)}{a\sqrt{(x+1)^2-2ax}} \quad (4.10)$$

where  $x$  is the normalized storage capacity  $\left(\frac{C}{S_b}\right)$  at point scale;  $a$  is the shape parameter describing the spatial variability of soil water storage capacity. The shape parameter  $a$  is then estimated through fitting the point-scale storage capacity data obtained from Equation (4.9) by minimizing the root mean square error (RMSE).

#### 4.2.3 Study watersheds

The estimations of mean annual runoff in 35 watersheds are diagnosed in this study. The drainage area of the watersheds varies from 2044 to 9889 km<sup>2</sup>. Table 5 shows the USGS gauge number and climate aridity index of these watersheds. The human interferences are minimum (Wang and Hejazi, 2011), and saturation excess is the dominated runoff generation in these watersheds. Daily precipitation and streamflow data during 1948 – 2003 are extracted from the MOPEX dataset (Duan et al., 2006), and the daily potential evaporation during this period is calculated based on the Hargreaves method (Hargreaves and Samani, 1985) by using the daily maximum, minimum, and mean temperature. The average soil water storage capacity and the shape parameter for these watersheds are estimated from the available data of climate, LULC, soil, and topography, and the predictions of mean annual runoff are diagnosed.

Table 5: The USGS gage stations, climate aridity index, the estimated potential maximum retention of curve number method ( $S_{CN}$ ), and the average soil water storage capacity ( $S_b$ ) for the study watersheds.

Index	Station Name	State	USGS Number	Gauge	Climate Index	Aridity	$S_{CN}$ (mm)	$S_b$ (mm)
1	Susquehanna River	NY	01503000			0.69	100	862
2	Chemung River	NY	01531000			0.84	95	518
3	Juniata River	PA	01567000			0.85	134	714
4	Rappahannock River	VA	01668000			0.85	152	792
5	Yadkin River	NC	02116500			0.71	153	1221
6	Chattahoochee River	GA	02339500			0.69	182	1559
7	Escambia River	FL	02375500			0.73	143	1075
8	Allegheny River	NY	03011020			0.68	153	1369
9	New River	VA	03168000			0.69	177	1494
10	Great Miami River	OH	03274000			0.89	63	301
11	Eel River	IN	03328500			0.92	68	304
12	East Fork White River	IN	03364000			0.83	68	378
13	Little Wabash River	IL	03381500			0.96	68	279
14	Fox River	WI	04073500			1.12	162	520
15	Auglaize River	OH	04191500			0.98	56	225
16	Maquoketa River	IA	05418500			1.19	72	209
17	Wapsipinicon River	IA	05422000			1.16	69	210
18	Rock River	WI	05430500			1.11	98	316
19	Pecatonica River	IL	05435500			1.11	66	214
20	Kishwaukee River	IL	05440000			1.03	70	255
21	Green River	IL	05447500			1.10	75	247
22	Iowa River	IA	05454500			1.18	65	191
23	Cedar River	IA	05458500			1.17	65	193
24	Kankakee River	IL	05520500			0.93	101	448

Table 5 (continued).

Index	Station Name	State	USGS Gauge Number	Climate Aridity Index	$S_{CN}$ (mm)	$S_b$ (mm)
25	Fox River	IL	05552500	1.04	88	321
26	Spoon River	IL	05570000	1.12	71	227
27	Kaskaskia River	IL	05592500	0.99	67	263
28	Blue River	KS	06884400	1.70	74	127
29	Thompson River	MO	06899500	1.16	65	195
30	Meramec River	MO	07019000	0.95	109	460
31	Chikaskia River	OK	07152000	1.82	77	121
32	Neosho River	KS	07183000	1.42	63	140
33	Deep Fork River	OK	07243500	1.40	87	197
34	Neches River	TX	08033500	1.14	174	540
35	Elm Fork Trinity River	TX	08055500	1.63	87	159

### 4.3 Results and discussion

#### 4.3.1 Estimated average soil water storage capacity

The potential maximum retention ( $S_{CN}$ ) is calculated based on the average CN in each watershed (Table 5). The average CN is computed based on LULC and hydrologic soil group. For examples, Figure 27a shows the LULC map for the Fox River watershed in Wisconsin and Figure 27d shows the LULC map for the Spoon River watershed in Illinois. The dominant land uses are agriculture (49%) and forest (33%) in the Fox River watershed, and agriculture (77%) and forest (15%) in the Spoon River watershed. The hydrologic soil groups are shown in Figure 27b (Fox River watershed) and Figure 27e (Spoon River watershed). Given the same LULC, the hydrologic soil group D is more favorable for runoff generation compared with group A. The



dominant hydrologic soil groups are group A (31%) and group B (19%) in the Fox River watershed, and group C/D (49%) and group B/D (20%) in the Spoon River watershed. The calculated CN for each grid cell is shown in Figure 27c (Fox River watershed) and Figure 27f (Spoon River watershed). The average CN is 61.0 for the Fox River watershed and 78.1 for the Spoon River watershed. Since the Spoon River watershed has a higher percentage of agricultural land and lower soil permeability, its average CN is higher than that for the Fox River watershed. Correspondingly, the calculated  $S_{CN}$  in the Fox River watershed (162 mm) is higher than that in Spoon River watershed (71 mm). The values of  $S_{CN}$  over the study watersheds vary from 56 mm (Auglaize River watershed) to 182 mm (Chattahoochee River watershed) as shown in Table 2.

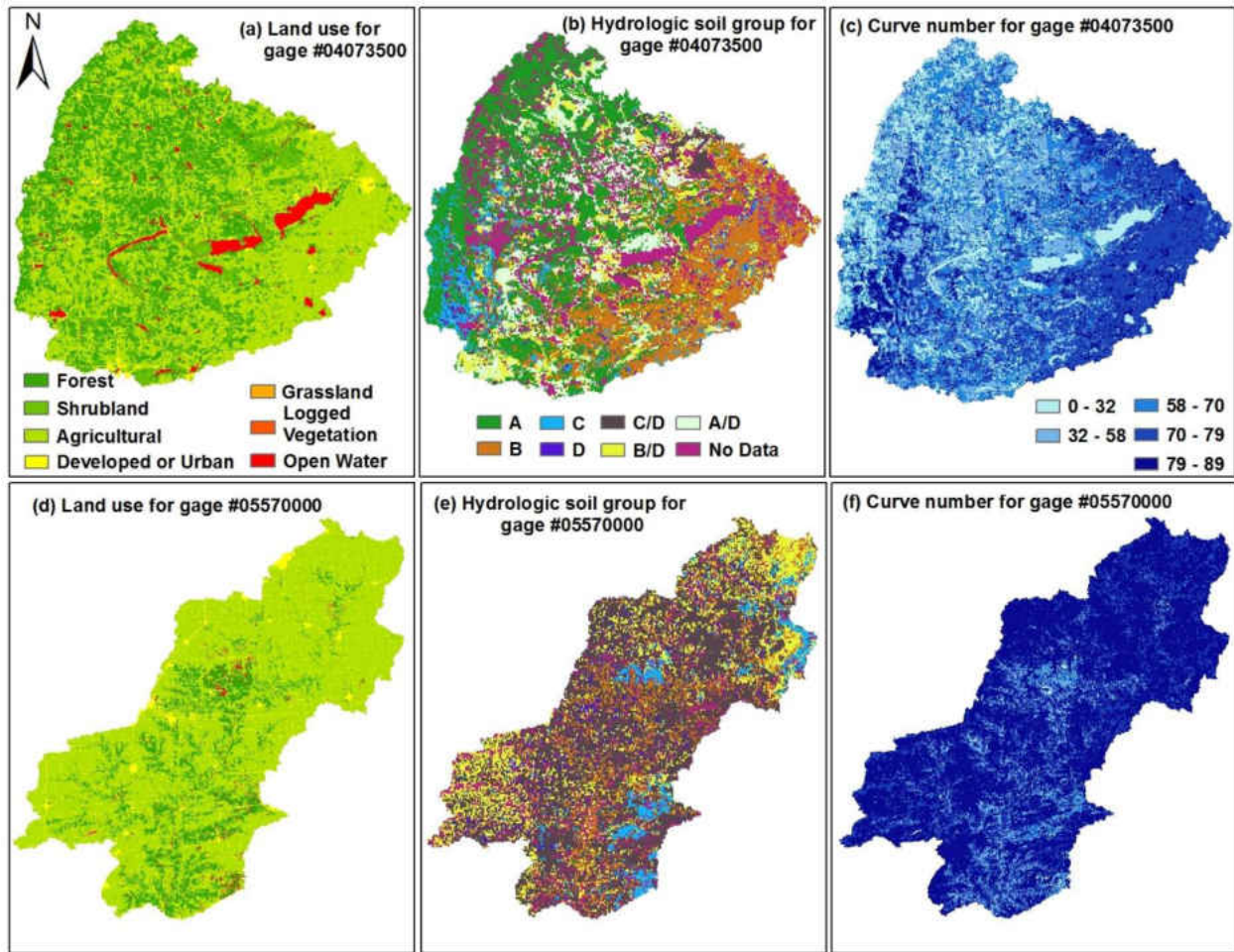


Figure 27: The spatial distribution of land use and land cover for Fox River watershed in Wisconsin (a) and Spoon River watershed in Illinois (d), the hydrologic soil groups for Fox River watershed (b) and Spoon River watershed (e), and the curve numbers for Fox River watershed (c) and Spoon River watershed (f).

The average soil water storage capacity is estimated based on the computed  $S_{CN}$  and climate aridity index shown in Equation (4.7). For examples, the climate aridity index in the Fox River watershed is 1.12 which is the same as that in the Spoon River watershed. The estimated  $S_b$  is 721 mm in the Fox River watershed and 314 mm for the Spoon River watershed. As shown in Table 2, the estimated  $S_b$  varies from 177 mm (Chikaskia River watershed) to 1870 mm

(Chattahoochee River watershed) over the study watersheds. Figure 28a shows the spatial distribution of the estimated  $S_b$ . Watersheds with higher  $S_b$  are mostly distributed in the eastern US, where the aridity index is relatively lower than that in the other watersheds.

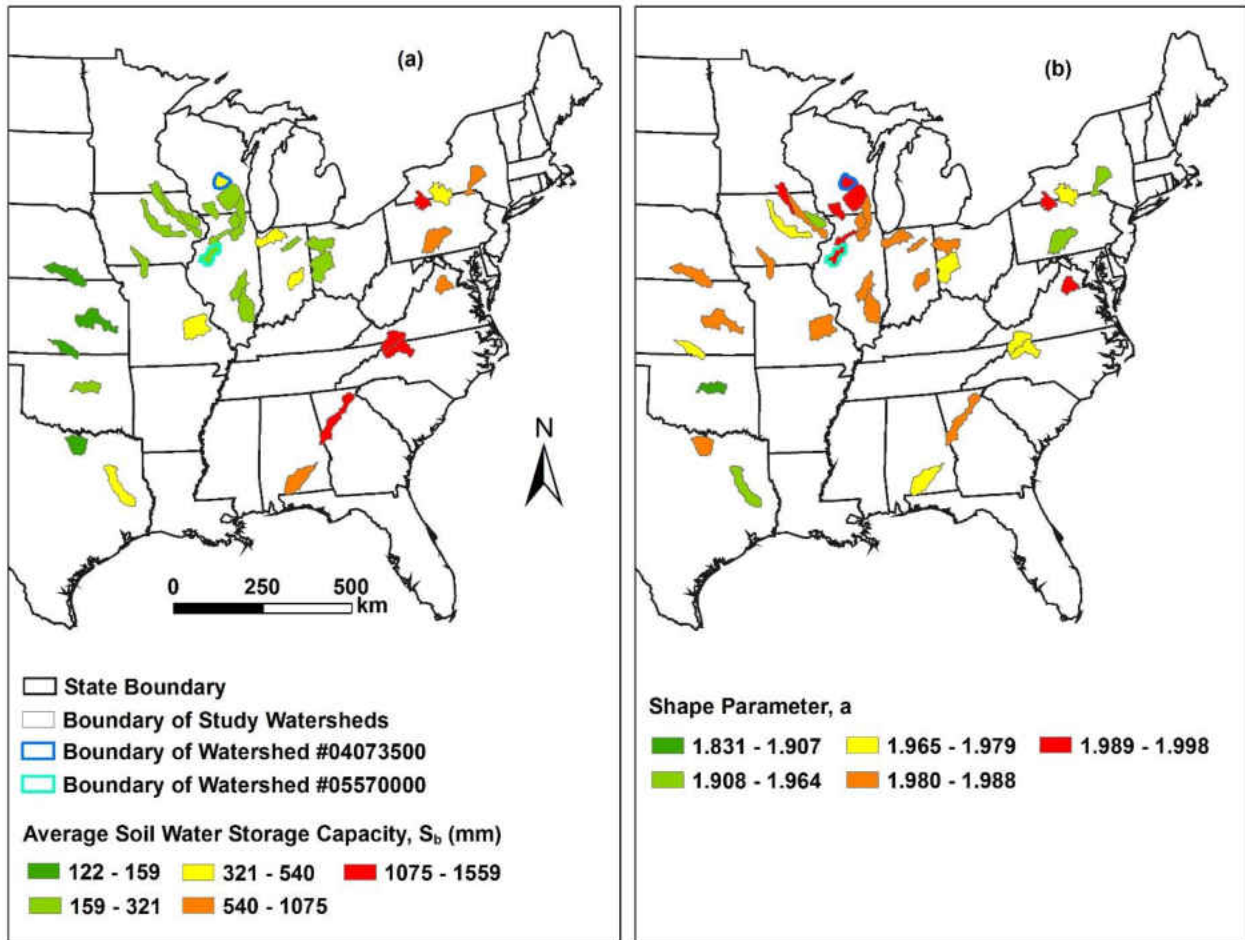


Figure 28: The estimated average soil water storage capacity ( $S_b$ ) as a function of  $S_{CN}$  and climate aridity index (a) and shape parameter from soil data (b).

#### 4.3.2 Estimated shape parameter

The shape parameter ( $a$ ) for the distribution of soil water storage capacity is estimated

based on the soil data in the gSSURGO database. For examples, the black circles in Figure 29 show the normalized storage capacity for the Fox River watershed (Figure 29a) and the Spoon River watershed (Figure 29b) based on the soil data in the gSSURGO database. As shown in Figure 29, the normalized CDF for both watersheds shows an S-shape. The estimated shape parameter is 1.996 for the Fox River watershed (RMSE = 0.58) and 1.990 for the Spoon River watershed (RMSE = 1.27) by fitting to the soil data. Higher value of shape parameter indicates less spatial variability; therefore, the spatial variability in the Spoon River watershed is higher than that in the Fox River watershed. The mean value of RMSE for the 35 study watersheds is 0.06. Figure 30b shows the estimated shape parameters for the study watersheds, which vary from 1.830 to 1.998.

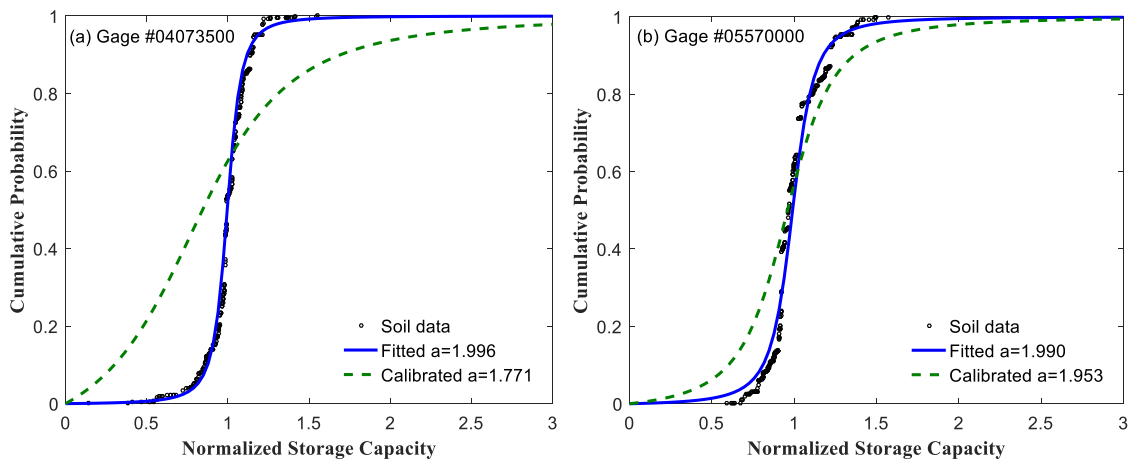


Figure 29: The estimated shape parameter for the spatial distribution of soil water storage capacity based on soil data and the calibrated shape parameter based on mean annual water balance in the Fox River watershed (a) and the Spoon River watershed (b).

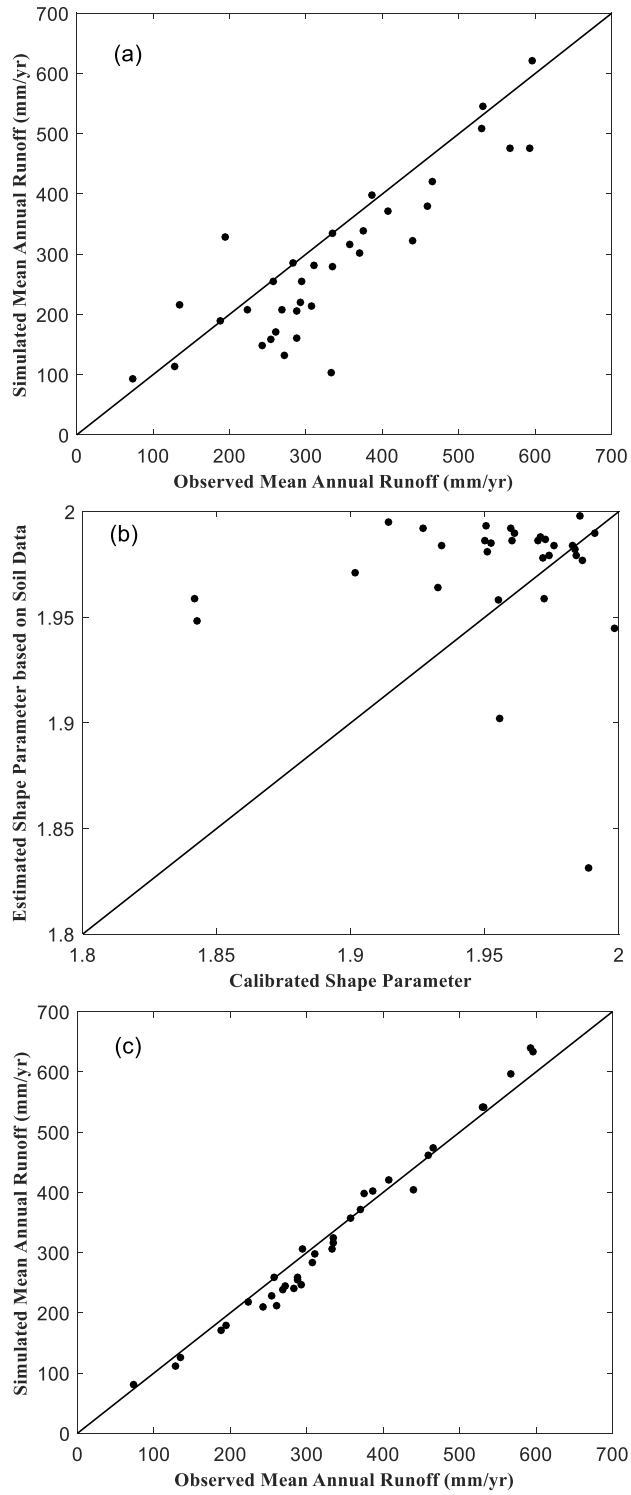


Figure 30: (a) Observed versus simulated mean annual runoff using shape parameter based on soil data; (b) Soil data-based versus calibrated shape parameter; and (c) Observed versus simulated mean annual runoff using shape parameter based on calibration.

### 4.3.3 Diagnosing mean annual runoff prediction

The estimated values of  $S_b$  and  $a$  based on climate, LULC, and soil data are applied to the mean annual water balance model. The comparison of simulated and observed mean annual runoff for the study watersheds is shown in Figure 30a. The RMSE for estimated mean annual runoff is 80 mm/yr. The water balance model captures 88.2% of the mean annual runoff; therefore, the methods for estimating  $S_b$  and  $a$  based on the available data are promising for predicting annual runoff in ungauged basins.

The water balance model with the estimated values of  $S_b$  and  $a$  underestimates the mean annual runoff in some watersheds, and the relative underestimation error is 11.8% on average among all the study watersheds. The underestimation of mean annual runoff could be due to the biased estimation of the shape parameter. As described in Section 4.3.2, the spatial variability of soil storage capacity is assumed to be equal with the spatial variability of the pore space in the shallow soil. The pore space at the point scale is calculated through the porosity and soil thickness. The thickness of the shallow soil in the gSSURGO database is quite uniformly distributed across the watershed, i.e., around 2 m; whereas, the actual soil thickness including the weathered bedrock is the elevation difference between the land surface and fresh bedrock, and can be highly heterogeneous due to the variable land surface and bedrock topography over the catchment.

To diagnose the effect of land surface and bedrock topography on mean annual water

balance, the shape parameter is calibrated using the observed streamflow. The streamflow data during 1948-2003 are divided into three periods: 1) the warm-up period (1948-1953); 2) the calibration period (1954-1973); and 3) the validation period (1974-2003). During the calibration, the estimated  $S_b$  based on CN is used, and  $a$  is the only free parameter to be calibrated. The calibration is conducted by minimizing the absolute error of the observed and simulated mean annual runoff through a global optimization method, i.e., Shuffled Complex Evolution Method (Duan et al., 1992). As shown in Figure 30b, most of the calibrated  $a$  are smaller than the estimated  $a$  based on soil data only. The performance of predicted mean annual runoff (during the validation period) is improved with the calibrated shape parameter (Figure 30c). The average of absolute error for the mean annual runoff is 7.1%.

The overestimation of shape parameter based on the soil porosity data underestimates the spatial variability of soil water storage capacity compared with the calibrated one as shown in Figure 29a for the Fox River watershed and Figure 29b for the Spoon River watershed. The slope at the normalized storage capacity around 1 for the estimated shape parameter is higher than that for the calibrated one. Therefore, the calibrated shape parameter indicates a larger spatial variability. The underestimation of the spatial heterogeneity of soil water storage capacity could be resulted from neglecting the effect of land surface and bedrock topography which cannot be referred from the soil database (gSSURGO) where the point-scale soil thickness is around 2 m.

To explore the impact of land surface topography on the spatial distribution of soil water

storage capacity, the soil data (i.e., porosity) is combined with the Height Above the Nearest Drainage (HAND) method proposed by Gao et al. (2019). HAND is the vertical elevation difference from a point to its nearest drainage point. The distribution of HAND was used for estimating the shape parameter of the spatial distribution of storage capacity. Therefore, the HAND method uses land surface topography data only for estimating the shape parameter. In our analysis, the porosity of the soil beyond the bottom layer in the soil database is assigned with the same value as the bottom layer. For example, if the HAND for a grid cell is 10.0 m and the porosity and depth of the bottom soil layer in the gSSURGO database is 0.2 and 2.0 m, respectively, the porosity for the soil from 2.0 m to 10.0 m depth is assigned with 0.2. Finally, the total volume of pores is calculated for each grid cell based on the soil porosity obtained from the gSSURGO database and the HAND value based on land surface topography.

Figure 31 shows the porosity-HAND based CDF of normalized soil water storage capacity for the Maquoketa River in Iowa (gauge #05418500). The stream initiation threshold used for calculating HAND is 40 km<sup>2</sup> which is 1% of the maximum flow accumulation (Maidment, 2002). The threshold affects the value of HAND but this is beyond the scope of this study. The best fit value of  $a$  for the porosity-HAND based CDF is 1.779, which overestimates the spatial variability of storage capacity compared with the calibrated shape parameter ( $a=1.905$ ). This is due to the assumption of the HAND method that the bedrock between a specific point and its nearest drainage point is horizontal and intercepts with the channel bed. However, the bedrock topography may



have various slopes in a watershed (Troch et al., 2002). Therefore, the true value of  $a$  (indicated by the calibrated one) potentially falls between the  $a$  obtained from soil data and the  $a$  based on soil and HAND. The bedrock topography from observation or models is needed to accurately estimate the shape parameter.

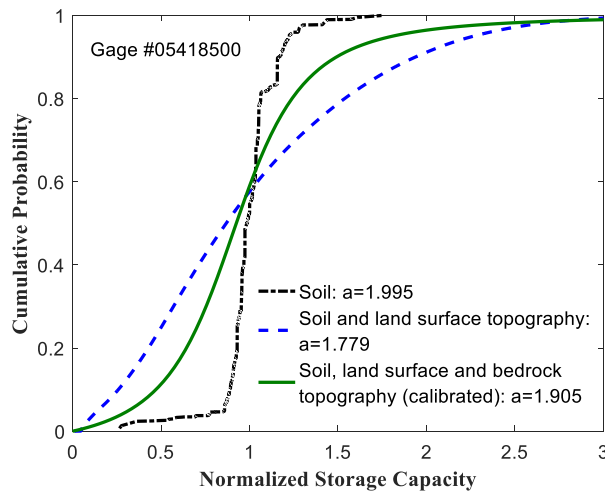


Figure 31: The effects of soil, land surface topography, and bedrock topography on the shape parameter of the spatial distribution of soil water storage capacity.

#### 4.4 Summary

A mean annual water balance model based on the concept of saturation excess runoff generation is used for predicting mean annual runoff in ungauged basins. The model takes the effect of climate variability into account explicitly since it is driven by daily precipitation and potential evapotranspiration at the daily time step. The distribution function, which leads to the SCS curve number method, is used for describing the spatial distribution of soil water storage capacity. The mean (i.e., average soil water storage capacity) and the shape parameter (i.e., the

spatial variability of soil storage capacity over the watershed) of the distribution function can be estimated from the available data. Based on the linkage of the distribution function and the SCS curve number method, a new method based on the existing observed data of watershed characteristics is proposed for estimating the average soil water storage capacity. The average soil water storage capacity ( $S_b$ ), as one of the parameters in the model, was estimated as a function of climate aridity index and curve number which is calculated based on land cover and soil data.

The developed mean annual water balance serves as a tool for diagnosing the potential for nonparametric modeling of mean annual runoff with a focus on the estimation of shape parameter ( $a$ ). The shape parameter, describing the spatial variation of soil water storage capacity, was first estimated based on the porosity and soil thickness data in the soil database (gSSURGO). The estimated values of  $a$  were tested in 35 watersheds. The results showed that the model with the estimated values of  $S_b$  and  $a$  underestimated the mean annual runoff by 11.8% on average over all the study watersheds. The underestimation of runoff is mainly caused by the underestimation of the spatial heterogeneity of soil thickness over the watershed. The Height Above the Nearest Drainage (HAND) was then calculated as the total soil thickness for estimating the total volume of the pore space. The result showed that topography is of great importance for determining the spatial variability of soil water storage capacity. The estimated shape parameter from porosity-HAND overestimated the spatial variability of the storage capacity compared with the calibrated  $a$ , which may result from the assumed bedrock in the HAND method. Future research will

investigate alternative methods for better estimating the spatial variability of soil water storage capacity over watersheds and test them in the proposed mean annual water balance model.

## CHAPTER 5 CONCLUSION

In this dissertation, the effects of best management practices (BMPs) on nitrate decrease in karst springs and the physical controls on groundwater flow in conduit network are evaluated, respectively. The research in this dissertation also diagnoses the prediction in mean annual runoff affected by the uncertainty in estimated distribution of soil water storage capacity. The present work fills the research gaps include the controls which are independent of the magnitude of the physical parameters on the contribution of conduit network to spring discharge under laminar and turbulent conditions are still unclear, and effects of BMP have not been evaluated for nitrate decrease in karst systems, as well as improves the prediction of mean annual runoff in ungauged basins.

First of all, a coupled Conduit Flow Process (CFPv2) and Conduit Mass Three-Dimensional (CMT3D) model was applied to evaluate nitrate removal for Silver Springs in Florida using blanket filters composed of biosorption-activated media (BAM). As the inputs of the model, the spatial and temporal variability of nitrate-N concentration in groundwater recharge was estimated as a function of population and land use, reflecting both point and non-point sources of nitrate. The coupled model estimates that conduit flow accounts for 48% of spring discharge and 47% of nitrate-N mass transport on average, and the contributions of conduit to flow and nitrate mass transport are higher during wet years. The effects of nitrate decrease in spring discharge was evaluated for two BMP scenarios, i.e., implementing BAM blanket filters in 26 stormwater

retention basins and 50% of the urban area. The effect of BMP for scenario 1 is limited; whereas, for scenario 2, the nitrate-N concentration in spring discharge would be decreased by 10.7% in a normal hydrologic year.

Secondly, this dissertation evaluates the controls on the contributions of single conduit and conduit network to spring discharge by employing three dimensionless physical factors (conduit-matrix hydraulic conductivity contrast,  $K_c/K$ ; relative roughness,  $\varepsilon/D$ ; Reynolds number,  $R_e$ ) as well as recharge ( $R$ ), conduit density ( $Cd$ ) and geometry. The results show that when flow in conduit(s) is laminar,  $K_c/K$ ,  $R_e$ , and  $Cd$  could pose significant controls on  $Q_c/Q$ . While, when conduit flow is turbulent, in addition to the three parameters ( $K_c/K$ ,  $R_e$ , and  $Cd$ ),  $Q_c/Q$  could also be controlled by  $\varepsilon/D$  and  $R$ . Meanwhile, when  $Cd$  is defined the same, changes in conduit geometry do not impact  $Q_c/Q$  whether it is in laminar or turbulent conditions. Further,  $Q_c/Q$  obtained from the evaluation results show well agreements with that from the two regional scale models developed both in present and previous studies, indicating given appropriate physical properties, the evaluations of controls on  $Q_c/Q$  could provide clues on the prediction of groundwater discharge in karst aquifers instead of building a more complex regional scale model.

Finally, this dissertation diagnoses the prediction in mean annual runoff affected by the uncertainty in estimated distribution of soil water storage capacity. Based on a distribution function, a water balance model for estimating mean annual runoff is developed, in which the effects of climate variability and the distribution of soil water storage capacity are explicitly

represented. As such, the two parameters in the model have explicit physical meanings, and relationships between the parameters and controlling factors on mean annual runoff are established. The estimated parameters from the existing data of watershed characteristics are applied to 35 watersheds. The results showed that the model could capture 88.2% of the actual runoff on average, indicating that the proposed new water balance model is promising for estimating mean annual runoff in ungauged watersheds. The underestimation of runoff is mainly caused by the underestimation of the spatial heterogeneity of soil storage capacity due to neglecting the effect of land surface topography. A higher spatial variability of soil storage capacity estimated through the Height Above the Nearest Drainage (HAND) indicated that topography plays a crucial role in determining the actual soil water storage capacity. The performance of mean annual runoff prediction in ungauged basins can be improved by employing better estimation of soil water storage capacity including the effects of soil, topography and bedrock.

## REFERENCES

- Alipour, M.H., Kibler, K.M., 2018. A framework for streamflow prediction in the world's most severely data-limited regions: test of applicability and performance in a poorly-gauged region of China, *Journal of Hydrology*, 557, 41-54. <https://doi.org/10.1016/j.jhydrol.2017.12.019>.
- Alipour, M.H., Kibler, K.M., 2019. Streamflow prediction under extreme data scarcity: a step toward hydrologic process understanding within severely data-limited regions, *Hydrological Sciences Journal*, 64(9), 1038-1055. [Doi:10.1080/02626667.2019.1626991](https://doi.org/10.1080/02626667.2019.1626991).
- Almasri, M.N., Kaluarachchi, J.J., 2007. Modeling nitrate contamination of groundwater in agriculture watersheds. *Journal of Hydrology*, 343, 211-229. [Doi:10.1016/j.jhydrol.2007.06.016](https://doi.org/10.1016/j.jhydrol.2007.06.016).
- Appleyard, S., 1995. The impact of urban development on recharge and groundwater quality in a coastal aquifer near Perth, Western Australia. *Hydrogeology Journal*, 3(2), 65-75. [Doi:10.1007/s100400050072](https://doi.org/10.1007/s100400050072).
- Assari, A., Mohammadi, Z., 2017. Assessing flow paths in a karst aquifer based on multiple dye tracing tests using stochastic simulation and the MODFLOW-CFP code. *Hydrogeology Journal*, 25 (6), 1679–1702. <https://doi.org/10.1007/s10040-017-1595-z>.
- Bear, J., 1972. *Dynamics of fluid in porous media*. New York, NY: Dover Publications.
- Berghuijs, W.R., Hartmann, A., Woods, R.A., 2016. Streamflow sensitivity to water storage changes across Europe, *Geophysical Research Letter.*, 43, 1980-1987. [Doi:10.1002/2016GL067927](https://doi.org/10.1002/2016GL067927).
- Bourdet, D., 2001. *Well test analysis: The use of advanced interpretation models*. Amsterdam, the Netherlands: Elsevier.
- Bradner, L.A., 1994. Ground-water resources of Okeechobee County, Florida. U.S. Geological Survey, Tallahassee, Florida. [Doi: 10.1111/gwat.12546](https://doi.org/10.1111/gwat.12546).
- Bratieres, K., Fletcher, T.D., Deletic, A., Zinger, Y., 2008. Nutrient and sediment removal by stormwater biofilters: A large-scale design optimization study. *Water Research*, 42 (14),

3930-3940. [Doi:10.1016/j.watres.2008.06.009](https://doi.org/10.1016/j.watres.2008.06.009).

Budyko, M.I., 1958. The Heat Balance of the Earth's Surface, U.S. Dep. of Commer., Washington, D. C.

Canion, A., McCloud, L., Dobberfuhl, D., 2019. Predictive modeling of elevated groundwater nitrate in a karstic spring-contributing area using random forests and regression-kriging. *Environmental Earth Sciences*, 78-271. [Doi:10.1007/s12665-019-8277-1](https://doi.org/10.1007/s12665-019-8277-1).

Cardenas, M.B., 2009. Stream-aquifer interactions and hyporheic exchange in gaining and losing sinuous streams. *Water Resources Research*, 45, W06429. [Doi:10.1029/2008WR007651](https://doi.org/10.1029/2008WR007651).

Castro, R.P., Avila, J.P., Ye, M., Sansores, A.C., 2018. Groundwater quality: analysis of its temporal and spatial variability in a karst aquifer. *Groundwater*, 56(1), 62-72. [Doi:10.1111/gwat.12546](https://doi.org/10.1111/gwat.12546).

Chang, N.B., Wanielista, M., Daranpob, A., Xuan, Z., Hossain, F., 2010. New performance-based passive septic tank underground drainfield for nutrient and pathogen removal using sorption media. *Environmental Engineering Science*, 27, 469-482. [Doi:10.1089=ees.2009.0387](https://doi.org/10.1089=ees.2009.0387).

Chang, N.B., Wanielista, M.P., Henderson, D., 2011. Temperature effects on functionalized filter media for nutrient removal in stormwater treatment. *Environmental Progress & Sustainable Energy*, 30, 309-317. [Doi:10.1002/ep.10479](https://doi.org/10.1002/ep.10479).

Chang, N.B., Xuan, Z., Marimon, Z., Islam, K., Wanielista, M.P., 2013. Exploring hydrobiogeochemical processes of floating treatment wetlands in a subtropical stormwater wet detention pond. *Ecological engineering*, 54, 66-76. [Doi:10.1016/j.ecoleng.2013.01.019](https://doi.org/10.1016/j.ecoleng.2013.01.019).

Chang, N.B., Wen, D., McKenna, A.M., Wanielista, M.P., 2018. The Impact of Carbon Source as Electron Donor on Composition and Concentration of Dissolved Organic Nitrogen in Biosorption-Activated Media for Stormwater and Groundwater Co-Treatment. *Environmental science & technology*, 52, 9380-9390. [Doi:10.1021/acs.est.8b01788](https://doi.org/10.1021/acs.est.8b01788).

Chang, N.B., Wen, D., Colona, B., Wanielista, M.P., 2019. Comparison of biological nutrient removal via two biosorption activated media between laboratory-scale and field-scale linear ditch for stormwater and groundwater co-treatment. *Water, Air, and Soil*



*Pollution*, 230, 151. <https://doi.org/10.1007/s11270-019-4193-y>.

Chang, Y., Wu, J., Liu, L., 2015. Effects of the conduit network on the spring hydrograph of the karst aquifer. *Journal of Hydrology*, 527, 517-530.

<http://dx.doi.org/10.1016/j.jhydrol.2015.05.006>.

Clark, M.M., 2009. *Transport Modeling for Environmental Engineers and Scientists*. John Wiley & Sons, Incorporated, Hoboken.

Coinly, H.H., 1945. Cyanosis in infants caused by nitrates in well water, *Journal of the American Medical Association*, 129(2). 112. [Doi:10.1001/jama.1945.02860360014004](https://doi.org/10.1001/jama.1945.02860360014004).

De Rooij, R., Perrochet, P., Graham, W., 2013. From rainfall to spring discharge: Coupling conduit flow, subsurface matrix flow and surface flow in karst systems using a discrete–continuum model. *Advances in Water Resources*, 61, 21–41. <https://doi.org/10.1016/j.advwatres.2013.08.009>.

Duan, Q., Sorooshian, S., Gupta, V., 1992. Effective and efficient global optimization for conceptual rainfall-runoff models, *Water Resources Research*, 28(4), 1015-1031. <https://doi.org/10.1029/91WR02985>.

Duan, Q., Schaake, J., Andreassian, V., Franks, S., Goteti, G., Gupta, H.V., Gusev, Y.M., Habets, F., Hall, A., Hay, L., Hogue, T., Huang, M., Leavesley, G., Liang, X., Nasonova, O.N., Noilhan, J., Oudin, L., Sorooshian, S., Wagener, T., Wood, E.F., 2006. Model parameter estimation experiment (MOPEX): an overview of science strategy and major results from the second and third workshops, *Journal of Hydrology*, 320, 3-17. [Doi:10.1016/j.jhydrol.2005.07.031](https://doi.org/10.1016/j.jhydrol.2005.07.031).

Dufresne, D., Drake, C.W., 1999. Regional groundwater flow model construction and wellfield site selection in a karst area, Lake City, Florida. *Engineering Geology*, 52, 129-139. [Doi:10.1016/S0013-7952\(98\)00066-0](https://doi.org/10.1016/S0013-7952(98)00066-0).

Duncan, J.M., Welty, C., Kemper, J.T., Groffman, P.M., Band, L.E., 2017. Dynamics of nitrate concentration-discharge patterns in an urban watershed. *Water Resources Research*, 53, 7349-7365. [Doi:10.1002/2017WR020500](https://doi.org/10.1002/2017WR020500).

Durden, D., Cera, T., Johnson, N., 2013. North Florida southeast Georgia (NFSEG) groundwater flow model conceptualization. St. Johns River Water Management District, Palatka, Florida, USA.

- Ermilio, J.F., 2005. Characterization study of a bio-infiltration stormwater BMP. Master Thesis. Villanova University.
- Exner, M.E., Hirsh, A.J., Spalding, R.F., 2014. Nebraska's groundwater legacy: nitrate contamination beneath irrigated cropland. *Water Resources Research*, 50, 4474-4489. [Doi:10.1002/2013WR015073](https://doi.org/10.1002/2013WR015073).
- Faulkner, G.L., 1973. Geohydrology of the cross-Florida barge canal area with special reference to the Ocala vicinity. United States Geological Survey, Tallahassee, Florida, USA.
- FDEP, 2006. Fifty-year retrospective study of the ecology of Silver Springs, Florida. Florida Department of Environmental Protection, Tallahassee, Florida, USA.
- FDEP, 2011. Silver Springs nutrient pathway characterization project final report. Florida Department of Environmental Protection, Tallahassee, Florida, USA.
- FDEP, 2012. Nutrient TMDL for Silver Springs, Silver Springs Group, and Upper Silver River (WBIDs 2772A, 2772C, and 2772E). Florida Department of Environmental Protection, Tallahassee, Florida, USA.
- FDEP, 2014. Integrated water quality assessment for Florida: 2014 sections 303 (d), 305 (b), and 314 report and listing update. Florida Department of Environmental Protection, Tallahassee, Florida, USA.
- FDEP, 2015. Basin management action plan for the implementation of total maximum daily loads adopted by the Florida Department of Environmental Protection in the Silver Springs basin management area for Silver Springs, Silver Springs group, and upper Silver River. Florida Department of Environmental Protection, Tallahassee, Florida, USA.
- Ford, D.C., Williams, P., 2007. *Karst Hydrogeology and Geomorphology*. John Wiley & Sons.
- Freeze, R.A., and Cherry, J.A., 1979, *Groundwater*. Englewood Cliffs, NJ, Prentice-Hall, 604 p.
- Fu, B.P., 1981. On the calculation of the evaporation from land surface [in Chinese], *Scientia Atmospherica Sinica*, 5, 23–31.

- Gallegos, J.J., Hu, B.X., Davis, H., 2013. Simulating flow in karst aquifers at laboratory and sub-regional scales using MODFLOW-CFP. *Hydrogeology Journal*, 21(8), 1749–1760. <https://doi.org/10.1007/s10040-013-1046-4>.
- Gao, H., Hrachowitz, M., Schymanski, S.J., Fenicia, F., Sriwongsitanon, N., Savenije, H.H.G., 2014a. Climate controls how ecosystems size the root zone storage capacity at catchment scale, *Geophysical Research Letter.*, 41, 7916-7923. [Doi:10.1002/2014GL061668](https://doi.org/10.1002/2014GL061668).
- Gao, H., Birkel, C., Hrachowitz, M., Tetzlaff, D., Soulsby, C., Savenije, H.H., 2019. A simple topography-driven and calibration-free runoff generation module, *Hydrology and Earth System Sciences.*, 23, 787-809. [Doi:10.5194/hess-23-787-2019](https://doi.org/10.5194/hess-23-787-2019).
- Gardner, K.K., Vogel, R.M., 2005. Predicting ground water nitrate concentration from land use. *Ground Water*, 43(3), 343-352. [Doi:10.1111/j.1745-6584.2005.0031.x](https://doi.org/10.1111/j.1745-6584.2005.0031.x).
- Gerrits, A.M.J., Savenije, H.H.G., Veling, E.J.M., Pfister, L., 2009. Analytical derivation of the Budyko curve based on rainfall characteristics and a simple evaporation model, *Water Resources Research.*, 45, W04403. [Doi:10.1029/2008WR007308](https://doi.org/10.1029/2008WR007308).
- Ghasemizadeh, R., Hellweger, F., Butscher, C., Padilla, I., Vesper, D., Field, M., Alshawabkeh, A., 2012. Review: groundwater flow and transport modeling of karst aquifers, with particular reference to the North Coast Limestone aquifer system of Puerto Rico. *Hydrogeology Journal*, 20, 1441-1461. [Doi:10.1007/s10040-012-0897-4](https://doi.org/10.1007/s10040-012-0897-4).
- Ghosh, D.K., Wang, D., Bilskie, M.V., Hagen, S.C., 2016. Quantifying changes of effective springshed area and wet recharge through recession analysis of spring flow. *Hydrological Processes*, 30, 5053-5062. <https://doi.org/10.1002/hyp.10970>.
- Giese, M., Reimann, T., Bailly-Comte, V., Marechal, J.-C., Sauter, M., Geyer, T., 2018. Turbulent and laminar flow in karst conduits under unsteady flow conditions: Interpretation of pumping tests by discrete conduit-continuum modeling. *Water Resources Research*, 54, 1918-1933. <https://doi.org/10.1002/2017WR020658>.
- Gomez J.D., Wilson J.L., Cardenas M.B., 2012. Residence time distributions in sinuosity- driven hyporheic zones and their biogeochemical effects. *Water Resources Research*, 48, W09533. [http://dx.doi.org/10.1029/2012WR012180](https://doi.org/10.1029/2012WR012180).
- Halihan, Y., Sharp, J., Mace, R.E., 2000. Flow in the San Antonio segment of the Edwards aquifer: Matrix, fractures, or conduits? In I.D. Sasowski & C.M. Wicks (Eds),

*Groundwater flow and contaminant transport in carbonate aquifers* (pp. 129-146).  
Rotterdam, the Netherlands: Balkema.

Harbaugh, A.W., 2005. MODFLOW-2005, the U.S. Geological Survey Modular Ground-Water Model: The Ground-Water Flow Process, Techniques and Methods 6–A16. United States Geological Survey, Reston, Virginia, USA Available at: <https://pubs.usgs.gov/tm/2005/tm6A16/PDF.htm>.

Hargreaves, G.H., Samani, Z.A., 1985. Reference crop evapotranspiration from temperature, *Applied Engineering Agriculture*, 1(2), 96-99.

Harper, H.H., 2014. Florida fertilizer ordinances-the good, the bad, and the ugly. Florida Stormwater Association 2014 Annual Conference.

Heffernan, J.B., Liebowitz, D.M., Frazer, T.K., Evans, J.M., Cohen, M.J., 2010. Algal blooms and the nitrogen-enrichment hypothesis in Florida springs: evidence, alternatives, and adaptive management. *Ecological Applications*, 20(3), 816-829.  
<https://doi.org/10.1890/08-1362.1>.

Hem, J.D., 1985. Study and interpretation of the chemical characteristics of natural water. U.S. Geological Survey, Water Supply Paper, 2254, 1-263.

Hickel, K., Zhang, L., 2006. Estimating the impact of rainfall seasonality on mean annual water balance using a top-down approach, *Journal of Hydrology*, 331(3-4), 409-424.

Ho, C.K., Webb, S.W., 1998. Capillary barrier performance in heterogeneous porous media. *Water Resources Research*, 34(4), 603-609. <https://doi.org/10.1029/98WR00217>.

Homer, C.G., Dewitz, J.A., Yang, L., Jin, S., Danielson, P., Xian, G., Coulston, J., Herold, N.D., Wickham, J.D., Megown, K., 2015. Completion of the 2011 National Land Cover Database for the conterminous United States-Representing a decade of land cover change information. *Photogrammetric Engineering and Remote Sensing*, 81(5), 345-354.

Hood A., Chopra, M., Wanielista, M.P., 2013. Assessment of biosorption activated media under roadside swales for the removal of phosphorus from stormwater. *Water*, 5(1), 53-66.  
[Doi:10.3390/w5010053](https://doi.org/10.3390/w5010053).

Hossain, F., Chang, N.B., Wanielista, M., Xuan, Z., Daranpob, A., 2010. Nitrification and denitrification in a passive on-site wastewater treatment system with a recirculation

- filtration tank. *Water Quality, Exposure and Health*, 2, 31-46. [Doi:10.1007/s12403-010-0022-7](https://doi.org/10.1007/s12403-010-0022-7).
- Hovorka, S., Mace, R.E., Collins, E.W., 1995. Regional distribution of permeability in the Edwards Aquifer. Edwards Underground Water District, San Antonio, TX. <http://x.doi.org/10.1029/2008WR007651>.
- Huang, M., Liang, X., Liang, Y., 2003. A transferability study of model parameters for the variable infiltration capacity land surface scheme, *Journal of Geophysical Research*, 108(D22), 8864. [Doi:10.1029/2003JD003676](https://doi.org/10.1029/2003JD003676).
- Huebsch, M., Fenton, O., Horan, B., Hennessy, D., Richards, K.G., Jordan, P., Goldscheider, N., Butscher, C., Blum, P., 2014. Mobilization or dilution? Nitrate response of karst springs to high rainfall events. *Hydrology and Earth System Sciences*, 18, 4423-4435. <https://doi.org/10.5194/hess-18-4423-2014>.
- Jeppson, R.W., 1976. *Analysis of flow in pipe networks*. Ann Arbor, MI: Ann Arbor Science.
- Katz, B.G., 2004. Sources of nitrate contamination of age of water in large karst springs of Florida. *Environmental Geology*, 46, 689-706. [Doi:10.1007/s00254-004-1061-9](https://doi.org/10.1007/s00254-004-1061-9).
- Katz, B.G., Sepulveda, A.A., Verdi, R.J., 2009. Estimating nitrogen loading to ground water and assessing vulnerability to nitrate contamination in a large karstic springs basin, Florida. *Journal of the American Water Resources Association*, 45(3), 607-627. <https://doi.org/10.1111/j.1752-1688.2009.00309.x>.
- Kiraly, L., 2002. Karstification and groundwater flow. Paper presented at the proceedings of the conference on evolution of karst: From pre-karst to cessation (pp. 155–190), Postojna-Ljubljana.
- Korom, S.F., 1992. Natural denitrification in the saturated zone: a review. *Water Resources Research*, 28(6), 1657-1668. [Doi:10.1029/92WR00252](https://doi.org/10.1029/92WR00252).
- Li, D., 2014. Assessing the impact of interannual variability of precipitation and potential evaporation on evapotranspiration, *Advances in Water Resources*, 70, 1-11. <https://doi.org/10.1016/j.advwatres.2014.04.012>.
- Liedl, R., Sauter, M., Hückinghaus, D., Clemens, T., Teutsch, G., 2003. Simulation of the development of karst aquifers using a coupled continuum pipe flow model.

*Water Resources Research*, 39 (3), 1057. <https://doi.org/10.1029/2001WR001206>.

Maidment, D.R. (Ed.), 2002. *ArcHydro: GIS for Water Resources*, ESRI Press, Redlands, Calif.

Marechal, J.-C., Ladouche, B., Dorflinger, N., Lachassagne, P., 2008. Interpretation of pumping tests in a mixed flow karst system. *Water Resources Research*, 44, W05401. <https://doi.org/10.1029/2007WR006288>.

McMahon, P.B., Burow, K.R., Kauffman, L.J., Eberts, S.M., Bohlke, J.K., Gurdak, J.J., 2008. Simulated response water quality in public supply wells to land use change, *Water Resources Research*, 45 (7), W00A06. [Doi:10.1029/2007WR006731](https://doi.org/10.1029/2007WR006731).

Milly, P.C.D., 1994. Climate, soil water storage, and the average annual water balance, *Water Resources Research*, 30(7), 2143-2156. [Doi:10.1029/94WR00586](https://doi.org/10.1029/94WR00586).

Moore, R.J., 1985. The probability-distributed principle and runoff production at point and basin scales, *Hydrological Sciences Journal*, 30(2), 273-297.

O'Reilly, A.M., Wanielista, M.P., Chang, N.B., Xuan, Z., Harris, W.G., 2012a. Nutrient removal using biosorption activated media: preliminary biogeochemical assessment of an innovative stormwater infiltration basin. *Science of the Total Environment*, 432, 227-242. [Doi:10.1016/j.scitotenv.2012.05.083](https://doi.org/10.1016/j.scitotenv.2012.05.083).

O'Reilly, A., Wanielista, M., Chang, N.B., Harris, W.G. Xuan, Z., 2012b. Soil property control of biogeochemical processes beneath two subtropical stormwater infiltration ponds. *Journal of Environmental Quality*, 41, 1-18. [Doi:10.2134/jeq2011.0204](https://doi.org/10.2134/jeq2011.0204).

O'Reilly, A., Chang, N.B., Wanielista, M., 2012c. Cyclic biogeochemical processes and nitrogen fate beneath a subtropical stormwater infiltration basin. *Journal of Contaminant Hydrology*, 133, 53-75. [Doi:10.1016/j.jconhyd.2012.03.005](https://doi.org/10.1016/j.jconhyd.2012.03.005).

O'Reilly, A.M., Chang, N.B., Wanielista, M.P., Xuan, Z., 2014. Groundwater Nutrient Reduction at Stormwater Infiltration Basins: Biogeochemical Assessment and Application of Biosorption Activated Media. 30th Annual ASCE Water Resources Seminar, Orlando, Florida.

Panno, S.V., Kelly, W.R., Martinsek, A.T., Hackley, K.C., 2006. Estimating background and threshold nitrate concentrations using probability graphs. *Ground Water*, 44(5), 697-709. [Doi:10.1111/j.1745-6584.2006.00240.x](https://doi.org/10.1111/j.1745-6584.2006.00240.x).

- Reed, E.M., Wang, D., Duranceau, S.J., 2017. Modeling anthropogenic boron in groundwater flow and discharge at Volusia Blue Spring (Florida, USA). *Hydrogeology Journal*, 25(1), 91-101. [Doi:10.1007/s10040-016-1461-4](https://doi.org/10.1007/s10040-016-1461-4).
- Reed, E.M., Wang, D., Duranceau, S.J., 2018. Evaluating nitrate management in the Volusia Blue springshed. *Journal of Environmental Engineering*, 144(3), 05018001. [Doi:10.1061/\(ASCE\)EE.1943-7870.0001324](https://doi.org/10.1061/(ASCE)EE.1943-7870.0001324).
- Reimann, T., Liedl, R., Birk, S., Bauer, S., 2013a. MODFLOW-CFPV2. Dresden Technical University, Dresden, GE.
- Reimann, T., Liedl, R., Birk, S., Bauer, S., 2013b. Modifications and Enhancements to CFPM1 Flow Subroutines and Addition of Transport Subroutines. Documentation available at [http://tudresden.de/die\\_tu\\_dresden/fakultaeten/fakultaet\\_forst\\_geo\\_und\\_hydrowissenschaften/fachrichtung\\_wasserwesen/igw/forschung/downloads/cfpv2](http://tudresden.de/die_tu_dresden/fakultaeten/fakultaet_forst_geo_und_hydrowissenschaften/fachrichtung_wasserwesen/igw/forschung/downloads/cfpv2).
- Reimann, T., Liedl, R., Giese, M., Geyer, T., et al. 2013c. Addition and Enhancement of Flow and Transport Processes to the MODFLOW-2005 Conduit Flow Process. NGWA Ground Water Summit, May 2013, San Antonio, TX.
- Peterson, E.W., Davis, R.K., Brahana, J.V., Orndorff, H.A., 2002. Movement of nitrate through regolith covered karst terrane, northwest Arkansas. *Journal of Hydrology*, 256, 35-47. [Doi:10.1016/S0022-1694\(01\)00525-X](https://doi.org/10.1016/S0022-1694(01)00525-X), 2002.
- Peterson, E.W., Wicks, C.M., 2006. Assessing the importance of conduit geometry and physical parameters in karst systems using the storm water management model (SWMM). *Journal of Hydrology*, 329, 294-305. <https://doi.org/10.1016/j.jhydrol.2006.02.017>.
- Phelps, G.G., 2004. Chemistry of ground water in the Silver Springs basin, Florida, with an emphasis on nitrate. U.S. Geological Survey, Reston, Virginia, USA.
- Pike, J.G., 1964. The estimation of annual runoff from meteorological data in a tropical climate, *Journal of Hydrology*, 12, 2116–2123.
- Porporato, A., Daly, E., Rodriguez-Iturbe, I., 2004. Soil water balance and ecosystem response to climate change, *American Naturalist*, 164(5), 625–632. [Doi:10.1086/424970](https://doi.org/10.1086/424970).

- Quinlan, J.F., Ewers, R.O., 1985. Ground water flow in limestone terranes: Strategy rationale and procedure for reliable, efficient monitoring of ground water quality in karst areas. In proceedings of the national symposium and exposition on aquifer restoration and groundwater monitoring (5th, Columbus, Ohio, pp. 197–243). Worthington, OH: National Water Well Association.
- Ritter, A., Munoz-Carpena, R., Bosch, D.D., Schaffer, B., Potter, T.L., 2007. Agricultural land use and hydrology affect variability of shallow groundwater nitrate concentration in south Florida. *Hydrological Processes*, 21, 2464-2473. [Doi:10.1002/hyp.6483](https://doi.org/10.1002/hyp.6483).
- Rivett, M.O., Buss, S.R., Morgan, P., Smith, J.W.N., Bemment, C.D., 2008. Nitrate attenuation in groundwater: a review of biogeochemical controlling processes. *Water Research*, 42, 4215-4232. [Doi:10.1016/j.watres.2008.07.020](https://doi.org/10.1016/j.watres.2008.07.020).
- Robertson, W.D., Blowes, D.W., Ptacek, C.J., Cherry, J.A., 2000. Long-term performance of in situ reactive barriers for nitrate remediation. *Ground Water*, 38(5), 689-698. [Doi:10.1111/j.1745-6584.2000.tb02704.x](https://doi.org/10.1111/j.1745-6584.2000.tb02704.x).
- Ronayne, M., 2013. Influence of conduit network geometry on solute transport in karst aquifers with a permeable matrix. *Advances in Water Resources*, 56, 27-34. <http://dx.doi.org/10.1016/j.advwatres.2013.03.002>.
- Sahu, M., Gu, R.R., 2009. Modeling the effects of riparian buffer zone and contour strips on stream water quality. *Ecological Engineering*, 35(8), 1167-1177. [Doi:10.1016/j.ecoleng.2009.03.015](https://doi.org/10.1016/j.ecoleng.2009.03.015).
- Salamah, S.K., 2014. The Effects of BAM as an Adsorptive Media on Phosphorus Removal in Stormwater. University of Central Florida Orlando, Florida.
- Sankarasubramanian, A., Vogel, R.M., 2002. Annual hydroclimatology of the United States, *Water Resources Research*, 38(6), 1083. [Doi:10.1029/2001WR000619](https://doi.org/10.1029/2001WR000619).
- SCS., 1972. *Hydrology. National Engineering Handbook, Supplement A, Section 4, Chapter 10*. Soil Conservation Service, US Department of Agriculture, Washington, DC.
- Sepulveda, N., 2002. *Simulation of ground-water flow in the intermediate and Floridan aquifer system in peninsular Florida*. United States Geological Survey, Tallahassee, Florida, USA.
- Sfriso, A., Marcomini, A., 1994. Gross primary production and nutrient behavior in a shallow



- coastal environment. *Bioresource Technology*, 47(1), 59-66. [Doi:10.1016/0960-8524\(94\)90029-9](https://doi.org/10.1016/0960-8524(94)90029-9).
- Shamrukh, M., Corapcioglu, M.Y., Hassona, F.A.A., 2001. Modeling the effect of chemical fertilizers on ground water quality in the Nile Valley aquifer, Egypt. *Groundwater*, 39(1), 59-67. [Doi:10.1111/j.1745-6584.2001.tb00351.x](https://doi.org/10.1111/j.1745-6584.2001.tb00351.x).
- Shao, Q., A. Traylen, Zhang, L., 2012. Nonparametric method for estimating the effects of climatic and catchment characteristics on mean annual evapotranspiration, *Water Resources Research*, 48, W03517. [Doi:10.1029/2010WR009610](https://doi.org/10.1029/2010WR009610).
- Shoemaker, W.B., Kuniansky, E.L., Birk, S., Bauer, S., Swain, E.D., 2007. Documentation of a Conduit Flow Process (CFP) for MODFLOW-2005: U.S. Geological Survey Techniques and Methods, Book 6, Chapter A24, 50p.
- Shultz, C.D., Gates, T.K., Bailey, R.T., 2018. Evaluating best management practices to lower selenium and nitrate in groundwater and streams in an irrigated river valley using a calibrated fate and reactive transport model. *Journal of Hydrology*, 566, 299-312. [Doi:10.1016/j.jhydrol.2018.09.005](https://doi.org/10.1016/j.jhydrol.2018.09.005).
- Shuster, E.T., White, W.B., 1971. Seasonal fluctuations in the chemistry of limestone springs: a possible means for characterizing carbonate aquifers. *Journal of Hydrology*, 14(2) 93-128. [https://doi.org/10.1016/0022-1694\(71\)90001-1](https://doi.org/10.1016/0022-1694(71)90001-1).
- Sirianuntapiboon, S., Kongchum, M., Jitmaikasem, W., 2006. Effects of hydraulic retention time and media of constructed wetland for treatment of domestic wastewater. *African Journal of Agricultural Research*, 1(2), 27-37.
- Smith, R.L., Miller, D.N., Brooks, M.H., 2001. In situ simulation of groundwater denitrification with formate to remediate nitrate contamination. *Environmental Science and Technology*, 35(1), 196-203. doi: 10.1021/es001360p. [Doi:10.1021/es001360p](https://doi.org/10.1021/es001360p).
- Smith, R.L., Bohlke, J.K., Garabedian, S.P., Revesz, K.M., Yoshinari, T., 2004. Assessing denitrification in groundwater using natural gradient tracer tests with <sup>15</sup>N: in situ measurement of a sequential multistep reaction. *Water Resources Research*, 40, W07101. [Doi:10.1029/2003WR002919](https://doi.org/10.1029/2003WR002919).
- Spiessl, S.M., Prommer, H., Licha, T., Sauter, M., Zheng, C., 2007. A process-based reactive hybrid transport model for coupled discrete conduit–continuum systems. *Journal of*

- Hydrology*, 347 (1-2), 23–34. <https://doi.org/10.1016/j.jhydrol.2007.08.026>.
- Sullivan, T.P., Gao, Y., Reimann, T., 2019. Nitrate transport in a karst aquifer Numerical model development and source evaluation. *Journal of Hydrology*, 573, 432-448. <https://doi.org/10.1016/j.jhydrol.2019.03.078>.
- Tang, Y., Wang, D., 2017. Evaluating the role of watershed properties in long-term water balance through a Budyko equation based on two-stage partitioning of precipitation, *Water Resources Research*, 53, 4142–4157. [Doi:10.1002/2016WR019920](https://doi.org/10.1002/2016WR019920).
- Toride, N., Leu, F.J., van Genuchten, M.T., 1999. The CXTFIT code for estimating transport parameters from laboratory or field tracer experiments. Research report 137, US Salinity Laboratory, USDA, ARS, Riverside, USA.
- Troch, P., Loon, E.V., Hilberts, A., 2002. Analytical solutions to a hillslope-storage kinematic wave equation for subsurface flow, *Advances in Water Resources*, 25(6), 637-649. [https://doi.org/10.1016/S0309-1708\(02\)00017-9](https://doi.org/10.1016/S0309-1708(02)00017-9).
- Troch, P. A., Carrillo, G., Sivapalan, M., Wagner, T., Sawicz, K., 2013. Climate-vegetation-soil interactions and long-term hydrologic partitioning: Signatures of catchment co-evolution, *Hydrology and Earth System Sciences*, 17, 2209-2217. <https://doi.org/10.5194/hess-17-2209-2013>, 2013.
- Trojan, M.D., Maloney, J.S., Stockinger, J.M., Eid, E.P., Lahtinen, M.J., 2003. Effects of land use on ground water quality in the Anoka Sand Plain aquifer of Minnesota. *Groundwater*, 41(4), 482-492. [Doi:10.1111/j.1745-6584.2003.tb02382.x](https://doi.org/10.1111/j.1745-6584.2003.tb02382.x).
- Turc, L., 1954. Le bilan d'eau des sols: Relation entre les precipitations, l'évaporation et l'écoulement, *Annalee Agronouiquee Serie A*, 5, 491–595.
- USCB, 1995. Census of population and housing. U.S. Census Bureau. Washington, D.C., USA.
- USDA, 2014. Gridded Soil Survey Geographic (gSSURGO) Database User Guide, U. S. Dep. of Agric., Nat. Resour. Conserv. Serv., Washington, D. C.
- U.S. EPA. The Qtracer2 Program For Tracer-Breakthrough Curve Analysis For Tracer Tests In Karstic Aquifers And Other Hydrologic Systems, 2002. U.S. Environmental Protection Agency, Office of Research and Development, National Center for Environmental Assessment, Washington Office, Washington, DC, EPA/600/R-02/001, 2002.

- Wang, D., Hejazi, M., 2011. Quantifying the relative contribution of the climate and direct human impacts on mean annual streamflow in the contiguous United States, *Water Resources Research*, 47, W00J12. [Doi:10.1029/2010WR010283](https://doi.org/10.1029/2010WR010283).
- Wang, D., Tang, Y., 2014. A one-parameter Budyko model for water balance captures emergent behavior in Darwinian hydrologic models, *Geophysical Research Letter*, 41, 4569–4577. [Doi:10.1002/2014GL060509](https://doi.org/10.1002/2014GL060509).
- Wang, D., 2018. A new probability density function for spatial distribution of soil water storage capacity leads to SCS curve number method, *Hydrology and Earth System Sciences*, 22, 6567-6578. [Doi:10.5194/hess-22-6567-2018](https://doi.org/10.5194/hess-22-6567-2018).
- Wen, D., Ordonez, D., McKenna A., Chang, N.B., 2019. Fate and transport processes of nitrogen in biosorption activated media for stormwater treatment at varying field conditions of a roadside linear ditch. *Environmental Research*, 181, 108915. [Doi:10.1016/j.envres.2019.108915](https://doi.org/10.1016/j.envres.2019.108915).
- Wen, D., Valencia, A., Lustosa, E., Ordonez, D., Rice, N., Shokri, M., Gao, Y., Kibler, K., Chang, N.B., Wanielista, M.P., 2019. Evaluation of green sorption media blanket filters for nitrogen removal at varying groundwater conditions in a stormwater retention basin. *Science of the Total Environment*, 22, 1-14. <https://doi.org/10.1016/j.scitotenv.2019.134826>.
- Wen, D., Valencia, A., Ordonez, D., Chang, N.B., Wanielista, W.P., 2020. Comparative nitrogen removal via microbial ecology between soil and green sorption media in a rapid infiltration basin for co-disposal of stormwater and wastewater. *Environmental Research*, 184, 109338. <https://doi.org/10.1016/j.envres.2020.109338>.
- Wei, X., Bailey, R.T., Records, R.M., Wible, T.C., Arabi, M., 2018. Comprehensive simulation of nitrate transport in coupled surface-subsurface hydrologic systems using the linked SWAT-MODFLOW-RT3D model. *Environmental Modelling & Software*, 1364-8152. [Doi:10.1016/j.envsoft.2018.06.012](https://doi.org/10.1016/j.envsoft.2018.06.012).
- Wood, E.F., Lettenmaier, D.P., Zartarian, V.G., 1992. A land-surface hydrology parameterization with subgrid variability for general circulation models, *Journal of Geophysical Research*, 97(D3), 2717-2728. <https://doi.org/10.1029/91JD01786>.
- Woods, R., 2003. The relative roles of climate, soil, vegetation and topography in determining

seasonal and long-term catchment dynamics, *Advances in Water Resources Research*, 37, 701-708. [https://doi.org/10.1016/S0309-1708\(02\)00164-1](https://doi.org/10.1016/S0309-1708(02)00164-1).

Worthington, S.R.H., 1999. A comprehensive strategy for understanding flow in carbonate aquifer. In: Palmer, A.N., Palmer, M.V., Sasowsky, I.D. (Eds.), *Karst Modeling, Special Publication*. 5, pp. 30–37.

Worthington, S.R.H., 2009. Diagnostic hydrogeologic characteristics of a karst aquifer (Kentucky, USA). *Hydrogeology Journal*, 17, 1665-1678. <https://doi.org/10.1007/s10040-009-0489-0>.

Worthington, S.R.H., 2015. Characteristics of channel networks in unconfined carbonate aquifers. *Bulletin of the Geological Society of America*, 127, 759-769. <https://doi.org/10.1130/B31098.1>.

Xiao, H., Wang, D., Hagen, S.C., Medeiros, S.C., Hall, C.R., 2016. Assessing the impacts of sea-level rise and precipitation change on the surficial aquifer in the low-lying coastal alluvial plains and barrier islands, east-central Florida (USA). *Hydrogeology Journal*, 24(7), 1791-1806. [Doi:10.1007/s10040-016-1437-4](https://doi.org/10.1007/s10040-016-1437-4).

Xu, Z., Hu, B. X., Davis, H., Cao, J., 2015. Simulating long term nitrate-N contamination processes in the Woodville Karst Plain using CFPv2 with UMT3D. *Journal of Hydrology*, 524, 72-88. [Doi:10.1016/j.jhydrol.2015.02.024](https://doi.org/10.1016/j.jhydrol.2015.02.024).

Xuan, Z., Chang, N.B., Daranpob, A., Wanielista, M., 2009. Initial test of a subsurface constructed wetland with green sorption media for nutrient removal in on-site wastewater treatment systems. *Water Quality, Exposure and Health*, 1, 159. [Doi:10.1007/s12403-009-0015-6](https://doi.org/10.1007/s12403-009-0015-6).

Xuan, Z., Chang, N.B., Wanielista, M., Hossain, F., 2010. Laboratory-scale Characterization of a green sorption medium for on-site sewage treatment and disposal to improve nutrient removal. *Environmental Engineering Science*, 27, 301-312. [Doi:10.1089/ees.2009.0256](https://doi.org/10.1089/ees.2009.0256).

Yang, H., Yang, D., Lei, Z., Sun, F., 2008. New analytical derivation of the mean annual water-energy balance equation, *Water Resources Research*, 44, W03410. [Doi:10.1029/2007WR006135](https://doi.org/10.1029/2007WR006135).

Yang, M., Yaquian, J.A., Annable, M.D., Jawitz, J.W., 2019. Karst conduit contribution to spring discharge and aquifer cross-sectional area. *Journal of Hydrology*, 578, 124037. <https://doi.org/10.1016/j.jhydrol.2019.124037>.

- Yao, L., Libera, D., Kheimi, M., Sankarasubramanian, A., Wang, D., 2020. The Roles of Climate variability on runoff at daily, monthly, inter-annual, and long-term scales, under review.
- Yokoo, Y., Sivapalan, M., Oki, T., 2008. Investigating the roles of climate seasonality and landscape characteristics on mean annual and monthly water balances, *Journal of Hydrology*, 357(3-4), 255-269. [Doi:10.1016/j.jhydrol.2008.05.010](https://doi.org/10.1016/j.jhydrol.2008.05.010).
- Zheng, C., Wang, P.P., 1999. MT3DMS: a Modular Three-dimensional Multispecies Transport Model for Simulation of Advection, Dispersion, and Chemical Reactions of Contaminants in Groundwater Systems; Documentation and User's Guide. U.S. Army Engineer Research and Development Center, Vicksburg, USA Contract Report SERDP-99-1.
- Zhang, L., Dawes, W.R., Walker, G.R., 2001. Response of mean annual evapotranspiration to vegetation changes at catchment scale, *Water Resources Research*, 37, 701-708. <https://doi.org/10.1029/2000WR900325>.
- Zhao, R.J., 1992. The Xinanjiang model applied in China, *Journal of Hydrology*, 135(1-4), 371-381.